A photograph of a rocky shoreline with water ripples and sediment waves. The water is blue and shows distinct wave patterns around the rocks. In the background, there are trees and a signpost.

Propagation of sediment waves associated with coarse gravel nourishments

F. Acevedo Goldaracena

This page is intentionally left blank

Propagation of sediment waves associated with coarse gravel nourishments

by

Fernando Acevedo Goldaracena

to obtain the degree of Master of Science
at the Delft University of Technology,
to be defended publicly on December 17th, 2020.

Student number: 4950798
Thesis committee: Dr. ir. A. Blom, TU Delft, supervisor
C. Ylla Arbós, TU Delft
Prof. dr. ir. M. Kok, TU Delft
Dr. ir. R. Schielen, RWS

This thesis is confidential and cannot be made public until December 17th, 2020.

An electronic version of this thesis is available at <http://repository.tudelft.nl/>.

“What we know is a drop, what we don’t know is an ocean”

— Isaac Newton

Preface

The present document marks the final step in my journey towards obtaining the degree of Master of Science at Delft University of Technology, as well as the first step into a future in the field of Hydraulic Engineering. Throughout this two-year journey I had the opportunity to dive into the field of River Morphodynamics, which is the main focus of this study, and the field of Flood Risk. More importantly, I had the opportunity to work alongside some of the brightest minds in my field of study, and I will be forever grateful for it.

In this research project, I had the opportunity to not only learn about rivers and sediment nourishments, but also to develop my research skills, which will with no doubt be of great use in my future. For this, I would like to personally thank both of my supervisors, Astrid and Claudia, for their patience, for sharing their expertise, and for offering their guidance and words of advice throughout this project, as well as my graduation committee members, Ralph and Matthijs for their valuable contributions.

I would like to thank my parents for their unconditional support throughout this journey, this would not have been possible without you. I would also like to thank my brother, as well as my cousins, who were always available whenever I was in need for a distraction, even though we are on opposite corners of the world.

I would also like thank all my friends: the ones who ventured into this journey with me, with whom I spent many hours facing the challenges that were thrown in our way, the ones who stayed in touch from abroad, with whom I could always count on when I needed someone to talk to, and the ones with whom I shared a house with, who were always there whenever I needed a break.

Fernando Acevedo Goldaracena
Delft, December 10th, 2020

This page is intentionally left blank

Abstract

Sediment nourishments have become an increasingly attractive alternative to deal with continuous bed degradation problems in the river system. When supplied to the river, sediment nourishments induce a sediment wave that propagates through the system causing changes in bed level and bed surface texture. In the present study we use a one-dimensional numerical model to analyse how the propagation of these sediment waves varies under different conditions.

We find that the propagation of the sediment wave tends to be predominantly dispersive for large spatial variations of the flow, which is the dominant case when the height of the wave is large in comparison to the flow depth, or when the sediment is dispersed over a large enough reach to lead to a backwater effect. In artificial sediment nourishments the height of the sediment wave is usually limited to prevent creating an additional obstacle to navigation, and it is then that the temporal variations in the flow, due to high discharge events for example, determine the propagation of the wave.

We study the morphodynamic response in a mixed-size sediment river system to a sediment nourishment, and identify the physical mechanisms that impact the propagation of mixed-sized sediment waves. In order to prevent it from being easily flushed downstream, the grain size distribution of the nourished sediment is typically selected to be coarser than the river bed. This reduces sediment mobility and enhances sediment deposition over the nourished reach, which in turn causes a deficit in sediment supply to the downstream reach and leads to the formation of a degradational wave.

The propagation celerity of the degradational wave is found to be significantly faster than that of the sediment wave, which means that the effects of the nourishments in a river system can be observed significantly further downstream than from where the front of the sediment wave is found. We find that the celerities of both the sediment wave and the degradational wave are predominantly affected by the adjustments in surface grain size in the system. These adjustments migrate in the river system as a fining wave, which both accelerates the sediment wave, and decelerates the degradational wave.

We learn that higher content of the finer fractions in the nourished sediment accelerate the evolution of the wave and lead to a predominantly translational behaviour. It also affects the magnitude of the incision depth, the closer the composition of the nourished sediment is to that of the bed surface, the less severe the scour. And even though it does not affect the propagation celerity of the degradational wave, it does impact how far downstream the wave travels, affecting a larger river reach the coarser the grain size composition of the sediment wave is.

Finally, we analyse the results from a nourishment pilot project carried out in the Bovenrijn from 2016-2019. We find that the propagation of the sediment wave associated with the nourishment is only observed during high discharge events. The wave is predominantly dispersive, and only during a prolonged extreme discharge event did the wave show slight translational behaviour. We observe that lateral sorting mechanisms caused the tracer sediment to have a different trajectory from the sediment wave, which highlights the limitations of using a one-dimensional model. We also observe that the changes in bed level are related to the changes in surface grain size, with sediment deposition over the nourished reach and bed degradation just downstream.

Contents

Preface	i
Abstract	ii
1 Introduction	1
1.1 Context	1
1.2 Scope	5
2 Theoretical background	7
2.1 Previous studies	7
2.1.1 “Bed” and “sorting” celerities	7
2.1.2 Experimental and field studies	9
2.2 Theoretical response	13
2.2.1 Bernoulli effect	13
2.2.2 Backwater effect	14
2.2.3 Increase in friction	15
2.2.4 Increase in grain size	16
2.2.5 Sorting waves	17
2.2.6 Dominant response	19
3 The model	20
3.1 Simplifications and assumptions	20
3.2 The model	21
3.3 Base case	21
3.3.1 Boundary conditions	21
3.3.2 Initial conditions	22
3.4 Model runs	23
3.4.1 Model runs A: Distribution of the nourishments	23
3.4.2 Model runs B: Grain size of the nourishments	23
4 Propagation of the adjustment waves	24
4.1 Unisize sediment case study	24
4.2 Mixed-size sediment case study	28
4.2.1 Morphodynamic response	28
4.2.2 Propagation of the sediment wave	30
4.2.3 Propagation of the degradational wave	32
5 Model results	36
5.1 Model runs A - Effects of changes in the height and length of the sediment wave	36
5.1.1 Propagation of the sediment wave	36
5.1.2 Propagation of the degradational wave	38
5.2 Model runs B - Grain size of the nourished sediment	41
5.2.1 Propagation of the sediment wave	41
5.2.2 Propagation of the degradational wave	44
5.2.3 Model run 4 - Decrease in grain size	46
6 Nourishment pilot project	49
6.1 Project specifications	49
6.2 Changes in bed level	52
6.3 Changes in surface grain size	58
6.4 Chapter conclusions	60

7	Discussion	62
8	Conclusions and Recommendations	64
8.1	Conclusions	64
8.2	Recommendations	67
A	Model convergence	70
B	Wiggles	72
	List of Figures	74

Introduction

1.1. Context

Over the past centuries the natural course of the Rhine river has been modified to fit societal purposes, causing the river to respond by adapting its geometry to fulfil its functions. Among other river interventions, the engineering training works of the 19th and 20th centuries, which consisted of extensive narrowing and shortening of the river, have led to an ongoing degradation of the river bed (Blom et al. 2016). Due to the problems this ensues for navigation, numerous sediment management measures have been implemented on the river over the past few decades.

The Rhine is one of the largest rivers and the busiest river in Europe, it serves as an inland waterway connection between the port of Rotterdam, the 11th busiest container port in the world, and the German hinterland. It has for a long time been a key to the economic and cultural development of the surrounding regions, and for these reasons, river authorities have made continuous efforts to keep the Rhine as a navigable waterway. Among these efforts, narrowing of the main river channel with the construction of groynes, maintenance dredging to remove sediment from places unfavourable for navigation, and fixing of the river course with dikes.



Figure 1.1: Rhine reach between Weisweil and Marlen. On top the meandering river reach before the normalisation works. On the bottom the same straightened river reach afterwards. (Hillebrand et al. 2017)

Continued interference in a river causes it to continuously adapt towards its equilibrium profile. This is defined by Blom et al. (2016) as the mean profile that the river approaches when flow, sediment supply, and base level vary around stable values for a long time in the absence of subsidence or uplift. Following from this definition of the equilibrium profile, it can be understood why the overall reduction in river width and length (Figure 1.1), via channel narrowing and normalisation works, has led to a large scale decrease in slope and associated ongoing bed degradation, as the Rhine attempts to approach its new equilibrium state. The latter is a product of the combination of all river interventions, as well

as changes in its boundary conditions due to sea level rise, change in sediment supply and increased flow variability.

The lowering of water levels due to bed degradation may be seen as beneficial when one considers its implications to flood safety, since a lower water level means relatively higher river dikes. However, the negative implications of bed degradation tend to outweigh the positive ones. If we consider that not every part of the river bed erodes as easily, the parts that are harder to erode lead to shallower areas in the river, which directly reduce the navigation capacity of the river as a waterway. Additionally, continuous bed degradation could threaten the stability of structures along the river, as well as negatively impact the ecology in the floodplains due to reduced groundwater levels.

To counteract bed degradation in the Rhine, where bed incision rates reach up to 2 cm/yr (Blom 2016), different sediment management measures have been implemented, both by German and by Dutch authorities. In order to prevent dredging activities from reducing the sediment available for transport, which are usually carried out to maintain the river channel navigable, it was required starting in 1992 that the dredged bed material be re-allocated back into the river.

The results of the aforementioned sediment management measure are presented in Figure 1.2 for the Niederrhein (Rhine-km 640-862). We present the total volumes of sediment dredged and its respective reallocation. From the data available, it is clear that this measure has been effectively implemented, as the total volumes for sediment extracted and sediment supplied sum to equal amounts. We can also see that the reallocation of these sediments is usually carried out immediately downstream of the dredged area, which prevents the effects from these measures to have an impact on other parts of the river.

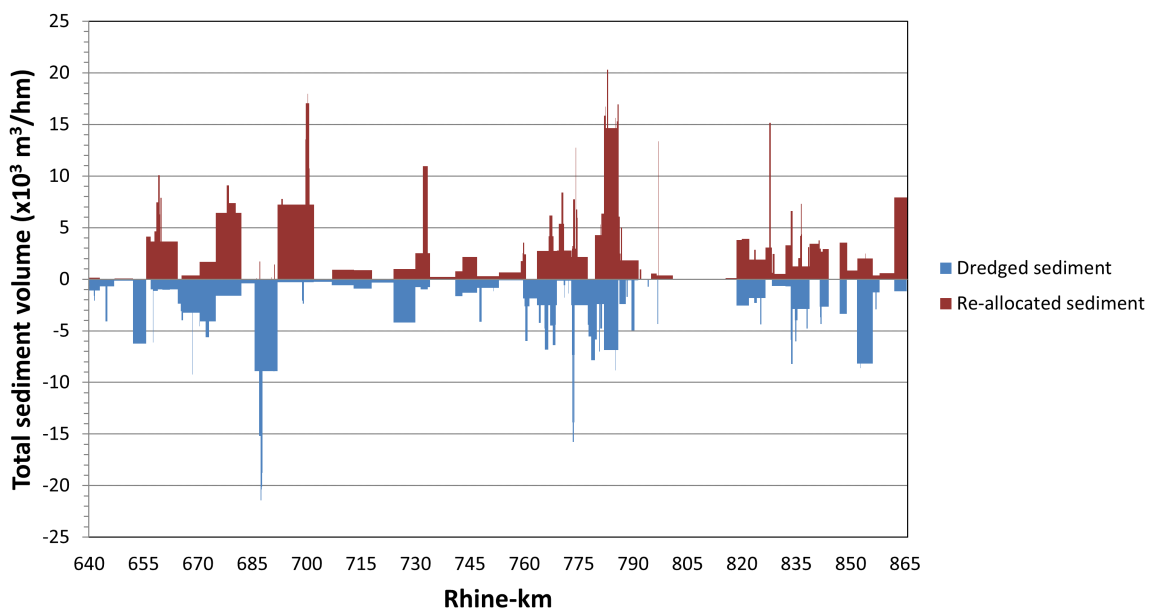


Figure 1.2: Total dredged and re-allocated sediment volumes in the Niederrhein between 1991-2010. As presented by Frings et al. (2014a).

Additionally, within the time period between 1989 and 2010 very coarse gravel nourishments were also carried out in this river reach. The total volumes for these are presented in Figure 1.3. We observe that of the total 6.4 Mt supplied within this period, about 3.6 Mt of it were allocated within the last 40 km of this reach, between Rhine-km 820-860 just upstream of the German-Dutch border. The grain size composition of this material ranged between 8-150 mm, which is significantly coarser than the existing bed surface. The purpose of this coarseness was to ensure the material was not easily eroded during mean discharge conditions, improving the stability of the river bed (Frings et al. 2014a).

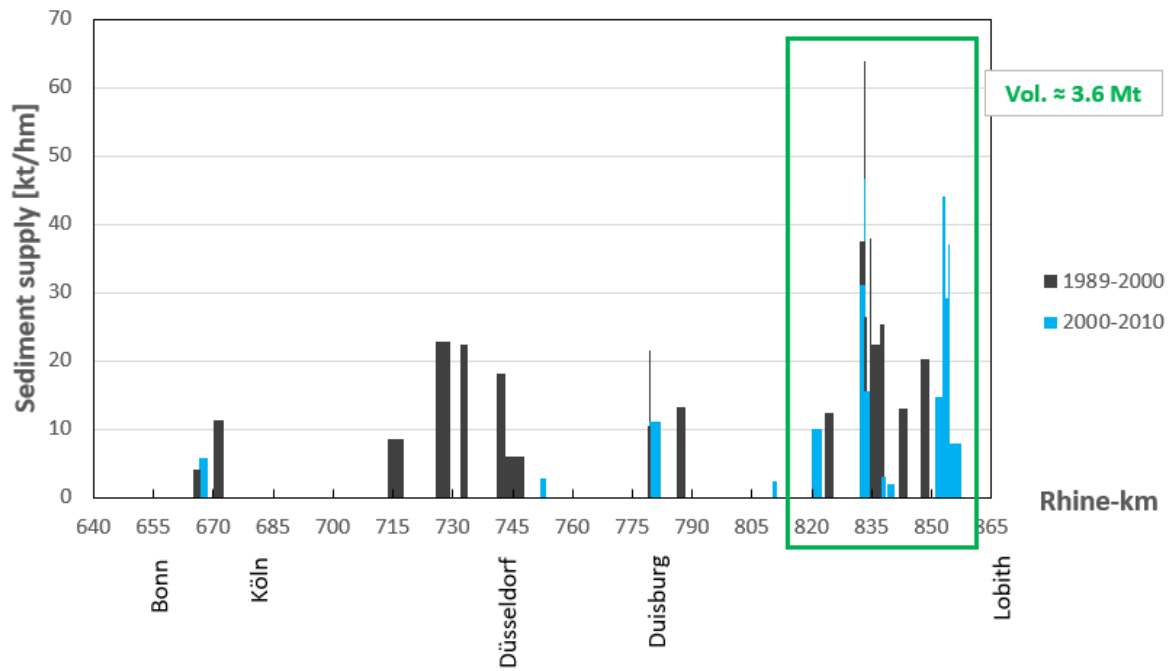


Figure 1.3: Total volume of nourished sediment with grain size of 8-150 mm in the Niederrhein between 1991-2010.

Lastly, in the year 2000 German authorities implemented a third sediment management measure to compensate for observed deficits in sediment supply downstream. This measure consisted in continuous nourishments with a grain size composition similar to that of the existing river bed, between 4-32 mm. In Figure 1.4. We present how these were distributed along the Niederrhein between 2000-2010, with the majority of the nourishments concentrating on the downstream end of this reach, between Rhine-km 810-850.

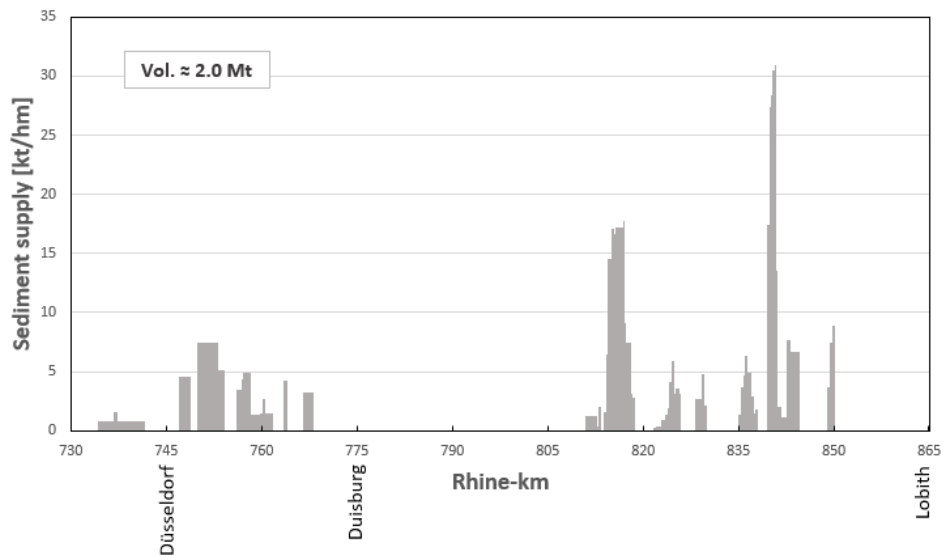


Figure 1.4: Total volume of nourished sediment consisting of additional bed-load supply (gravel of 4-32 mm) in the Niederrhein between 2000-2010.

Studies based on data analysis have shown a significant decrease in bed degradation rates along the Niederrhein in response to the implemented sediment management measures (Quick et al. 2019).

However, the consequences of these measures on the downstream reaches have not yet been thoroughly analysed.

When sediment coarser than the bed surface is fed through artificial nourishments to the river, these induce a propagating gravel front that causes a coarsening of the river bed over time. This in turn increases the shear stress needed to mobilise this coarser bed sediment, reducing bed degradation, and consequently also decreasing the volume of sediment transported downstream. This induces a degradational wave that travels downstream significantly faster than the nourished sediment itself (Blom 2016).

The temporal coarsening of the bed surface via artificial sediment nourishments enhances bed degradation downstream. This implies that sediment nourishments such as the ones presented in Figure 1.3 for the Niederrhein could likely already have negative consequences for the trends in bed level in the Dutch Rhine downstream.

Just downstream of the German-Dutch border the Rhine bifurcates into the Waal and the Pannerdensch Kanaal (Figure 1.5). The Waal is the largest of the two branches, designed to carry approximately 2/3 of the incoming discharge. Flood defences downstream are designed for this specific partitioning, and different bed degradation trends for each of the branches influence this discharge partitioning, and therefore endangers them.

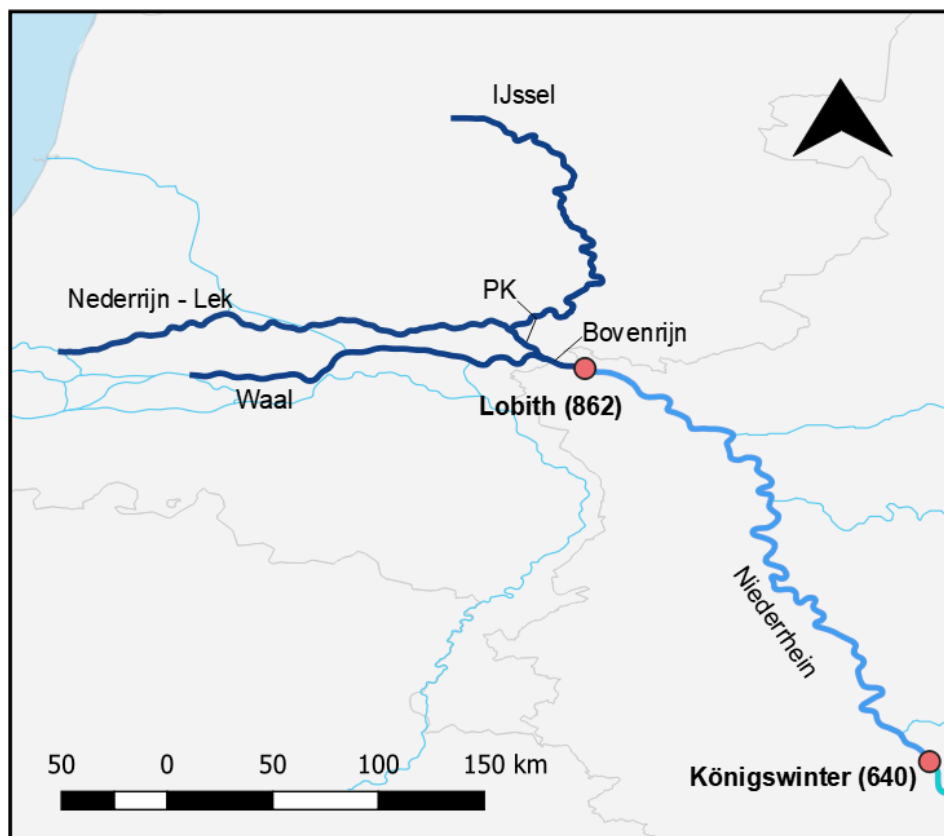


Figure 1.5: Upper Rhine delta and downstream reach of the German Rhine (Niederrhein), city boundaries with respective (Rhine-km). PK: Pannerdensch Kanaal.

The Rhine river gravel-sand transition (GST) zone is located in the upper Rhine delta. This is explained by Blom et al. (2017a) as an abrupt decrease in characteristic grain size often observed in alluvial rivers, from about 10 to 1 mm. In the river Rhine this transition is not as abrupt as reported in other smaller rivers, as it stretches for over 50 kilometres, from Rhine-km 820 to Rhine-km 870 (Frings et al. 2014a).

The decrease in bed degradation rates observed in the Niederrhein after the sediment management measures were implemented is not quite carried into the Dutch Rhine. While incision rates have been negligible in the Bovenrijn since around 1985, incision still persists in the upstream reach of the Waal (Rhine-km 870-920) at approximately 1-1.5 cm/yr over the past 20 years (Ylla Arbós et al. 2019).

Dutch authorities have started looking at sediment nourishments as a possible measure to counteract bed degradation in this reach. A pilot project was implemented in 2016, where a total volume of 70,000 m^3 sediment slightly coarser than the bed was supplied to a 2.3 km reach. The objective of this project is to improve the understanding of how nourishments propagate and the effects they have on the river system, in order to determine whether or not nourishments become a part of the river management in the future (Koolstra et al. 2019).

1.2. Scope

The objective of this research project is to analyse the changes in a river system caused by sediment nourishments, not only over the reach where they are supplied, but also upstream and downstream of it. We study the different factors (such as the grain size composition of the nourishments) that influence the downstream propagation of the nourished sediment, and the changes in bed level it induces.

We use a one-dimensional numerical model to provide insight on the impact sediment nourishments have on the river system, assessing what these sediment management measures mean for bed elevation and bed surface texture. We address the following research questions:

1. What adjustment waves can be observed in a river system after a sediment nourishment?
2. What physical processes determine the propagation celerity of the adjustment waves?
3. What is the impact of variations in the height and length of the sediment wave induced by the nourishment on the adjustment waves?
4. What is the impact of variations in the grain size distribution of the nourishments on the adjustment waves?
5. How do these results compare to a nourishment field experiment?

Research question (1) is addressed in chapter 2, where we present a comprehensive review of the existing studies on the propagation of bed material and grain size adjustment waves. We analyse the theoretical hydrodynamic and morphodynamic response of a river system, considering the different mechanisms in play after a nourishment supply of material coarser than the bed surface. We then identify the adjustment waves that we can expect to propagate in the river system after said nourishment supply.

In Chapter 3 we describe the numerical model used in this research project, providing an overview of the simplifications and assumptions made for the model runs. We motivate the selected input parameters, as well as the initial and boundary conditions. An overview of each set of model runs is described with their specifications, linking the methodology followed to each of the research questions.

In Chapter 4 we address research question (2). We complement the theoretical analysis with a case study of sediment nourishments with unisize and mixed size sediment compositions. We compare the morphodynamic responses in each of the models and determine the main physical processes that cause changes in the propagation celerity of the adjustment waves.

Chapter 5 is divided in 2 sections, in the first we address research question (3). We set-up a series of model runs in which we vary the length over which a constant volume of sediment nourishments are distributed. This causes changes in the flow velocities for each of the model runs, while keeping the base parameters constant. We study the changes in the propagation of the adjustment waves for each of these model runs.

In the second section of Chapter 5 we analyse the impact of variations in the grain size composition of the nourishments on the system response, and on the evolution and propagation of the resulting adjustment waves. We aim to answer research question (4) with a set of model runs in which we vary the grain size composition of the nourishments, and study the changes in the results.

In Chapter 6 we address research question (5), by analysing the results from the pilot nourishment project carried out in the Bovenrijn in 2016, and by comparing this results to the analysis made with the 1-D model. We aim to better identify the limitations of the model, as well as provide a better understanding in the effectiveness of a 1-D to study these physical processes.

Theoretical background

We begin this chapter with a literature review with the objective to introduce important concepts that are treated in this research project. We present first the different studies that deal with the propagation celerity of perturbations in a river system. Then we analyse the results from existing experimental and field studies on the propagation of sediment waves.

We then study the theoretical hydrodynamic and morphodynamic response of a river reach to a sediment nourishment. We identify the different adjustment waves of bed level, as well as surface grain size for the different physical processes that influence the response of the river system to a sediment nourishment.

2.1. Previous studies

Various studies have been made regarding the propagation of nourishments on gravel-bed rivers. With their increase in popularity as a counteracting measure to problems related to bed degradation, it has become more important to understand how they propagate in a river system, based on the sediment composition and the way the nourishments are supplied, as these factors vary the response of the system and the overall effectiveness of the nourishments.

In this section, we first present the analytical solution obtained to estimate the celerity of perturbations in flow, bed level and grain size changes. This is then followed by a brief summary on experimental studies that have treated the physical behaviour of sediment waves with varying grain sizes. Finally we take a look at reports on data analysis from field experiments regarding sediment nourishments in rivers.

2.1.1. “Bed” and “sorting” celerities

Sediment nourishments induce temporal changes in bed level and bed surface texture in the river system. To be able to study these morphodynamic changes, the active layer model proposed by Hirano (1971) is to this day the most commonly used sediment continuity model for mixed-sized sediment (Equation 2.1). It is able to relate sediment bed load transport to the size of sediments available at the bed surface, while keeping track of the development of stratigraphy.

$$(1 - p) \left[\frac{\partial F_{ak} L_a}{\partial t} + F_{lk} \frac{\partial}{\partial t} (z_b - L_a) \right] = - \frac{\partial q_{sk}}{\partial x} \quad (2.1)$$

where p represents the porosity of the bed surface, F_{ak} is the volume fraction content per grain size in the active layer, L_a the thickness of the active layer, F_{lk} the volume fraction content per grain size of the interface, z_b represents bed elevation, and q_{sk} the sediment transport per unit width per grain size fraction [m^2/s]. In this model (Hirano 1971) introduces the concept of the active layer, defined as the volume of sediment that interacts with the flow and gives rise to bed load fluxes, regulating the exchange with the substrate layers underneath.

Stecca et al. (2014) used the active layer model by Hirano (1971) to derive grain size specific active and substrate layer mass conservation equations. They then used this model in conjunction with the Saint-Venant equations for free-surface flow (i.e. equations of conservation of mass and momentum), and the Exner equation for conservation of sediment mass for unisize sediment, to build a system matrix for a mathematical analysis. By finding approximations of the eigenvalues of this matrix, they found expressions that provide an analytical approximation of the propagation velocities of small-amplitude perturbations to bed elevation (“bed” waves) and to perturbations of the grain size distribution of the active layer (“sorting” waves). A schematisation of these waves is presented in Figure 2.1.

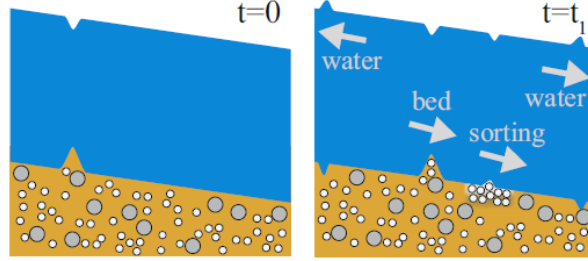


Figure 2.1: Schematic of the effect of a perturbation in bed elevation in a mixed sediment case as depicted by (Chavarrías, Guglielmo Stecca, et al. 2018). A perturbation in bed elevation introduces perturbations in flow, bed level and surface grain size distribution, hereby referred to as “water”, “bed”, and “sorting” waves respectively.

The findings from Stecca et al. (2014) for the celerity of the bed waves coincide with the results obtained in a previous study by De Vries (1965) for quasi-steady flow, given by Equation 2.2. The drawback of this equation is that for flow close to critical conditions (i.e. for Froude numbers roughly within the range $0.8 < Fr < 1.2$), the bed wave celerity (λ_{bed}) becomes unrealistically large and no longer valid. When λ_{bed} is positive, the bed wave travels in the downstream direction for well-developed subcritical flow, and upstream for supercritical flow.

$$\lambda_{bed} = \frac{u\psi}{1 - Fr^2}, \quad \text{with} \quad \psi = \frac{\partial q_s}{\partial q} \quad (2.2)$$

Furthermore, Stecca et al. (2014) improved on the work by Ribberink (1987) who first identified and derived an equation for the celerity of the sorting waves, by taking into account grain size selective transport. In their equation (Eq. 2.3), they considered one eigenvalue for each active layer equation, such that there are distinct celerities ($N - 1$) depending on the total number of unique characteristic grain sizes (N). It is also applicable to all Froude regimes as well as degradational conditions, as long as the solution remains hyperbolic. However, it is important to note that in order to derive this equation, a constant active layer thickness was assumed, as well as high-transport conditions (i.e. all size fractions k are sufficiently mobile).

$$\lambda_{sort,k} = \frac{Q_{bk}(1 - F_{Ik}) + F_{Ik}Q_{bN}}{uL_a} \quad \text{for} \quad 1 \leq k \leq N - 1 \quad (2.3)$$

The sorting celerity λ_{sort} is inversely proportional to the thickness of the active layer L_a , consistent with the previous findings by Ribberink (1987). The volume fraction content per grain size of the interface F_{Ik} is defined by Equation 2.4 following Hirano (1971), for aggradational conditions $\frac{\partial}{\partial t}(z_b - L_a) > 0$, and for degradational conditions $\frac{\partial}{\partial t}(z_b - L_a) < 0$.

$$F_{Ik} = \begin{cases} F_{ak} & \text{if } \frac{\partial}{\partial t} (z_b - L_a) > 0 \\ f_{sk} (z = z_b - L_a) & \text{if } \frac{\partial}{\partial t} (z_b - L_a) < 0 \end{cases} \quad (2.4)$$

While these equations (2.2 and 2.3) have been derived for small amplitude perturbations, they are still relevant to the present study, as they provide insight on the relations that describe the propagation of the adjustment waves, as well as on the physical processes that drive them.

2.1.2. Experimental and field studies

Using a physical model in a flume, Berkhout (2015) studied the propagation of a bed level step with different grain size compositions, with the objective to gain insight on its physical behaviour by comparing the resulting celerities from the physical model, to the ones obtained analytically with the solution presented by Stecca et al. (2014) in Equations 2.2 and 2.3, as well as to the celerities obtained with the use of a numerical model.

In their results for the experiments with mixed-sized sediment, presented in Figure 2.2 Berkhout (2015) found the bed level step composed of the coarser sediment fraction to be preceded by a degradational wave. The formation of this degradational wave can be explained by the increase in surface grain size induced by the bed level step, the coarsening of the bed surface decreases sediment mobility and therefore the amount of sediment available for transport downstream, such that the flow downstream of the step compensates for the reduced sediment supply by eroding the bed surface.

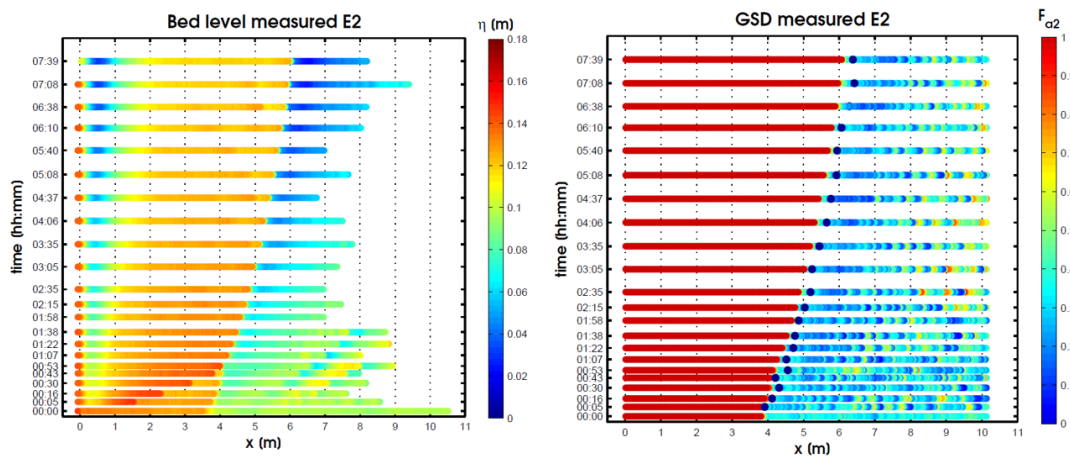


Figure 2.2: Results from experimental studies by Berkhout (2015) for the propagation of a shoal composed of coarse sediment. On the left, bed level measurements depicting the formation of a scour downstream of the shoal. On the right, measurements of the gravel volume content in the active layer, showing the fining of the surface downstream of the shoal.

As presented on the right hand-side of Figure 2.2, Berkhout (2015) found in their physical model that the degradational wave is accompanied by a fining of the bed surface. An explanation for this finding is that over the coarsened reach, the sediment deposition of the coarser fraction becomes relatively larger than that of the finer fraction, which causes a relative fining of the sediment supply to the downstream reach.

The main advantage of a physical model is that it is able to represent certain physical processes that a numerical model is either unable or would require significant computational time. Among these processes are changes in surface friction related to surface grain size, as well as unsteady fluid motions associated with turbulent flow. However, a numerical model does have a certain advantage in that it makes it easier to set-up multiple model runs under identical conditions, which allows for a comparison

of different results with varying control parameters.

In their study, Berkhout (2015) compare the results from the physical model to that of a numerical model set up with the same conditions and parameters. They identified that the depth of the incision is larger in the experimental results than in the numerical simulations, possibly due to the latter being unable to properly predict the increased sediment mobility caused by turbulent flow at this location. Another potential explanation for this discrepancy between the models could be related to the observed changes in surface grain size, in the physical model the degradational wave is accompanied by a significant fining of the bed surface, and a deeper incision could be the result of this finer surface being more mobile, and hence easier to erode.

Another notable difference observed in the numerical simulations, is that the fining of the active layer in the bed surface just downstream of the coarsened reach does not happen to the same extent as observed in the physical model. In comparison, in the results for the numerical model the fining of the bed surface associated with the degradational wave is much milder. Berkhout (2015) hypothesised that this difference could be due to the numerical model not representing vertical sorting processes and flow velocity patterns related to turbulent flow that could enhance this fining of the surface texture.

The hypothesis by Berkhout (2015) explains that the fining of the surface texture was a result of a combination of dune sorting and flow velocity patterns in the recirculation zone downstream of the step. Due to vertical sorting, the coarse sediment fractions being transported by the nourishment wave first avalanche to the trough of the preceding degradational wave, afterwards the flow in the recirculation zone mobilises only the finer fractions, as it has a lower magnitude, and these cover the coarser ones buried in the bottom. A similar process can be observed with migrating bed forms, as the coarse material tends to gather underneath (Figure 2.3).

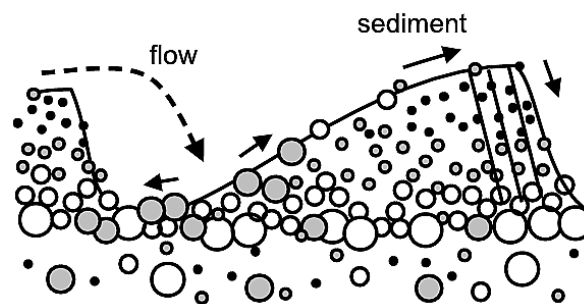


Figure 2.3: Accumulation of the coarser sediment fractions in the trough of migrating bed forms due to vertical sorting, as depicted by Blom et al., (2003)

On the left hand-side of Figure 2.2 we can also observe that the celerity of the degradational wave is significantly higher than that of the bed wave, as the former propagates significantly further downstream than the latter during the same amount of time. This goes hand in hand with the findings by Ribberink (1987) that imply that the sorting waves tend to be several times faster than the bed waves.

The differences observed in the celerities of the bed and sorting waves by both Berkhout (2015) and Ribberink (1987) imply that if we considered a river reach, where the surface has been coarsened by sediment nourishments for example, the degradational wave that precedes the coarsened reach migrates downstream significantly faster, and affects a reach larger and further downstream than from where the nourishments are supplied.

We consider a different approach to this topic by reviewing other studies that have focused on analysing the propagation of natural sediment waves. While these studies primarily focus on the propagation of very large-amplitude sediment waves, they still provide valuable insight on the role of the grain size composition of sediment augmentations on the propagation of sediment waves, as well as explain the influence of the Froude number on whether these waves propagate through translation or dispersion.

The translational behaviour of a sediment wave as described by Lisle et al. (2001) can be identified when all of the features of the wave, leading and trailing edge, apex, and centre of mass propagate in the same direction with a similar celerity. This means that a purely translational wave does not deform over time, but is rather simply advected through the river system. On the other hand, in a purely dispersive wave, the centre of mass of the wave tends to remain in place while the amplitude becomes smaller over time, as presented in Figure 2.4

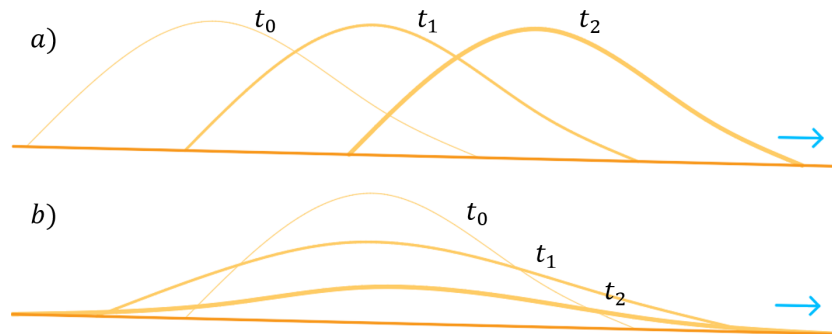


Figure 2.4: On top (a) the evolution of a purely translational sediment wave. On bottom (b) the evolution of a purely dispersive sediment wave.

To better understand the routing of bed material through river channels, by studying the evolution of sediment waves of bed material in a model gravel-bed river, Lisle et al. (1997) found that large-amplitude waves tend to have a more predominantly dispersive behaviour. The dispersion of the sediment wave is driven by sediment transport gradients that favour deposition of the upstream and downstream ends, and erosion of the wave crest. This wave behaviour, however, is predominantly observed in flow close to critical conditions, as the Froude number in their experiment was estimated at 0.90. This is later confirmed by Lisle et al. (2001) as they observed that significant wave translation requires a low Froude number, and low wave amplitude, which can only be achieved by a large wave after it has significantly decayed.

Furthermore, Lisle et al. (1997) observed that slight sediment migration was only observed nearing the end of their experiment, once the wave had decayed to a small fraction of its initial amplitude, and the longitudinal slope hardly varied. They concluded that the longitudinal slope plays a strong role in the initial evolution of the sediment wave, and only after the wave has significantly decayed do other flow processes cause the wave to migrate downstream with a more translational behaviour.

They then reproduced these processes with a numerical model, which showed that changes in bed slope do not cause a significant change in the pattern of wave evolution observed. In their results, they found that even with the presence of two-dimensional features in their physical model, the evolution of the wave was well represented by their one-dimensional numerical model. Additionally, Lisle et al. (2001) found that field evidence also show similar results to the observations in their experiments, even when compared to fully three-dimensional flow behaviour.

To complement their analysis, Lisle et al. (2001) also studied the effects of the grain size distribution of the sediment wave on its evolution. They hypothesised that due to the clear dependence of the rate of wave evolution on the bed load transport rate, while finer grain size composition may promote translation of the sediment wave, it mainly increases the bed load transport rates and thus simply accelerates wave evolution.

The effects of the grain size distribution of sediment waves was then also later assessed by Sklar et al. (2009), in their experiments they analyse the evolution of sediment pulses of different grain size compositions and volumes. They concluded that sediment pulses composed of finer materials to have a more translational behaviour. A similar conclusion was made for sediment pulses of smaller volumes,

again confirming the findings of Lisle et al. (2001) that translation of sediment waves is observed more predominantly once the wave has decayed, and the variations in longitudinal slope become smaller.

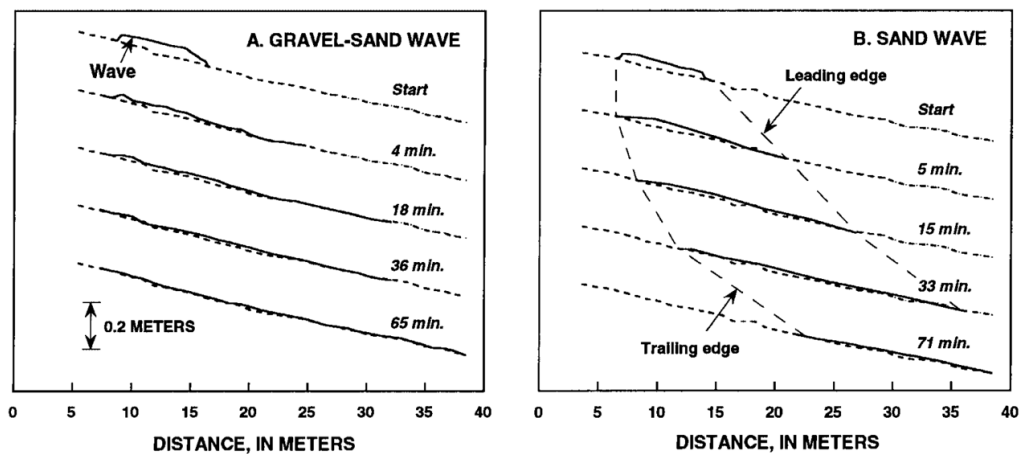


Figure 2.5: On the left (A) the evolution of a gravel sand sediment wave. On the right (B) the evolution of a sand sediment wave. As depicted by Lisle et al. (2001).

The understanding sediment routing becomes increasingly important when considering sediment nourishments projects, whether for river restoration or maintenance of channel as a waterway for navigation. This highlights the importance of knowing how the sediment will disperse depending on its volume and grain size composition, and the effect it will have on the river bed surface. Such efforts have been not only in experimental studies as was the case for Lisle et al. (2001), Sklar et al. (2009), and Venditti et al. (2010), among others, but also through data analysis of tracer recovery in nourishments.

Emmanouil (2017) analysed the data from a sediment nourishment project carried out downstream of the dam at Iffezheim (Figure 1.5) in the Rhine river. The nourishments were composed of sediment overall slightly coarser than the bed, with grain sizes varying from 4 to 63 mm. The propagation of the sediment was analysed with measurements of tracer concentration. The results indicated that the apex of the wave decayed to about 15% of its initial concentration value over the first 10 months while showing almost no translation, while the tail remained fairly static. Over the next 4 years results showed significant slowing down of the wave decay, and a very dispersive-dominated evolution, as the leading edge of the wave propagated further, and at a faster pace than the centre of mass, while the tail barely moved.

From the field experiment in Iffezheim, Emmanouil (2017) also analysed the propagation of the tracer sediment per grain size fraction. The results showed that the coarser fractions clearly propagate at a slower rate. However, a certain grouping of the grain sizes within the ranges 4-8 mm and 8-16 mm also occurred, which could be an indicator of sediment hiding of the smaller fractions. This means that the level of exposure of the finer grains to the flow could explain their reduced mobility, since the larger particles may tend to hide them and hinder their propagation through the system.

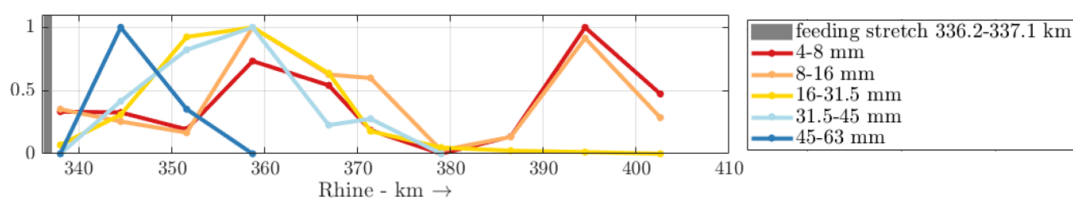


Figure 2.6: Normalised tracer concentration per grain size fraction, almost 5 years after nourishments, as depicted by Emmanouil (2017)

2.2. Theoretical response

In this section we present the morphodynamic response of a river system after a sediment nourishment. We separate the morphodynamic response for each of the effects that play a role in it, and use them to determine the adjustment waves that are observed in a river system after a sediment nourishment with coarse material.

The objective of this section is to better understand the driving processes behind the different morphodynamic responses of a river system to a sediment nourishment, and to determine the different scenarios that must be considered for different dominant mechanisms.

The four effects that we analyse are:

1. Bernoulli effect.
2. Backwater effect.
3. Increase in grain size.
4. Increase in friction.

2.2.1. Bernoulli effect

Let us first assume a river reach in equilibrium, where a volume of sediment is supplied uniformly over a portion of it, with the same grain size composition as the bed surface. The nourishments cause an immediate increase in bed level over the reach where it is supplied. The sudden increase in bed level alters the flow, and induces a morphodynamic response in which the river will try to adjust back to its equilibrium state by eroding the supplied sediment from the bed.

If we neglect energy losses due to friction, the energy head remains constant over space ($\frac{d\langle H \rangle}{ds} = 0$). Following Bernoulli's principle (Eq. 2.5), the sudden increase in bed level causes an increment in flow velocity over the nourished reach. This is explained by an inertia-dominated response of the flow, where the potential energy of the flow (piezometric head d), is converted to kinetic energy (velocity head $u^2/2g$). In Figure 2.7 we present the associated schematic of the Bernoulli effect, where the flow velocities over the nourished reach are increased.

$$\langle H \rangle = d_I + \frac{u_I^2}{2g} = d_{II} + \frac{u_{II}^2}{2g} \quad (2.5)$$

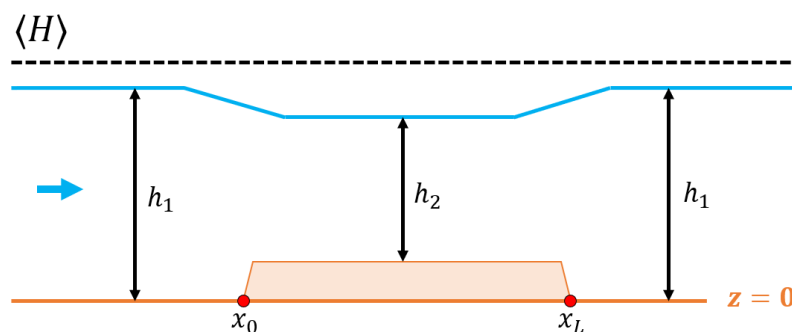


Figure 2.7: Energy balance and Bernoulli effect over a bed level step, neglecting energy losses due to friction ($\frac{d\langle H \rangle}{ds} = 0$).

The increased velocities over the nourished reach increase sediment transport rates, which are then accompanied by a morphodynamic response. In Figure 2.8 we present a schematisation of this initial morphodynamic response, where the increase in flow velocity at the upstream end of the nourishments (x_0) is met with an incisional wave, and the decrease of flow velocity at the downstream end (x_L) is met with a sedimentation front or a downstream-migrating hump.

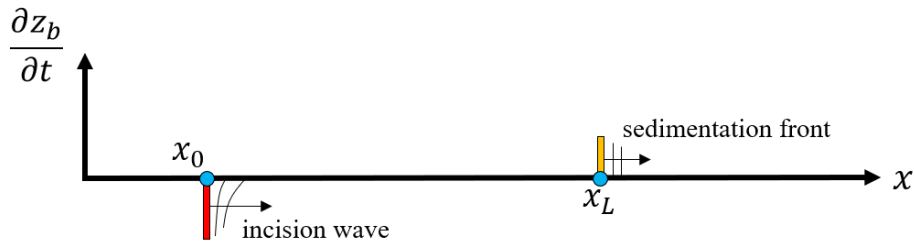


Figure 2.8: Morphodynamic response corresponding to the increase in velocity caused by the Bernoulli effect.

2.2.2. Backwater effect

In Figure 2.9 we study the backwater effect caused by the bed level increase due to the nourishments, the equilibrium flow depth (d_e) remains the same, but for the nourished reach this flow depth is now found at a higher water level than for the unaltered reaches. The water level information in a system with subcritical flow travels from downstream to upstream. This means that over the nourished reach the flow depth (d) adjusts with a M2 backwater curve, with flow depth increasing in the upstream direction. And in the upstream reach the flow depth adjusts with a M1 backwater curve, with flow depth decreasing in the upstream direction.

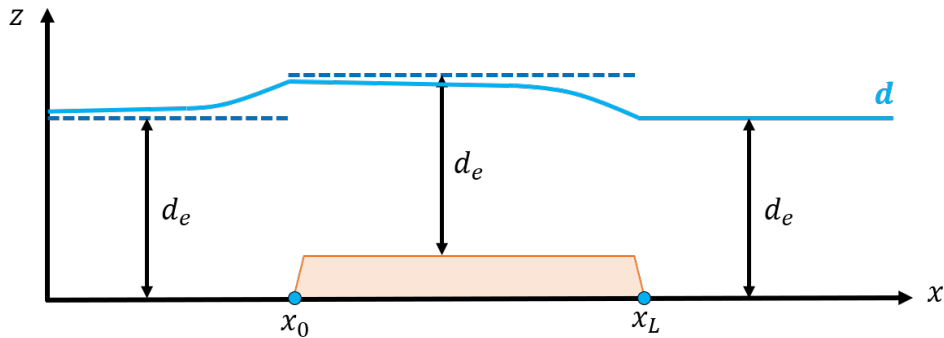


Figure 2.9: Initial flow response and backwater effect.

The corresponding flow velocities to this backwater effect are presented in Figure 2.10. In this figure we see that the equilibrium flow velocity ($u_e = \frac{q}{d_e}$) remains unchanged, as there are also no changes in discharge (q) and equilibrium flow depth. The corresponding flow velocity (u) to the observed flow depth in Figure 2.9 is seen to decrease along the upstream reach, and decrease over the nourished reach.

The respective morphodynamic response to these velocity changes is depicted in Figure 2.11. The steep velocity gradients at the boundaries of the nourished reach (x_0 and x_L) lead to a similar morphodynamic response as observed for the Bernoulli effect, with an incisional wave on the upstream end, and a sedimentation front on the downstream end. Additionally, the spatial gradient in flow velocity over the upstream reach leads to bed aggradation, and to bed degradation over the nourished reach.

By comparing Figures 2.8 and 2.11 we can draw the conclusion that the morphodynamic responses from both effects (Bernoulli and backwater) complement each other, as both lead to the downstream migration of an incisional wave and a sedimentation front starting from the same locations. For simplicity we refer to this downstream-migrating accumulation of sediment as a “sediment wave”.

As the river system attempts to adjust back to its equilibrium state, the sediment wave associated with the sediment nourishment is transported in the downstream direction. The shape of this wave deforms due to the spatial gradients in flow velocity caused by the backwater effect. As the height of the wave decays over time, the gradients in sediment transport become milder, and the sediment wave slows

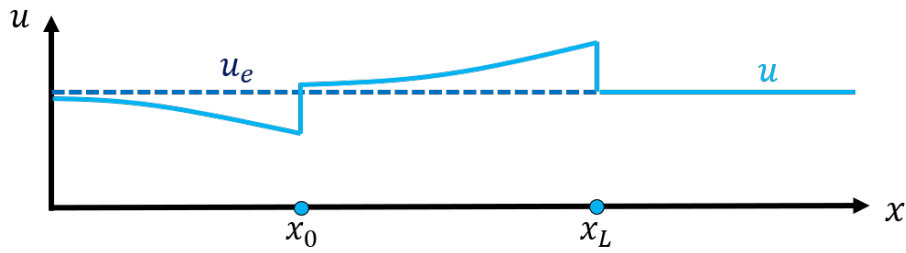


Figure 2.10: Flow velocity gradients corresponding to the backwater effect.

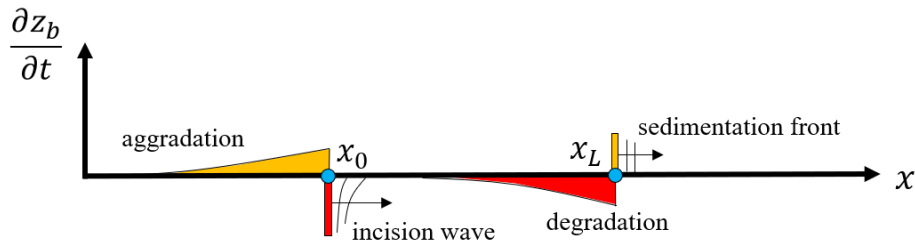


Figure 2.11: Morphodynamic response to the backwater effect.

down.

2.2.3. Increase in friction

One of the disadvantages of using a numerical model to study the hydrodynamics of a system is that changes in friction are often hard to account for. In this section we analyse the hydrodynamic and corresponding morphodynamic response to an increase in surface friction over the nourished reach.

Over the nourished reach the increase in surface grain size also leads to an increase in surface friction. This increase in friction causes the equilibrium flow depth of the nourished reach to be larger, which leads to the backwater effect presented in Figure 2.12.

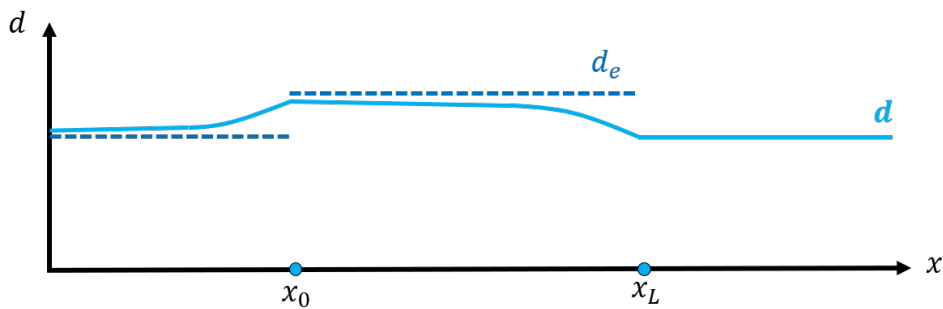


Figure 2.12: Resulting backwater curves for an increase in surface friction over the nourished reach.

The spatial gradients in flow depth observed in Figure 2.12 lead to the initial morphodynamic response presented in Figure 2.13, due to the consequent gradients in sediment transport.

We observe that the increase in friction enhances degradation over the nourished reach, and favours aggradation upstream. This is a similar response as the one observed for the backwater effect in Figure 2.11. From which we can conclude that even though we assume a constant value for the friction coefficient in our numerical simulations, the morphodynamic response corresponding to the increase in friction simply enhances the already observed response for the Bernoulli and backwater effect depicted earlier.

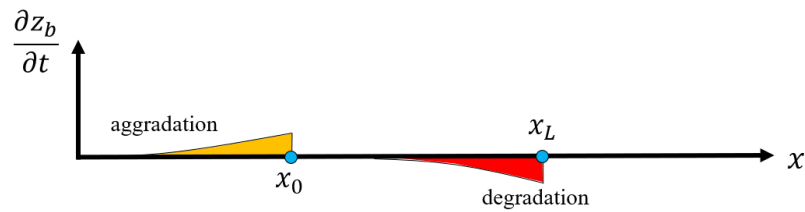


Figure 2.13: Morphodynamic response to an increase in friction.

2.2.4. Increase in grain size

In gravel-bed rivers the river bed is typically composed by grains of significantly different sizes. In fact, it has been studied that the bed surface of river channels tends to get finer in the downstream direction. This phenomenon, downstream fining, is commonly attributed to be caused by particle abrasion and selective transport, among others.

Let us now address a river system where the composition of the bed load and bed surface is described by multiple, discrete characteristic grain size fractions. We analyse the case of a nourishment supply distributed uniformly over a portion of the river, composed of sediments coarser than the bed surface.

The coarser composition of the nourished sediment causes a decrease in sediment mobility over the reach where it is supplied, which consequently also reduces the amount of sediment transported downstream. This effect can be represented by the sediment transport gradients drawn in Figure 2.14.



Figure 2.14: Sediment transport gradients resulting from a coarsening of a river reach.

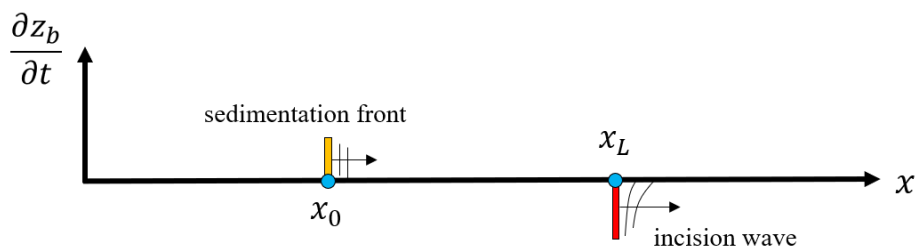


Figure 2.15: Morphodynamic response to coarse sediment nourishments.

In Figure 2.15 we describe the morphodynamic response to a coarse sediment nourishment. The negative gradient in sediment transport at the upstream end of the nourished reach (x_0) is met with a sedimentation front, or a migrating hump. The positive gradient at the downstream end of the nourished reach (x_L) is met with a downstream-migrating incisional wave.

This morphodynamic response is the complete opposite as that observed in the previous section (Figure 2.11) for the Bernoulli and backwater effect. The sediment wave described earlier is now preceded by a “degradational” wave.

2.2.5. Sorting waves

Additional to the adjustment waves related to bed level changes described earlier, when we study a case with mixed size sediment we also have the adjustment waves related to the changes in the grain size distribution of the bed surface. These waves are referred to as sorting waves, as described earlier (Figure 2.1).

First we consider the sorting waves in response of the temporal coarsening of the bed surface. Over the nourished reach, sediment mobility of the finer fraction is reduced, while the transport of the coarser fraction remains unchanged from the initial situation. The equilibrium surface texture also remains unchanged after the nourishments. This is depicted in Figure 2.16.

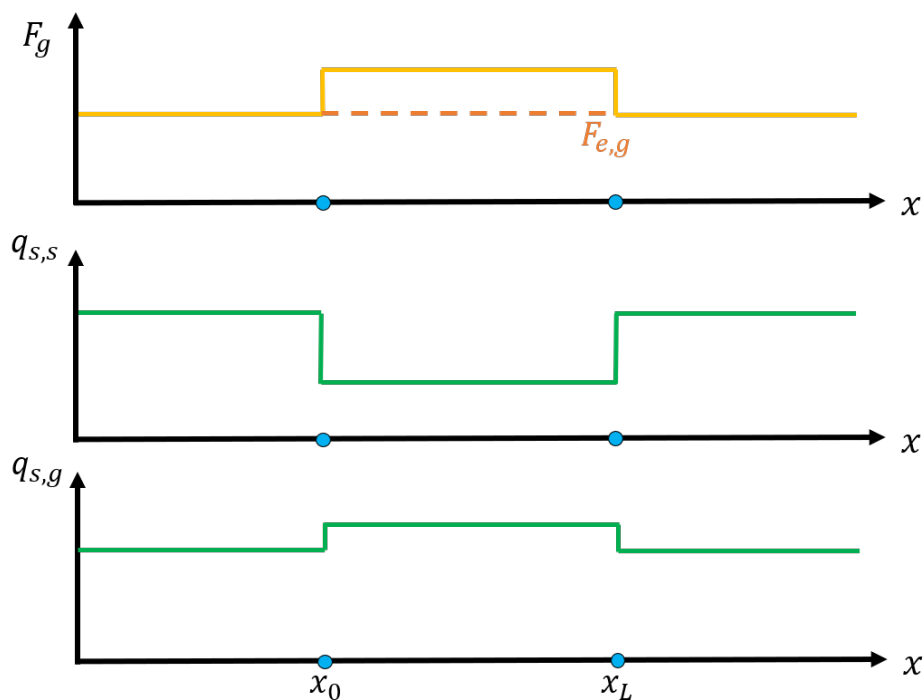


Figure 2.16: At the top, surface content of the coarser fraction (F_g) with respect to the equilibrium surface texture ($F_{e,g}$). At the bottom sediment transport gradients for the finer fraction ($q_{s,s}$) and the coarser fraction ($q_{s,g}$).

The resulting sorting waves in the system can be deduced from the difference in sediment transport for each of the fractions. Over the nourished reach, the surface texture tends to get finer due to reduced mobility of the finer fractions. Downstream of it, the surface tends to get coarser due to the reduced supply of the finer fraction from upstream. This is schematised in Figure 2.17.

The sorting waves depicted in Figure 2.17 can be explained with the following physical reasoning. In gravel-bed rivers with a mixed-size grain size distribution the bed load tends to be significantly finer than the bed surface, this is due to the river adjusting its bed slope and surface composition in order to be able to transport the coarser sediment fractions, which generally leads to the formation of an armour surface layer. It is then the finer sediment bed load that is transported to the coarsened reach, where it starts accumulating as a downstream-migrating aggradational wave due to the reduced sediment mobility over this reach, causing a fining of the bed surface with respect to the initial situation with coarse nourishments. Additionally, this causes the supply of the finer sediment bed load to the reach

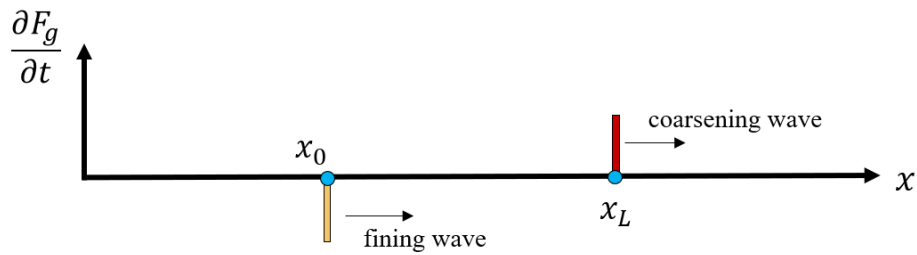


Figure 2.17: Sorting waves resulting from an increase in grain size.

downstream of the nourishment to be reduced, which is met with a downstream-migrating coarsening of the bed surface.

We now analyse the changes in surface texture in response to the spatial gradients in flow velocity caused by the Bernoulli and backwater effects. We assume that due to the non-linear relation between flow velocity and sediment transport, a change in flow velocity causes a steeper gradient in the sediment transport of the finer fraction than of the coarser fraction. The resulting transport gradients considering the flow velocities drawn for the backwater effect in Figure 2.10 are presented in Figure 2.18.

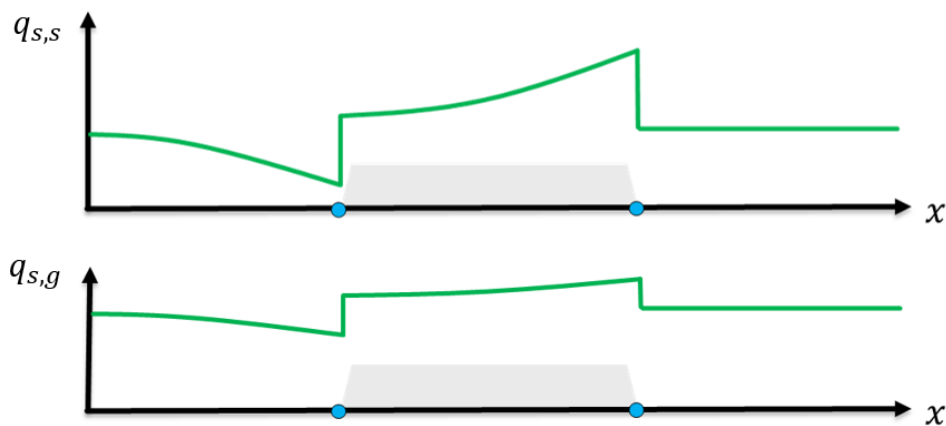


Figure 2.18: Sediment transport gradients corresponding to the backwater effect for each grain size fraction.

We determine the resulting sorting waves by comparing the gradients in sediment transport per fraction. In the upstream reach, flow velocities are reduced due to the M1 backwater curve, which leads to a fining of the bed surface. This reduces the supply of the finer sediment to the nourished reach, leading to a coarsening wave. Over the nourished reach flow velocity increases due to the M2 backwater curve, causing a coarsening of the bed surface. The transport of the finer fraction is now larger than that of the coarser fraction at the downstream end (x_L), which leads to a fining wave. This is schematised in Figure 2.19.

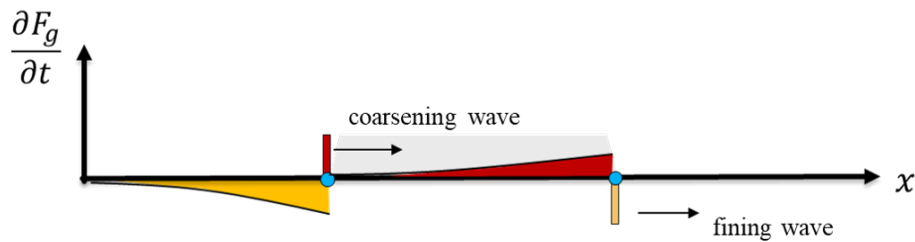


Figure 2.19: Changes in grain size and sorting waves resulting from the gradients in flow velocity due to the backwater effect.

2.2.6. Dominant response

Throughout this section we have described the different adjustment waves that are present in a river system after a nourishment supply. We distinguish between the morphodynamic responses corresponding to the Bernoulli effect, the backwater effect, the increase in friction, and the increase in surface grain size for the case with mixed-size sediment. In reality, the morphodynamic response of the system is a combination of all of these effects. We also distinguish between the two types of adjustment waves, bed waves which originate due to changes in bed level, and sorting waves which form due to changes in surface grain size.

To distinguish the adjustment waves that are observed in a river system after a nourishment we first analyse a case with unisize sediment. Since there are no changes in grain size, only bed waves (and not sorting waves) are observed in the system. These correspond to the schematics shown in Figures 2.8 and 2.11. With an incision wave originating at the upstream end of the nourished reach (x_0) and a sedimentation front at the downstream end (x_L).

In a mixed-size sediment system, the combined morphodynamic response will depend on which of the effects is more dominant over the other. We first consider the morphodynamic response corresponding to the Bernoulli and backwater effect (Figure 2.11) to be dominant. This is the case when the increase in flow velocity caused by the Bernoulli effect is enough to prevent a deficiency in sediment supply on the reach downstream of the nourishment. De Way (2014) shows that this happens for low discharges, or in cases where the increase in bed level caused by the nourishment is large with respect to flow depth, such that the Froude number approaches its critical value. For this scenario, the bed waves again correspond to that of Figures 2.8 and 2.11, and the sorting waves to that of Figure 2.19, with a coarsening wave at x_0 and a fining wave at x_L .

Generally, the volume of nourished sediment is estimated such that the increase in bed level does not create problems for navigation, as a minimum flow depth needs to be maintained even during low discharges. This means that the increase in grain size caused by nourishment tends to be the dominant effect dictating the initial morphodynamic response of the system. In this response we observe the bed waves depicted in Figure 2.15, with a sedimentation front at the upstream end of the nourished reach (x_0) and a incisional wave at the downstream end (x_L), as well as the sorting waves depicted in Figure 2.17, with a fining wave originating at x_0 and a coarsening wave at x_L .

The model

When sediment nourishments are supplied over a river reach, they induce direct changes to bed elevation, as well as to bed surface texture depending on the grain size of the nourished sediment. These changes propagate through the system as adjustment waves. The aim of this study is to analyse the dependence of the evolution of these adjustment waves on the way the sediments are supplied, on the grain size of the nourished sediment, and on the bed surface texture.

3.1. Simplifications and assumptions

In engineered rivers with a fixed planform, the river tends to evolve towards an equilibrium state by adjusting its bed slope and bed surface texture. Due to the large difference in time scales at which the flow rate varies and the channel slope changes, there is generally insufficient time for the latter to adjust to the short-term variations of the flow. This means that while variability of the flow rate is essential to analyse changes induced by extreme events, such as floodplain mechanisms, meander cutoffs and movement of huge boulders, these high discharge events are less important when one is interested in modelling long-term morphodynamic change (Blom et al. 2017b).

For simplicity, we assume that pressure is hydrostatic along the water column, which means that the water surface elevation equals the piezometric head, and that the 1D St Venant equations for depth-averaged flow are valid. We also consider the flow in the river system to be steady and characterised by a representative water discharge, which means that the spatial change in water depth can be described by the backwater equation (3.1).

$$\frac{\partial d}{\partial x} = \frac{i_b - i_w}{1 - Fr^2} \quad (3.1)$$

where the term on the left-hand side represents the spatial gradient in flow depth, and on the right-hand side i_b is the river bed slope, i_w the friction slope or energy head loss per unit of space, and Fr the Froude number.

The model is set up with the following simplifications and assumptions:

1. We assume a rectangular cross-section, and do not distinguish between flow through the main channel and the floodplains.
2. The main channel width is considered constant along the analysed reach and fixed. The width is so large that the hydraulic radius can be assumed to be equal to the flow depth.
3. The model neglects subsidence and uplift, as well as sea level rise and delta outbuilding, since the temporal scale of these changes is considerably larger than the one considered in this study.
4. We only consider bed material load (both bed load and the component of suspended load that is bed material load).
5. The non-dimensional friction coefficient (c_f) is assumed constant, and independent of the flow parameters and surface texture.
6. We assume a constant value of the porosity of the bed sediment.

3.2. The model

We use the one-dimensional research code Elv to make the model runs, which solves for the flow, bed elevation, and bed surface texture in a decoupled manner. The model provides a numerical solution to the backwater equation (Eq. 3.1) in a space-marching manner, from the downstream end in the upstream direction with the assumption that the flow is subcritical ($Fr < 1$), using a first-order explicit Euler scheme. Bed elevation and surface texture are solved using the *Hirano* (1971) equation for sediment continuity in mixed-sized sediment systems, and are updated after each time step. For further details we refer to Blom et al. (2017b).

Numerical settings consist a streamwise grid size of $\Delta x = 50$ m, and a time step $\Delta t = 0.5$ days, such that the stability of the numerical model is ensured by satisfying the Courant-Friedrich-Levy (CFL) condition. The total domain length is set to 200 km. The choice for the grid size was made small enough such that convergence of the model results was found. This means that we ensure that the choice for the time and spatial steps does not influence the results of the model. In Appendix A we present the model results for different time and spatial steps, we show that for smaller values of these steps the variations in the results become less significant until we find convergence in the solution.

3.3. Base case

For the input parameters of the base case we draw inspiration from the river geometry of the downstream end of the Niederrhein, and the Bovenrijn. We assume a main channel width of 300 m, a value of the porosity of bed sediment of 0.4, and take a dimensionless friction coefficient of 0.007 which is reasonable for this river reach according to previous calibrated models (Paarlberg et al. 2007) and (Arkesteyn et al. 2019). Studies on the Hirano active layer model suggest that the active layer thickness is usually related to either a characteristic grain size of the bed surface or to the dimension of the bedforms in the system (Chavarrías et al. 2019). Studies on the geometry of bedforms show that in the river Waal the height of the bedforms reach up to 1 m (Van der Mark et al. 2008), we assume this value to remain constant in the model. These input parameters are summarised in Table 3.1.

To select the characteristic grain sizes, we assume the river sediment to be bi-modal as is typical for gravel-bed streams (Blom et al. 2017b). For the finer sand fraction, grain sizes range from 0.063 mm to 2 mm, for which we find a median value on the phi-scale of $D_s = 0.5$ mm. Similarly, for the coarser gravel fraction, the grain sizes range from 2 mm to 128 mm, for which a value of $D_g = 16$ mm is found.

Parameters	Values	Units
Channel width (B)	300	[m]
Friction coefficient (c_f)	0.007	[-]
Porosity (p)	0.4	[-]
Active layer thickness (L_a)	1	[m]
Sand grain size (D_s)	0.5	[mm]
Gravel grain size (D_g)	16	[mm]

Table 3.1: Specifications of the base case.

3.3.1. Boundary conditions

For lowland rivers with a mild bed slope, the water flow can be assumed to be subcritical (with $Fr \ll 1$), and thus three boundary conditions are required to obtain a unique solution of the system; two hydrodynamic boundary conditions, one upstream and the other downstream, and one morphodynamic boundary condition upstream.

The upstream hydrodynamic boundary condition is the representative water discharge, as explained previously, this will be assumed steady and thus constant over time. The mean discharge measured during the 1991-2010 period at Rees (Rhine-km 837) equals $2311 \text{ m}^3/\text{s}$ (Frings et al. 2014b). However, due to the non-linear relation between the water discharge and sediment transport, the representative

discharge tends to be larger than the mean value (Blom et al. 2017b). For simplicity we assume a value of $2500 \text{ m}^3/\text{s}$. Additionally, to avoid backwater effects at the downstream boundary, we consider normal flow as the boundary condition at this end.

Short-term temporal variations of the mean sediment supply from upstream lead to a discrepancy between the instantaneous sediment transport capacity and the instantaneous sediment supply rate. This leads to persistent downstream-migrating adjustment waves of bed elevation and surface texture. This is commonly referred to as a hydrograph boundary layer (Arkesteijn et al. 2019). We avoid this not only by assuming a steady water discharge as mentioned previously, but also by imposing a constant sediment supply on the upstream boundary.

For this morphodynamic boundary condition upstream, the estimated bed load transport rates are taken from the data found in the sediment budget analysis done by Frings et al. (2014) which covered the period from 1991 to 2010. Even though there is a known uncertainty of these values (of around 200%), they are representative of the river system up to their order of magnitude. More importantly, the calculated sediment fluxes per fraction are known, and already account for the input from artificial sediment nourishments, as well as from the major tributaries in the upstream reaches. These values are presented in Table 3.2.

Parameters	Values	Units
Water discharge (Q_w)	2500	[m ³ /s]
Gravel transport ($D_g = 16 \text{ mm}$)	0.56	[Mt/a]
Sand transport ($D_s = 0.5 \text{ mm}$)	0.11	[Mt/a]
Total bed load transport (Q_s)	0.67	[Mt/a]

Table 3.2: Upstream boundary conditions.

3.3.2. Initial conditions

Using the above parameters and boundary conditions, a solution for the equilibrium bed slope and bed surface texture can be found. To do this, we choose the Ashida and Michiue [1972] transport relation (3.2), which has a threshold below which transport is negligible and allows us to account for hiding effects.

$$q_{sk}^* = a(\theta_k - \theta_{ck})(\sqrt{\theta_k} - \sqrt{\theta_{ck}}) \quad (3.2)$$

where q_{sk}^* is the dimensionless sediment transport per fraction k . The coefficient a is assumed equal to 17, and θ_{ck} equal to 0.05 multiplied by a hiding factor (ξ_k) that depends on grain size, represented by equations 3.3 and 3.4. In which, D_m is the geometric mean grain diameter of the bed material.

$$\text{For } \frac{D_k}{D_m} < 0.4, \quad \xi_k = 0.85 \frac{D_m}{D_k} \quad (3.3)$$

$$\text{For } \frac{D_k}{D_m} \geq 0.4, \quad \xi_k = \left[\frac{\log_{10}(19)}{\log_{10}\left(\frac{19D_k}{D_m}\right)} \right]^2 \quad (3.4)$$

Finally, θ_k is the Shields parameter, for which the only remaining unknown variable is the flow velocity, which directly on the bed slope.

Considering two different sizes of sediment (gravel and sand), the resulting transport relation for each fraction gives a system of two equations with two unknown variables, the equilibrium bed slope and bed surface gravel content, for which an analytical solution can be found iteratively (Blom et al. 2017b). The resulting values for the given parameters are presented in Table 3.3.

Parameters	Values	Units
Equilibrium bed slope (i_{be})	1.31e-04	[-]
Surface gravel content (F_g)	78	[%]
Surface sand content (F_s)	22	[%]

Table 3.3: Initial conditions.

3.4. Model runs

In this section we describe the objective of each of the model runs and its specifications, a summary of which is presented in Table 3.4. We set an initial base run with gravel nourishments, with a sediment composition of 100% gravel ($D_g = 16mm$). These are located 50 km downstream of the upstream end and are distributed over 20 km, far enough downstream so that effects on bed level upstream of the nourishments can be observed, and sufficiently upstream that they can propagate along the domain (total 200 km).

3.4.1. Model runs A: Distribution of the nourishments

The objective of this set of model runs is to gain insight on the evolution of the adjustment waves induced by the gravel nourishments, and better understand the physical processes that drive them. We do so by comparing the changes in the propagation celerities of the waves for different schematisations of the nourishments.

The total volume of the nourishments is set at 3 Mt for all model runs, a number that roughly resembles the total volume of the bed stabilisation nourishments carried out in the lower end of the Niederrhein during the 1991-2010 period (Figure 1.3). For simplicity, the total volume of nourishments is supplied uniformly and all at once. For each of the runs we vary the length over which the nourishments are distributed, and keep the same starting upstream location.

This set of model runs allows us to study the changes to the propagation celerity of the adjustment waves caused by the variation in length and consequently also height of the nourished gravel, providing an answer to research question (2) of this study.

3.4.2. Model runs B: Grain size of the nourishments

For this set of model runs we vary the grain size composition of the artificial nourishments. The aim of this set of model runs is to better understand the impact of the grain size composition of the nourishments not only on the dispersion of the nourished sediment, but also on the propagation celerity of the adjustment waves. With these results we provide an answer to research question (3) of this study.

Initially, we set the nourishments in the model to be composed entirely of coarse gravel ($D_g = 16$ mm), for this set of model runs we increase the content of the sand fraction ($D_s = 0.5$ mm) in the nourishments in each run as specified in Table 3.4.

The values for the sand fraction content in the nourishments are selected such that for the first 3 sets of model runs the nourished sediment remains coarser than the bed surface. In the final model run the nourished sediment has a finer grain size composition than the bed surface, which allows us to assess how this changes the system response, as well as the propagation celerity of the adjustment waves.

Set	Control variable	Run 1	Run 2	Run 3	Run 4
A	Distribution length (ΔL)	10 km	15 km	20 km	40 km
B	Sand fraction content in nourishments ($F_{N,S}$)	0	6.25%	12.5%	25%

Table 3.4: Specifications of the model runs.

Propagation of the adjustment waves

This chapter is divided in two sections: in the first section we present the results for a numerical simulation assuming unisize sediment, with the aim to better understand the propagation of the adjustment waves when they are not influenced by an increase in grain size. This means that the observed morphodynamic response is that of Figure 2.11. In this section we also present in more detail the methodology followed to analyse the evolution of the sediment wave induced by the nourishment.

In the second section we present the results for a numerical simulation with mixed size sediment, with the choice of parameters described in Section 3.3 with a nourishment composed fully of the coarse gravel fraction. Similarly to how it was done for the case study with nourishments in unisize sediment, we study the combined morphodynamic response of the river system, and determine the dominant physical mechanisms that drive the propagation of the the corresponding adjustment waves.

4.1. Unisize sediment case study

We show how the propagation of the adjustments waves described in Section 2.2 for a unisize case (Figure 2.8 can be studied with the numerical research code Elv. We use the model results to analyse the propagation of the associated sediment wave, and determine the changes in its celerity over time.

For this model run we make the same assumptions described in Section 3.1. For numerical settings, we choose a spatial step of 100 m, a time step of 1 day to comply with the CFL condition, and a total domain length of 150 km. The rest of the parameters remain the same as for the ones described for the base case in Section 3.3, with the only change being that we assume a single characteristic grain size of 2 mm, and solve for the corresponding equilibrium bed slope of the system ($i_{be} = 5.5e-05$) so that it starts from an equilibrium state.

A total volume of 1 Mt of sediment nourishments are supplied uniformly over a 20 km river reach, a single supply of the nourished sediment is carried out at the beginning of the simulation, which means that the entire volume is supplied all at once.

We analyse the morphodynamic and hydrodynamic response of the system in Figures 4.1 and 4.2 respectively. In these figures we present 3 instances in time of bed level and flow velocity, at the beginning of the simulation ($t = 0$), 10, and 50 years afterwards.

As seen in Figure 4.2, the flow velocity pattern along the domain matches with the one depicted in Figure 2.10 for the backwater effect. Additionally, a clear increase in flow velocities is observed over the nourished reach, as expected due to the Bernoulli effect. We also observe that these flow velocities decrease the longer the nourishment wave decays in the system.

We study the propagation of the centre of mass or “centroid” of the sediment wave. The centroid is estimated as the median of the distribution of cumulative bed elevation difference, as shown in Figure 4.3. To calculate the centroid of the sediment wave, we estimate the change in bed elevation (Δz) caused directly by the nourishment at each given spatial step (Δx), and calculate the change in volume bed elevation per unit width (ΔV) for each step. We add the total change in volume V_T and estimate

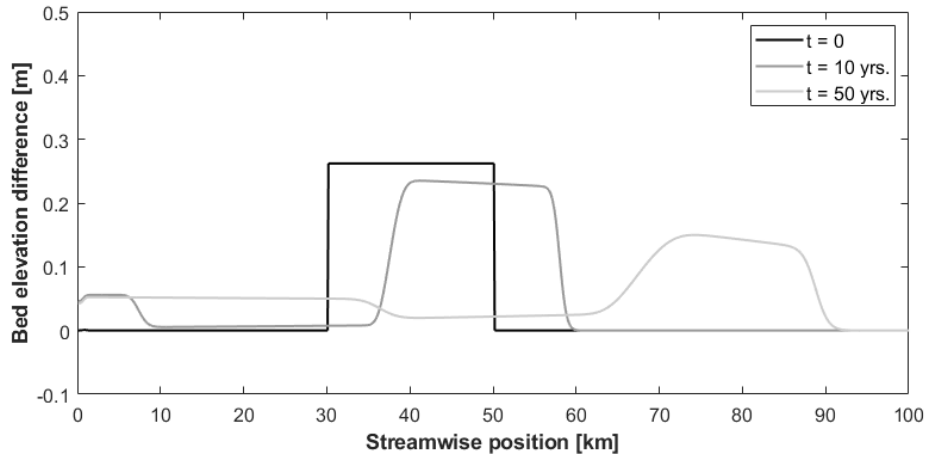


Figure 4.1: Bed elevation difference [m] with respect to initial bed level at times $t = 0, 10,$ and 50 years. Flow direction from left to right.

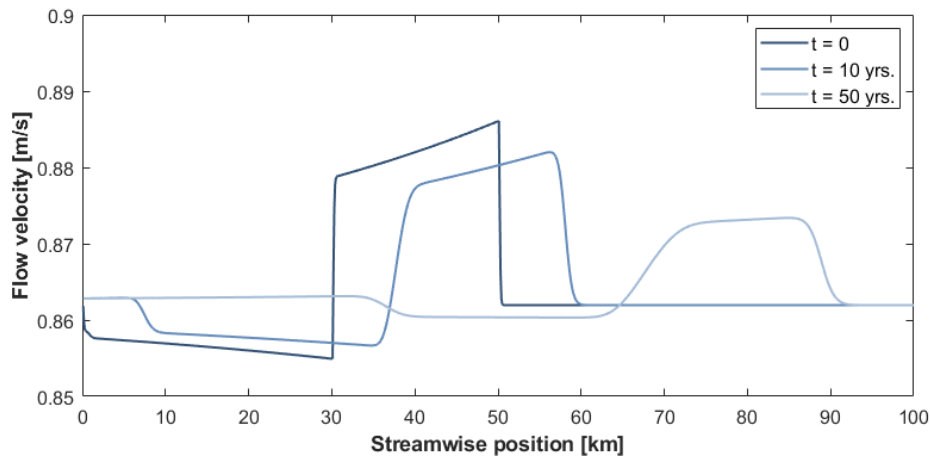


Figure 4.2: Flow velocity [m/s] at times $t = 0, 10,$ and 50 years. Flow direction from left to right.

with it the rate of increase in volume per spatial step. We determine the centroid of the sediment wave (x_c), by calculating the point before and after which 50% of the increase in sediment volume has accumulated. The centroid of the wave is thus the median of the cumulative elevation difference. Similarly, the front (x_{95}) and tail (x_{05}) of the sediment wave are estimated as the 95th and 5th percentiles of the cumulative elevation difference, respectively.

By estimating the location of both the wave front and wave tail, we are able to assess whether the evolution of the sediment wave is predominantly translational or dispersive. A comparison between the two behaviours can be made by studying the lengthening of the wave with respect to the displacement of the wave centroid, as presented in Figure 4.4. The wavelength (l) is simply calculated as the distance between the wave front and the wave tail.

In Figure 4.4 we explain the difference between a purely translational and a purely dispersive wave evolution. For a purely translational wave, the centroid would propagate downstream without lengthening of the wave, showing a completely horizontal line in the plot. For a purely dispersive wave, the line would be vertical, as the wave lengthens without displacement of the centroid.

If we make a critical observation of the changes in bed elevation difference presented in Figure 4.1, we can already deduce that the evolution of the sediment wave in this model run is predominantly trans-

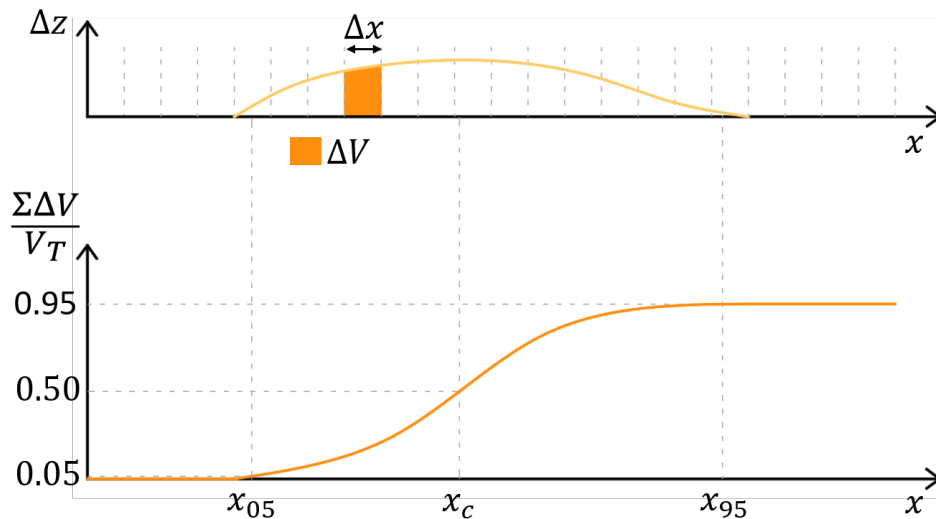


Figure 4.3: Estimation of the sediment wave tail (x_{05}), centroid (x_c), and front (x_{95}).

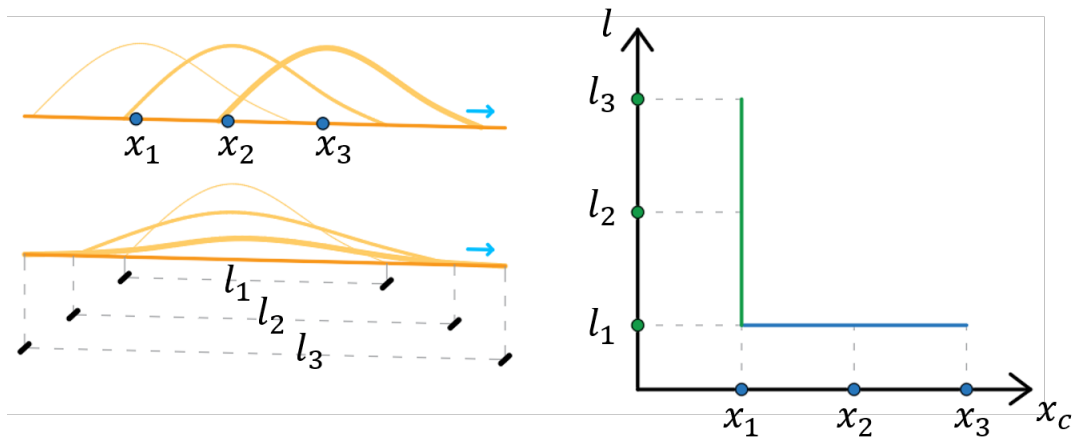


Figure 4.4: On the left, the evolution of a purely translational sediment wave (top) and a purely dispersive sediment wave (bottom). On the right, the comparison between the location of the wave centroid (x_c) and the wavelength (l), for a purely translational wave (blue) and a purely dispersive wave (green).

lational, even after 50 years the wave retains most of its properties and its is clearly distinguishable in the system. We study this in more detail in Figure 4.5 where we plot the displacement of the sediment wave centroid with respect to its initial position over time against the wavelength.

The results of this model run show a predominantly translational behaviour of the sediment wave, made evident by the ratio between the displacement of the wave centroid and the wavelength. In Figure 4.5 we observe that the wave centroid travels downstream a distance of over 60 km, and lengthens less than 2 km.

We use the results from the numerical simulation to estimate the propagation celerity of the sediment wave centroid. In Figure 4.6 we compare the numerical values of the celerities to the analytical values of the celerities of small amplitude bed waves obtained with Equation 2.2, as described in the Section 2.1.1.

The results show that the propagation of the sediment wave slightly slows down over time. This can be related to the decrease in flow velocity as the wave diffuses and lengthens over time. However, the decay in wave celerity is so slight for both numerical and analytical calculations that an average value of 0.75 km/yr and 0.47 km/yr can be approximated.

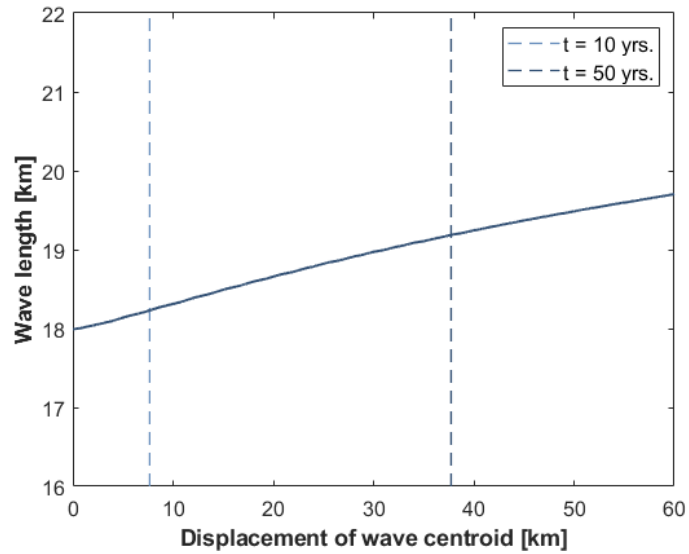


Figure 4.5: Displacement of the centroid of the sediment wave with respect to its initial position in the streamwise direction, the dashed lines indicate the location of the centroid at times $t = 10$ and 50 years.

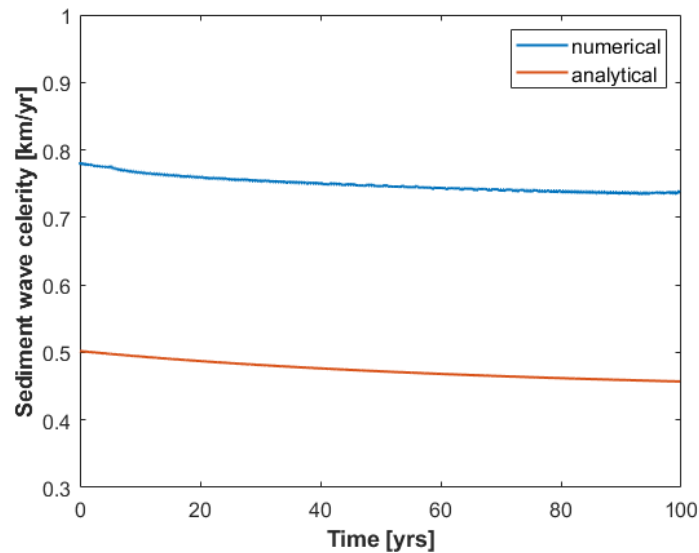


Figure 4.6: Celerity of the sediment wave centroid estimated with the results for the numerical simulation (blue) and with the analytical solution (orange).

Although the celerities obtained with the numerical simulation are of a different order of magnitude than the analytical ones, the equations for the latter have been derived for waves of a significantly smaller amplitude. Nevertheless, they do provide valuable insight on how the wave tends to gradually slow down over time as it decays and lengthens.

4.2. Mixed-size sediment case study

In this section we analyse the results for the numerical simulations of the model set up with the specifications for the base case described in Section 3.3. To this base case we add a volume of 3 Mt of coarse gravel sediment, distributed over a 20 km reach of a river system initially at equilibrium. The sediment is supplied uniformly over the 20 km reach and all at once. We use the same method described in Section 4.1 to study the propagation of the adjustments waves through the system.

We aim to identify the main differences in the morphodynamic response of the river system with respect to the unisize case, and identify how these differences impact not only the evolution of the sediment wave, but also the changes in celerity of the adjustment waves.

4.2.1. Morphodynamic response

We first present the results for bed elevation difference at different times in the model run in Figure 4.7a, and the changes in surface grain size in Figure 4.7b. We observe that the changes in bed level and surface grain size observed in these figures correspond to the morphodynamic response presented in Figure 2.15, which means that with the given initial conditions, the increase in surface grain size is the dominant effect dictating the morphodynamic response of the system.

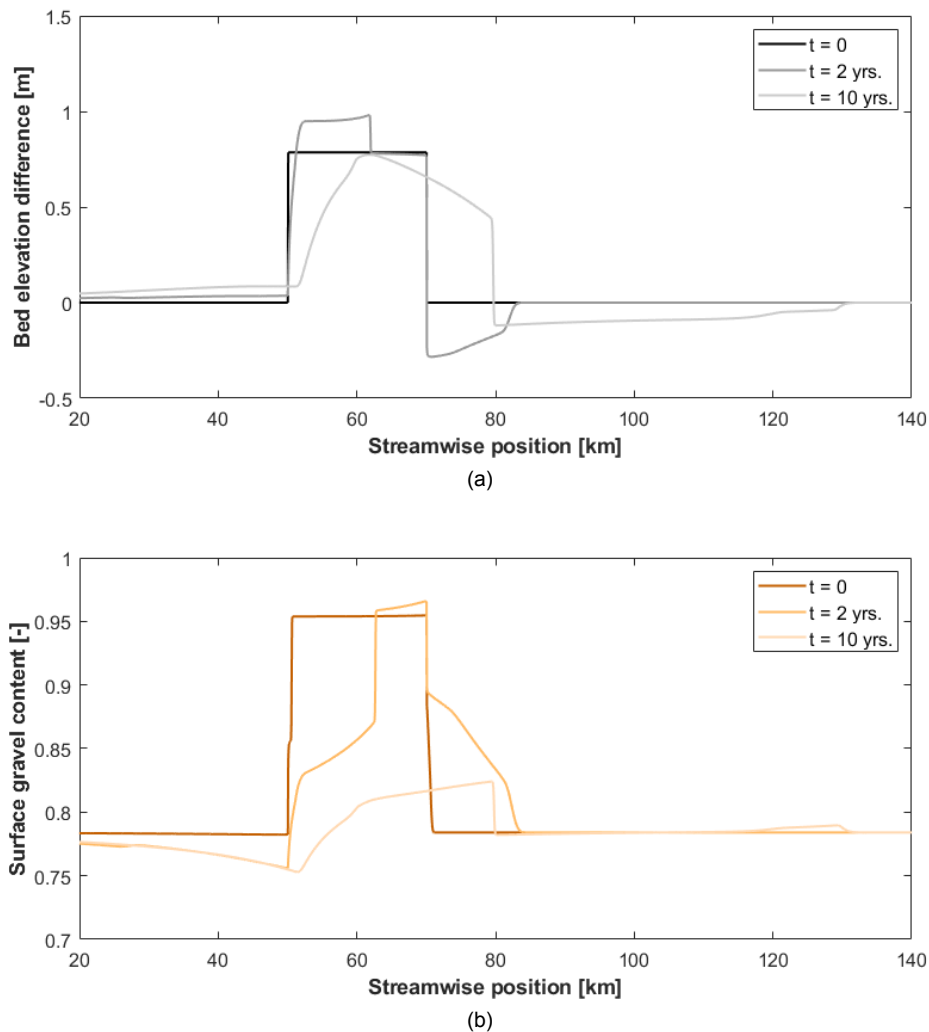


Figure 4.7: Base case results for times $t = 0, 2,$ and 10 years. At the top (a) bed elevation difference [m] with respect to initial bed level. At the bottom (b) Bed surface gravel content [-]. Flow direction from left to right.

We identify two bed waves in the system response, a hump which increases bed level on top of the sediment wave, starting from its upstream end (km-50), and a degradational wave on the downstream end of the sediment wave (km-70). We also identify two sorting waves, a fining wave which decreases surface gravel content at the upstream end (km-50), and a coarsening wave at the downstream end (km-70).

In Figure 4.7a we can already observe that at $t = 10$ years, the degradational wave has propagated significantly farther downstream than the sediment wave. This means that if the purpose of the sediment nourishments is to counteract bed degradation along the river system, one must consider the negative impact not only immediately downstream of the nourished reach, but actually much further downstream as well.

The migration of the adjustment waves causes changes in flow velocity, sediment transport. The model results for these parameters are presented in Figure 4.8. The changes in flow velocity can be understood by studying the Bernoulli and backwater effect, as explained in detail in Section 2.2. These changes in flow velocity over time are presented in Figure 4.8a. Here we see that the increase in bed level over the nourished reach causes a significant increase in flow velocities, and that the corresponding backwater curves to this changes in bed level lead to a negative gradient in flow velocity over the upstream reach, and a positive gradient over the nourished reach.

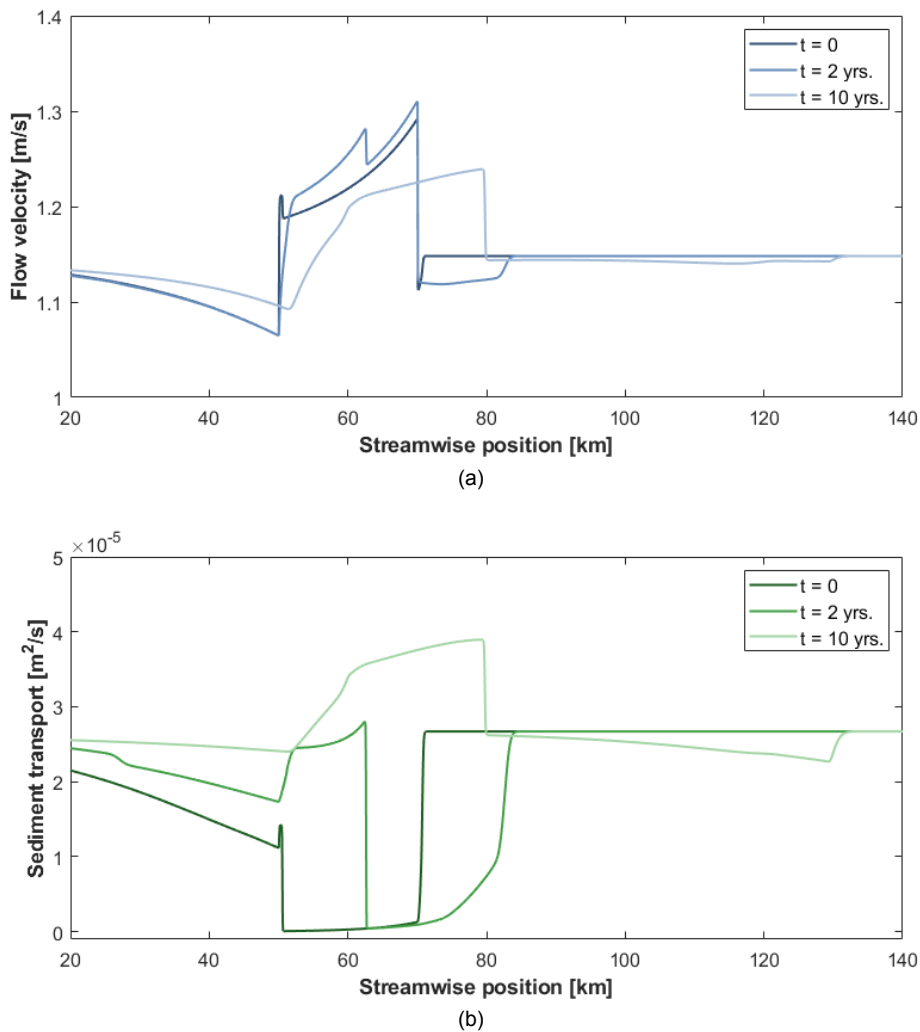


Figure 4.8: Base case results for times $t = 0, 2,$ and 10 years. At the top (a) Flow velocities [m/s] along the domain. At the bottom (b) Total sediment transport rates per unit width [m^2/s] along the domain. Flow direction from left to right.

Due to the non-linear relation between flow velocity and sediment transport, one would normally expect the gradients in sediment transport to follow a similar pattern as the flow velocity, but with more exaggerated gradients. In Figure 4.8b, where we present the sediment transport rates for both sediment fractions over the domain at different times, we see that this is not the case over the nourished reach due to the increase in grain size, which significantly reduces sediment mobility.

Initially, the sediment transport rate over the nourished reach becomes lower than the transport upstream and downstream, despite the increase in flow velocity over this reach. This is characteristic of a morphodynamic response corresponding to an increase in surface grain size.

Over time, as we can observe for the results at $t = 10$ years, the sediment transport rates along the nourished reach have significantly increased, and now correspond to the flow velocity gradients observed in Figure 4.8a. This means at this time period, due to the adjustments in bed surface grain size along the domain, the dominant physical effect driving the morphodynamic response of the system is the backwater effect.

We can see in Figures 4.7a and 4.7b that as the fining wave propagates through the domain, sediment transport rates significantly increase due to the improved sediment mobility. The opposite happens for the coarsening wave downstream of the nourishments. These two sorting waves propagate at different rates, with the fining wave being faster than the coarsening wave. This means that the fining wave eventually catches up with the latter, and the gradients in surface grain size along the domain become significantly milder.

As seen for $t = 10$ years in Figure 4.7b, even though the spatial gradients in surface grain size are milder than at the initial situation, they still indicate changes along the domain with respect to the equilibrium situation (no gradients). The gradients now correspond to those shown in Figure 2.19 for the backwater effect. Over the upstream reach, flow velocities are lower and surface becomes finer. Over the nourished reach, flow velocities are higher and surface texture coarsens.

4.2.2. Propagation of the sediment wave

We first study the dispersion of the sediment wave by comparing the lengthening of the wave with respect to the displacement of the wave centroid, this is presented in Figure 4.9. The wave centroid (x_c), tail (x_{05}) and front (x_{95}) are calculated with the percentiles of the cumulative elevation difference, similarly to how it was done for the unisize case following the method described in Figure 4.3.

The results in Figure 4.9 show that initially, the wave tends to shorten instead of lengthen, which is due to the wave tail propagating faster than the wave front. The main reason behind this initial behaviour of the wave is that the adjustments in surface grain size first occur at the wave tail (see Figure 4.7b), where reduced sediment mobility favours sediment deposition from upstream, such that during the initial period after the nourishment, the sediment at the wave front tends to be coarser and hence less mobile.

Afterwards, once the celerity of the sediment wave front increases and the wave begins to lengthen, it has a combined dispersive-translational behaviour, and as the wave decays its behaviour becomes increasingly translational, which coincides with the observations made by Lisle et al. (2001) on the behaviour of sediment waves.

Even though the cases studied are different, a comparison can still be made between the behaviour of the sediment waves for the unisize and the mixed-size sediment cases. The main difference is found in the initial behaviour of the sediment wave for the mixed-size case, where due to the differences in sediment mobility between the wave tail and the wave front, the wave appears to shorten. This highlights the importance of the adjustments in surface grain size in the propagation of the waves.

From Figure 4.9 it is clear that the celerity of the sediment wave is not the same at every location of the wave (centroid, front and tail). Therefore, we study how the propagation celerity of the waves at its front, tail, and centroid varies over time. These results are presented in Figure 4.10. The celerities

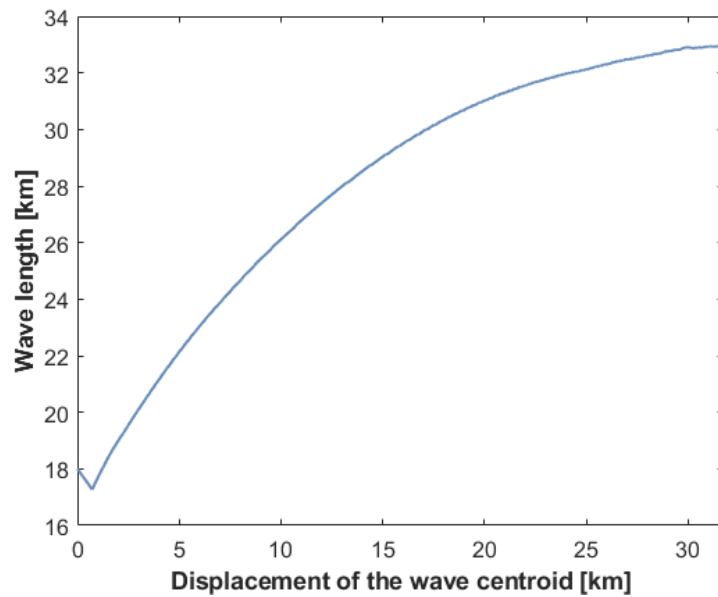


Figure 4.9: Dispersion of the nourishment wave with respect to its centroid.

are calculated based on the location of the wave at every time step, and because this location is found for discrete grid sizes, the computed celerity oscillates or wiggles around its true values, which are approximated by taking the 1-year moving average of the estimated celerity at each time step, a more detailed explanation on these wiggles is given in Appendix B.

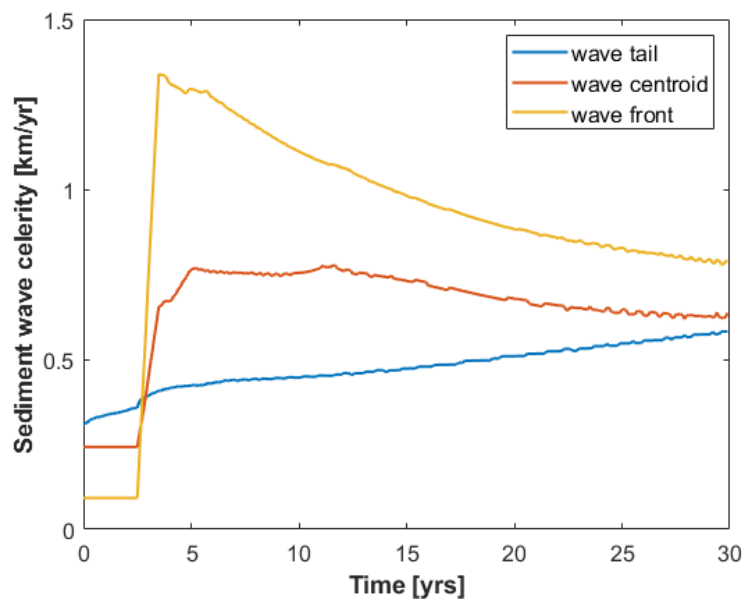


Figure 4.10: 1-year moving average value of the celerity [km/yr] of the sediment wave tail (blue), centroid (red), and front (yellow).

We can clearly distinguish in Figure 4.10 a behavioural change between two time periods: during the first three years the sediment wave tail propagates faster, as the fining wave migrates along the nourished reach. Afterwards, once sediment mobility has been increased due to the adjustment in grain size of the bed surface, it is the sediment wave front that propagates at a significantly faster rate.

The celerity of the sediment wave tail gradually increases as the behaviour of the wave tends to be more predominantly translational (see Figure 4.9). For both the sediment wave front and centroid an abrupt increase in celerity is found due to the adjustments in surface grain size over the nourished reach. Over time, as the sediment wave decays and lengthens, and the sediment transport gradients level, the celerity of the wave centroid and front gradually decreases.

In Figure 4.11 we compute the analytical celerity using Equation 2.2 for the propagation celerity of small amplitude bed waves. We compare the results for the analytical celerity to the results obtained from the numerical model for the sediment wave centroid.

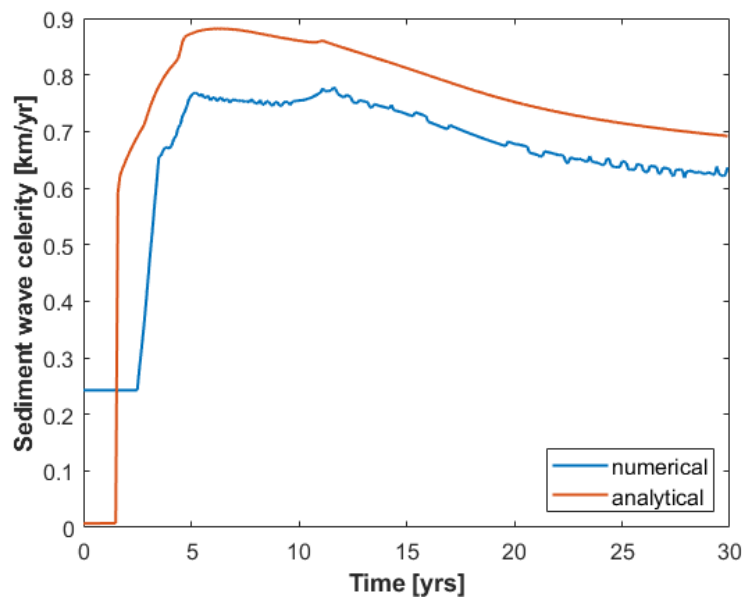


Figure 4.11: Celerity of the sediment wave centroid estimated with the results for the numerical simulation (blue) and with the analytical solution (orange)

The results in Figure 4.11 show that the values obtained analytically provide a reasonable estimate for the celerity of the sediment wave, even though it is derived for small amplitude bed waves. More importantly, we observe that the change in celerity over time follows a very similar decreasing pattern for both estimates, and that this pattern is also observed for sediment transport rates over time, which indicates the dependency of the propagation of the sediment wave to sediment transport.

Therefore, the changes found for the sediment wave celerity over time are a clear indication that for a mixed-size sediment case, there are two main effects that control the propagation celerity of the wave: 1) the spatial gradients in flow velocity, which are a function of the height of the sediment wave and the flow depth due to the Bernoulli and backwater effects, respectively and 2) the spatial gradients in grain size, which directly influence sediment mobility along the nourished reach.

4.2.3. Propagation of the degradational wave

For the propagation of the degradational wave we are mainly interested in two aspects of the wave: 1) first we analyse how far downstream the degradational wave propagates with respect to the nourishment wave, 2) then we study the changes in the celerity of the degradational over time, with the aim to gain a better understanding on the parameters it depends on.

We estimate the location of the degradational wave front from the model results using the same logic as for the sediment wave. The only difference is that now the values for the cumulative elevation difference are negative. We determine the upstream boundary of the degradational wave, that is the point after which we start adding the negative volumes, as the first point downstream of the sediment wave

front where the bed elevation difference is zero. If we look back at the results for bed level change in Figure 4.7a, this upstream boundary would be located at $x = 70$ for $t = 0$, and at $x = 80$ for $t = 10$ yrs. The degradational wave front is then the 95th percentile of this cumulative elevation difference. The wave tail and centroid are then estimated as the 5th percentile and the median, respectively.

We analyse the propagation of each part of the degradational wave (front, tail, and centroid) as done for the sediment wave. The results for the degradational wave are presented in Figure 4.12. Even though the displacement of the wave tail initially indicates a small translation of the degradational wave, the wave front clearly propagates much further away during this time, which highlights the dominantly dispersive behaviour of this wave. Afterwards, we can see that the degradational wave front moves steadily away from the wave centroid, which means that while bed degradation can be seen to be affecting a larger reach of the river over time, the majority of it remains near the wave tail.

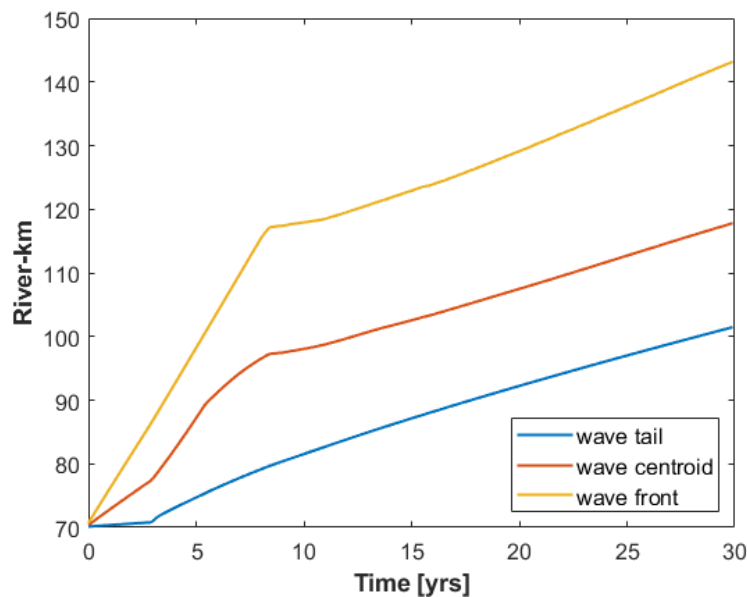


Figure 4.12: Streamwise location of the degradational wave tail (blue), centroid (red) and front (yellow) over time [yrs].

The propagation of the degradational wave is affected by the adjustments in surface grain size, but at different times. This is observed in Figure 4.13, where we present the propagation over time of the degradational wave front, together with the fining wave front and the sediment wave front.

In Figure 4.13 we see that the fining wave, which reduces the gradients in surface grain size along the domain, significantly changes the way in which both the sediment and the degradational wave propagate. In particular, the sediment wave accelerates and the degradational wave decelerates, and as we see in this figure, this happens at different times for each of the waves, which means that the degradational wave manages to propagate far away from the sediment wave, before it is abruptly slowed down.

The front of the degradational wave propagates in a different way than the centroid and the tail. In Figure 4.14 we analyse the results for the propagation celerity of each location of the wave. The wiggles observed in this plot occur for the same reason explained for Figure 4.10 (Appendix B). We identify that the celerity of the degradational wave tail has the same behaviour as the sediment wave front, as well as a similar order of magnitude. This means that the initial propagation of the tail is quite slow, until it abruptly accelerates due to the changes in surface grain size. The results also show that after the fining wave front has overtaken the degradational wave (roughly at $t = 8$ years, depicted in Figure 4.13) the wave celerity for all 3 locations varies around a similar small range of values close to 1 km/yr, which is of the same order of magnitude as the celerity of the sediment wave.

In order to analyse the relation between surface grain size and the degradational wave celerity, we

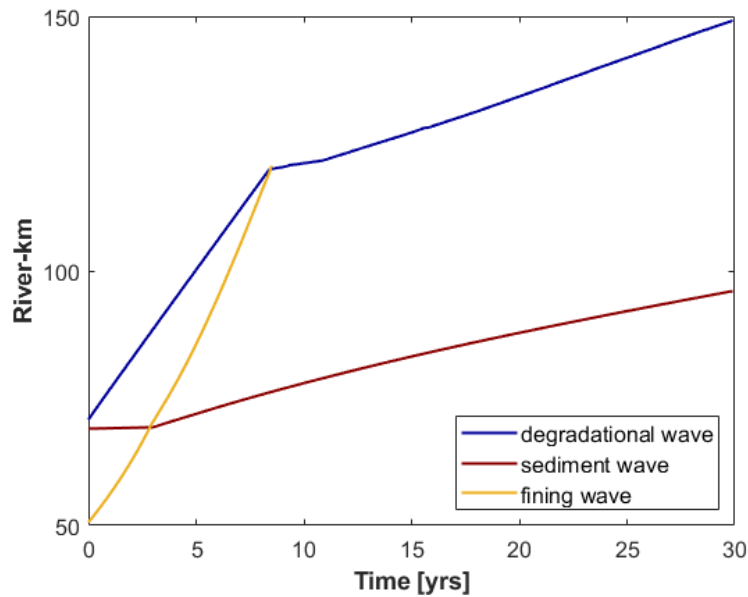


Figure 4.13: Streamwise location of the **front** of the degradational wave (blue), sediment wave (red), and fining wave (yellow) over time.

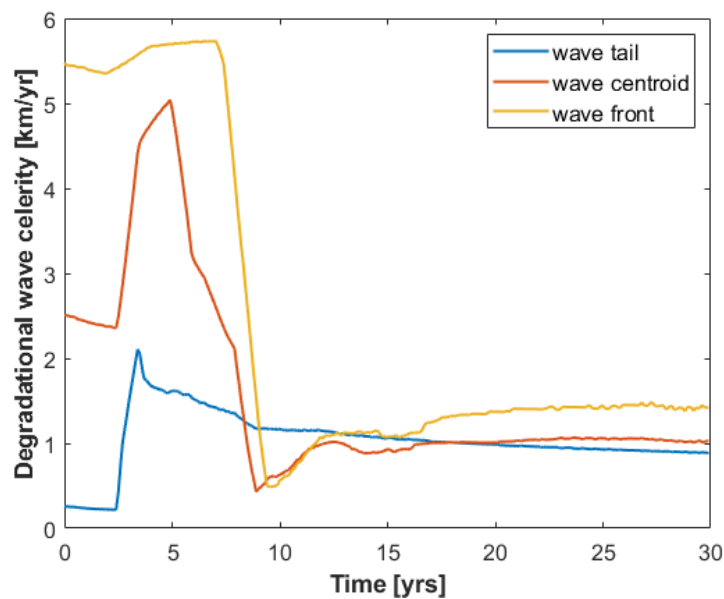


Figure 4.14: 1-year moving average value of the celerity [km/yr] of the degradational wave tail (blue), centroid (red), and front (yellow).

present in Figure 4.15 the estimated values for the analytical celerity of the wave, calculated following the derivations by Stecca et al. (2014) for a small amplitude sorting wave (Equation 2.3). These values are then compared to the ones obtained from the numerical simulation for the degradational wave front.

The results presented in Figure 4.15 show that there is a clear mismatch in the initial values of the celerities. We hypothesise that this occurs because the equation for the analytical celerity is derived to estimate the characteristic propagation of the wave, and as we observed in Figure 4.14, the initial values of the celerity vary a lot for each location of the degradational wave, as it is still forming and growing. This is supported by the fact that for the time period afterwards ($t > 8$ yrs), where the shape

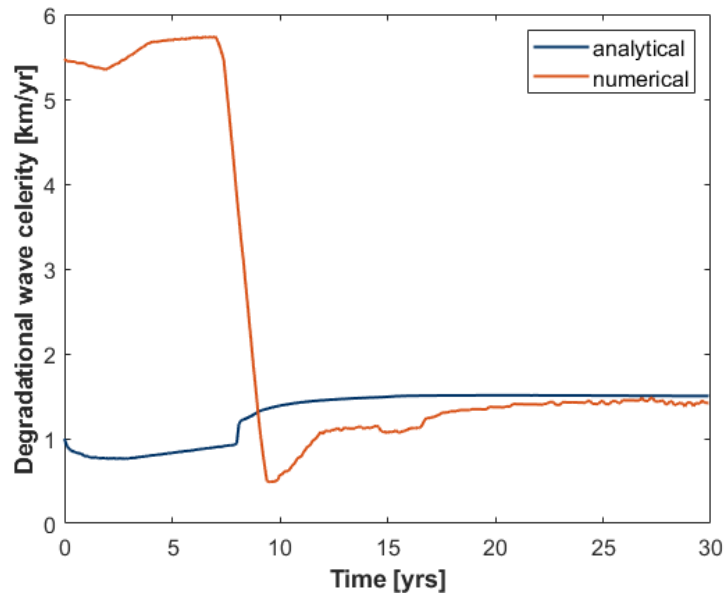


Figure 4.15: Celerity of the degradational wave front estimated with the results for the numerical simulation (red) and with the analytical solution (blue).

of the degradational wave remains fairly similar, the propagation celerity estimated analytically coincides with the numerical one.

The celerity of the centroid of the sediment wave provides a good average estimate of how fast it propagates in the river system, by comparing to the celerity degradational wave front which indicates how far downstream the river system is affected by the sediment nourishments (presented in Figure 4.16), we observe that not only is the celerity of the degradational wave an order of magnitude higher during the initial time period, but it remains higher than the celerity of the sediment wave even after it has significantly slowed down.

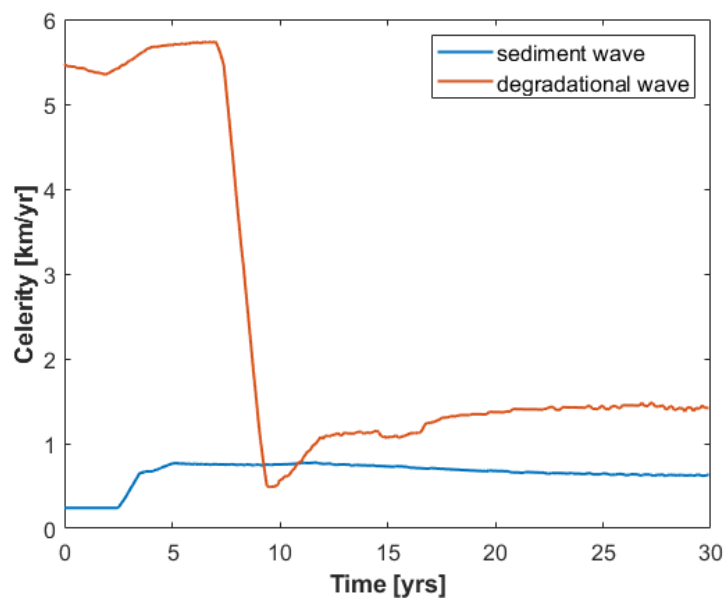


Figure 4.16: 1-year moving average value of the celerity [km/yr] of the centroid of the sediment wave (blue), and the front of the degradational wave (red).

5.1. Model runs A - Effects of changes in the height and length of the sediment wave

In this section we present a series of model runs in which we vary the distribution length of the nourishments, while keeping their volume and grain size composition constant. We define the distribution length (ΔL) as the total distance of the river reach over which the nourishments are supplied. By keeping the total volume of the nourished sediment constant, this also means that the increase in bed level induced by the nourishments is different for each model run as well. The specifications for the nourishments in each of the runs are presented in Table 5.1.

Runs	1	2	3	4
Vol [Mt]	3	3	3	3
x_0 [km]	50	50	50	50
x_L [km]	60	65	70	90
ΔL [km]	10	15	20	40
$F_{N,s}$ [-]	0	0	0	0

Table 5.1: Nourishment specifications of the model runs

where x_0 is the most upstream coordinate of the nourished reach, x_L the most downstream coordinate, and $F_{N,s}$ the percentage sand content in the nourishments grain size composition. Please note that the specifications used for model run 3 are the same described for the base case with nourishments discussed in Section 4.2.

By keeping the total volume of the nourished sediment constant, we simultaneously vary the distribution length of the nourishments, and the direct increase in bed level caused by the nourishments. We expect that for a shorter distribution length (i.e. taller sediment wave), both the backwater and Bernoulli effects are stronger and therefore lead to higher flow velocities. This allows us to assess the influence of changes in the flow in the propagation of the sediment and degradational waves.

5.1.1. Propagation of the sediment wave

We first study the evolution of the sediment wave for each of the model runs by determining whether their behaviour is predominantly dispersive or translational. The analysis is done by comparing how much the wave lengthens with respect to the displacement of the wave centroid. The results for each model run are presented in Figure 5.1.

The behaviour of the waves is increasingly translational for the longer, lower waves. This means that this translational behaviour becomes more predominant as the waves decay and lengthen over time.

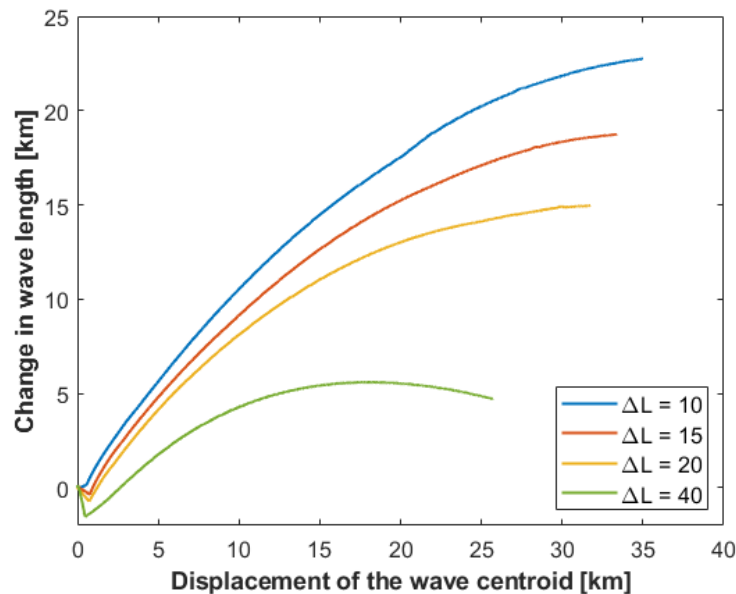


Figure 5.1: Changes in wave length with respect to the displacement of the wave centroid for the sediment waves in the set of model runs A. ΔL indicates the length in [km] of the nourished reach in each model run.

This type of behaviour can be explained if we consider the spatial gradients in flow velocities for each case. The shorter, taller waves induce larger changes in the flow due to the backwater and Bernoulli effects, this causes the flow velocities at the front of the wave to become significantly higher than at its tail, which leads to wave dispersion. Similarly, for the longer, lower waves the spatial gradients in flow velocity are milder, and the velocities at the tail and front of the wave are not so different, which leads to wave translation.

We can use a similar logic to hypothesise what the behaviour of a sediment wave would be for different values of the water discharge. High discharge values lead to an increase of the water depth, this causes the ratio between the flow-depth and height of the sediment wave to become larger as well. This causes the backwater and Bernoulli effects to become less dominant, which leads to milder spatial gradients in flow velocity. This means that during a high discharge event, the downstream propagation of the wave is not only accelerated to the ensuing larger flow velocities, but also that this propagation will tend to be have a more translational behaviour rather than dispersive.

The initial behaviour of the sediment waves is determined by their length, and consequentially the time it takes for the adjustments in grain size to affect the entire nourished reach. We observe that for the longer waves, where this adjustment in surface grain size takes more time, there is a more predominant initial wave shortening due to the differences in surface grain size and sediment mobility along the nourished reach.

We analyse the celerity of the sediment wave for each model run by studying the propagation of the wave centroid over time. The results for this analysis are presented in Figure 5.2. We observe that the celerities are larger for the shorter, taller waves due to the increase in flow velocity caused by the Bernoulli and backwater effects. As the waves decay and the flow velocities approach their initial equilibrium values, the celerities for all the waves converge to approximately the same value. The waviness in the celerity values observed at $t = 10-15$ yrs for $\Delta L = 15$ km, and at $t = 25-30$ yrs for $\Delta L = 40$ km is caused by tiny perturbations in bed level reaching the end of the numerical domain, and therefore no conclusions should be drawn from these specific values.

The initial, abrupt increase in the celerity of the sediment waves occurs later for the longer waves, as it takes more time for the adjustments in surface grain size to propagate through the nourished reach.

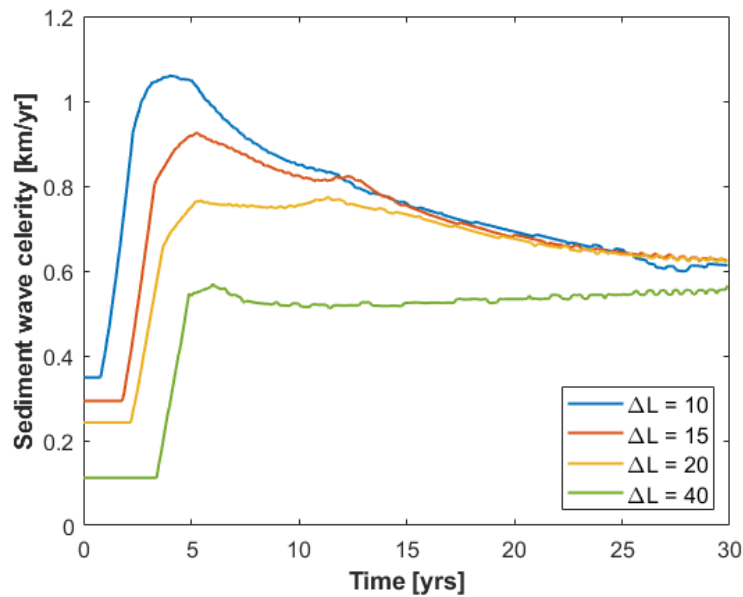


Figure 5.2: 1-year moving average value of the celerity [km/yr] of the centroid of the sediment wave, set of model runs A. ΔL indicates the length in [km] of the nourished reach in each run.

Even though the shorter, taller waves propagate faster due to the increased flow velocities, the abrupt increase in wave celerity due to the adjustments in surface grain size is far more significant in all of the model runs.

One of the main takeaways from this analysis is the importance of changes in grain size in the sediment waves associated with sediment nourishments. We learn that when the nourished sediment is coarser than the bed, it induces not only a degradational wave that negatively impacts the downstream reaches, but also a fining wave that significantly changes the mobility of the sediment wave (Figure 4.13). This highlights the importance of monitoring the changes in grain size of a nourished reach to make a better assessment of how the nourished sediment propagates in the river system, as well as to better understand how the nourishments are affecting the surface grain size of the river reach.

5.1.2. Propagation of the degradational wave

We study how the changes in the distribution length of the nourishments impacts the degradational wave that forms downstream of it. We analyse how the maximum depth of incision varies over time for each run, how far downstream the degradational wave propagates under different flow conditions, and the changes in degradational wave celerity between the model runs.

In Figure 5.3 we present the results for the maximum depth of incision for each of the model runs. The trend we observe in all of the model runs is that the incision first grows, which happens during the time period when the adjustments in surface grain size are still occurring in the nourished reach upstream of the degradational wave. Afterwards, when the fining wave and also a smaller aggradational wave that accompanies the fining reaches the degrading reach, the ongoing degradation is mitigated, which is why we see the maximum incision depth decrease in size. The incision finally reaches some form of stability once surface grain size along the entire affected reach has adjusted back to nearly its equilibrium values.

We expect the maximum incision depths to be found for the taller sediment waves, since for these waves the backwater and Bernoulli effects are more dominant, and the gradients in flow velocity become larger. This holds true for all but the first model run with the shortest distribution length (ΔL). We hypothesise that this occurs because the increase in flow velocity becomes large enough, that it is

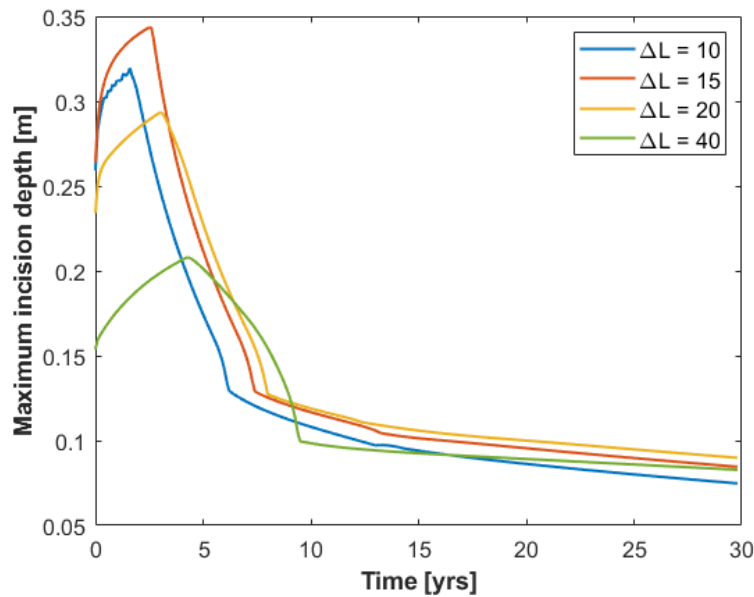


Figure 5.3: Maximum depth of the incision [m] over time [yrs], set of model runs A. ΔL indicates the length in [km] of the nourished reach in each run.

able to mobilise a larger volume of the coarse gravel fraction of the nourished sediment. This would increase the sediment supply to the downstream reach, and cause the incision to become less severe. It is important to note, that for such a tall sediment wave, effects related to flow separation and turbulent flow might become more relevant.

The maximum incision depth occurs just downstream of the sediment wave, or rather at the tail of the degradational wave, which was observed in the experimental studies by Berkhout (2015). This means that if there is a risk that the degradation preceding the nourishment could endanger a structure in the river, such as a bridge pier for example, limiting the increase in bed level caused by the sediment nourishments also helps limiting the depth of the scour.

We present the results for the celerities of the degradational wave front over time in Figure 5.4. In this figure we observe that in all model runs, regardless of the height and length of the sediment wave, the initial wave celerity is approximately the same. After an abrupt deceleration, which occurs at different times for each run, the degradational wave celerity is once again the same for all model runs.

From Figure 4.14 we learn that the abrupt deceleration of the degradational wave occurs due to adjustments in grain size over the degrading reach. From this set of model runs the abrupt deceleration of the wave occurs at different times for each run, taking more time for the longer sediment waves. This occurs because the length of the nourished reach is different for each run, and it is logical that the larger this length the longer it takes for the adjustments in grain size to occur along the entire affected reach.

The results show that even though the depth of the incision is affected by the changes in flow velocity, the celerity with which the degradational wave propagates is not. This means that to determine how far downstream the river bed will be affected by the degradational wave, it will not depend so much on the flow conditions, but rather on the total length of the coarsened reach. This is also observed in Figure 5.5, where we compare the distance travelled by the degradational wave front in each of the model runs.

A physical explanation behind this reasoning is that even though higher flows are more effective at eroding the river bed, higher flows also carry more sediment downstream, and this additional sediment can compensate for the deficit in sediment supply in the downstream reach. On the other hand, for

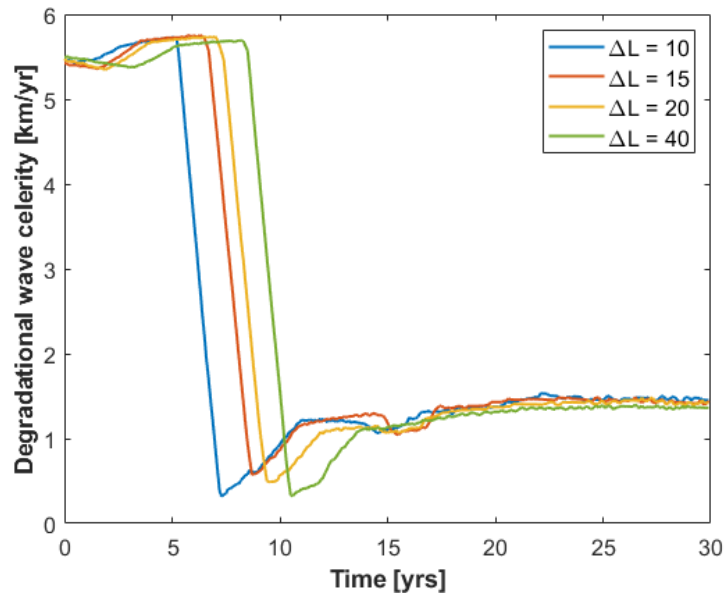


Figure 5.4: 1-year moving average value of the celerity of the front of the degradational wave, set of model runs A. ΔL indicates the length in [km] of the nourished reach in each run.

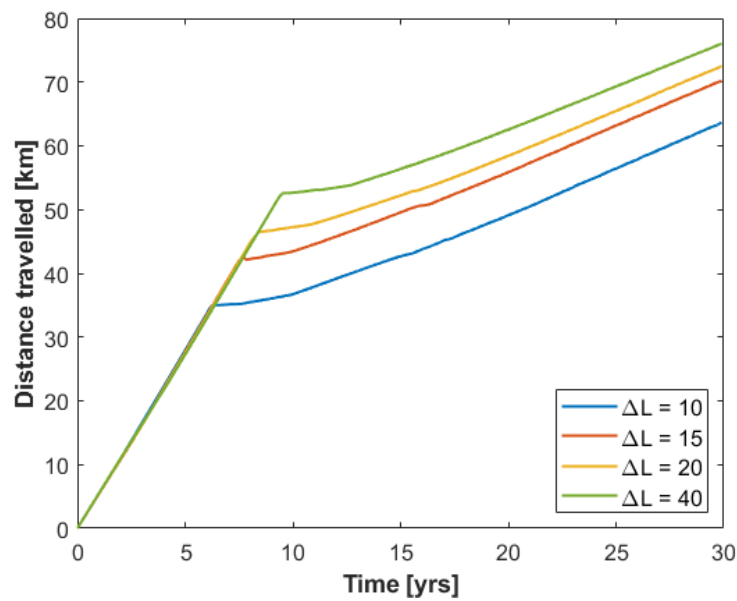


Figure 5.5: Distance travelled by the front of the degradational wave, set of model runs A. ΔL indicates the length in [km] of the nourished reach in each run.

lower flows where this deficit in sediment supply is enhanced, the flow velocities are lower and thus less capable of eroding the river bed.

5.2. Model runs B - Grain size of the nourished sediment

In this section, we aim to study the impact of changes to the grain size composition of the nourishments to the system response. In order to analyse these changes we set up a one-dimensional model of a river system with the specifications for the base case described in Chapter 3. To this river system we add a nourishment supply with a total volume of 3 Mt, supplied uniformly over a 20 km reach and all at the same time. In each of the model runs we vary the grain size composition of these nourishments, and analyse the changes to bed level and bed surface grain size for each of the runs.

The sediment in the system is described by 2 characteristic grain size classes, sand ($D_s = 0.5$ mm) and gravel ($D_g = 16$ mm). We impose a constant bed load composed of 83% sand and 17% gravel, and estimate the equilibrium surface texture to be composed of 22% sand and 78% gravel. We consider this composition of the surface texture to guarantee that in at least three of the model runs (runs 1-3) the composition of the nourishments is coarser than the bed surface, and then analyse a fourth model run (run 4) in which the composition of the nourishments is finer than the bed surface. The specifications for each model run is presented in Table 5.2.

Runs	1	2	3	4
Vol [Mt]	3	3	3	3
ΔL [km]	20	20	20	20
$F_{N,S}$ [-]	0	6.25%	12.5%	25%

Table 5.2: Specifications of the nourishments in each model run.

With this selection of model runs we define the following objectives: 1) we study how the dispersion of the sediment wave along the system changes with increasing contents of the finer sediment fraction; 2) we determine the changes in the sediment wave celerity associated with its grain size composition; 3) we analyse how increments of volume fraction content of sand in the nourishments impact the size and propagation of the degradational wave, which means studying changes in the depth of the incision as well as changes to the propagation celerity of the degradational wave front; 4) we study how the combined morphodynamic response changes when the composition of the nourishments is finer than the bed surface (model run 4).

5.2.1. Propagation of the sediment wave

Previous studies on the propagation of bed material waves have addressed how the grain size composition of the waves affect their evolution. In their study Lisle et al. (2001) found that finer sediment tends to increase the translational behaviour of sediment waves, and that it mainly accelerates wave evolution by increasing sediment transport rates. Our aim is to use the results from the model to assess if these changes are observed with increased sand content in the nourishments, to better understand the physical processes behind these changes, and get an estimate on the significance of these changes with each model run.

To assess whether the behaviour of the sediment wave is translational or dispersive (see Figure 2.4), we compare the displacement of the wave centroid to the wave length. The wave length is calculated as the distance measured between the tail of the wave and the front of the wave, which are estimated as the 5% percentile and 95% percentile of the cumulative elevation difference of the wave, respectively. In Figure 5.6 we present the resulting dispersion of the wave for each of the model runs.

The results shown in Figure 5.6 show that there is a clear relation between the sand content in the nourishments ($F_{N,S}$) and the translational behaviour of the wave. For the runs with a larger nourishment sand fraction, the wave centroid is displaced further downstream with less lengthening. Additionally, the results show that an increased content of sand in the nourishments accelerates the initial evolution

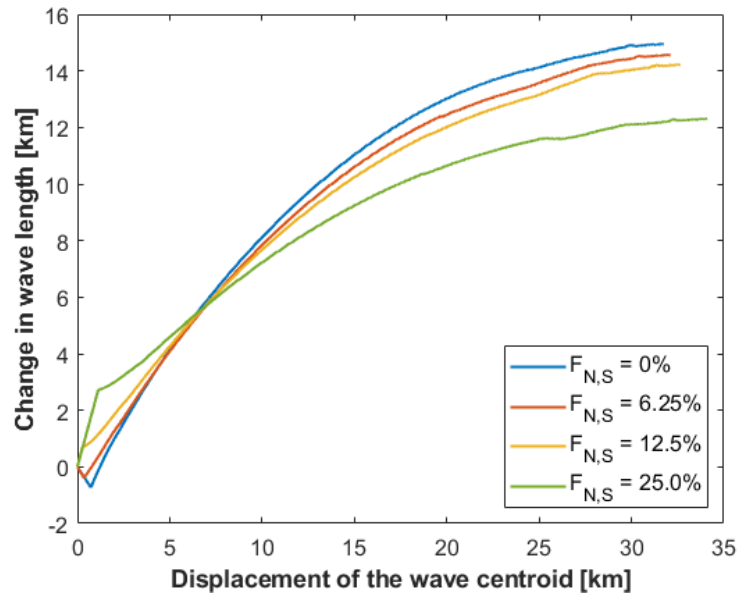


Figure 5.6: Changes in wave length with respect to the displacement of the wave centroid of the sediment waves in the set of model runs B. $F_{N,S}$ indicates the fraction content of sand [% volume] in the nourished sediment in each model run.

of the wave, this is particularly true for the model run with the largest amount of sand content ($F_{N,S} = 25\%$) as the wave lengthens significantly more than the others without barely any displacement of the centroid. The behaviour of the wave in this model run ($F_{N,S} = 25\%$) is significantly different because the initial morphodynamic response of the system differs to that of the other model runs, we elaborate this in more detail in Section 5.2.3.

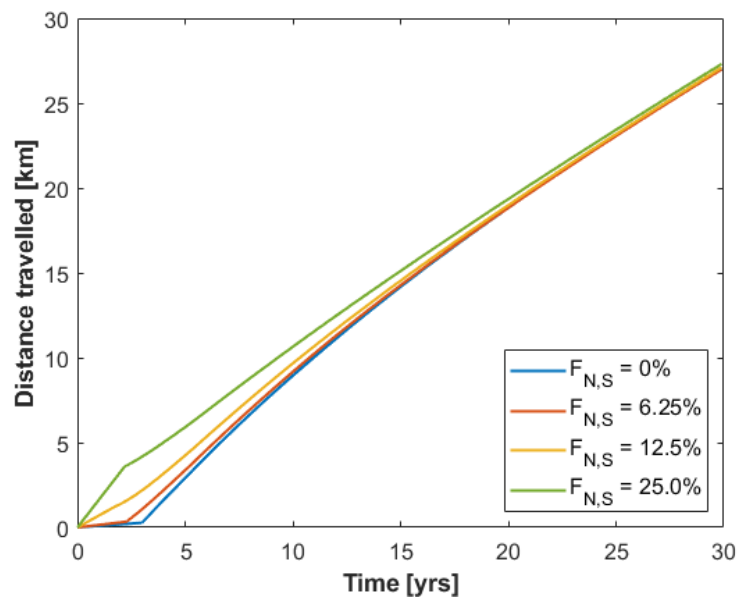


Figure 5.7: Distance travelled [km] over time by the front of the sediment wave, set of model runs B. $F_{N,S}$ indicates the fraction content of sand [% volume] in the nourished sediment in each model run.

In order to better understand how the content of the finer fractions in the nourishments influence the initial evolution of the wave, we analyse how far downstream the wave front propagates for each of the model runs. The results of this analysis are presented in Figure 5.7.

The following conclusions regarding the dispersion of the sediment wave can be drawn from Figure 5.7. The first confirms the findings by Lisle et al. (2001) that increased content of the finer fractions in the wave mainly accelerate its evolution, this conclusion is drawn from the fact that the wave front propagates further in the initial years after the nourishments for increasing sand content ($F_{N,S}$). The second conclusion is that regardless of their initial propagation and sediment composition, in all of the model runs the final displacement of the wave front is the same, this is highlighted in the figure as all lines converge shortly after 20 years.

We analyse the celerity of the sediment wave for each of the model runs, in order to determine the changes to the propagation of the wave with respect to its grain size composition. This comparison allows us to assess whether an increased content of finer sediment in the nourishments improve the mobility of the wave. The results of this analysis are presented in Figure 5.8, the celerities are obtained according to the displacement of the wave centroid.

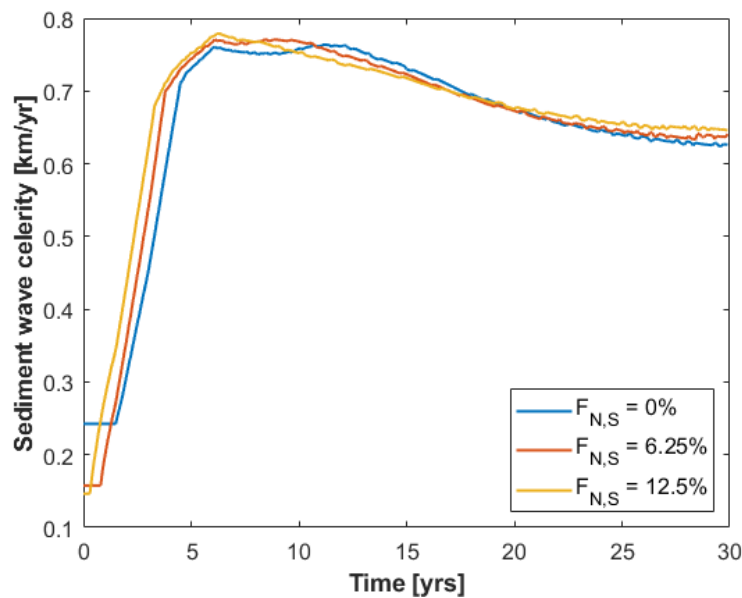


Figure 5.8: 1-year moving average value of the celerity [km/yr] of the centroid of the sediment wave, set of model runs B (runs 1-3). $F_{N,S}$ indicates the fraction content of sand [% volume] in the nourished sediment in each model run.

The main takeaways from these results are that the initial celerities of the sediment waves are largest for the first run ($F_{N,S} = 0\%$) despite a lower content of sand, and that even though the celerities vary around similar values, they are generally higher for the model run with the largest sand content in the nourishments. A physical explanation for this results is given by how the height of the sediment wave varies over time, and the effects this has on the flow velocities due to the Bernoulli effect. In Figure 5.9 we present the change in the maximum height of the sediment wave over time.

To understand these changes in height of the sediment wave we must go back to the theoretical morphodynamic response presented in Figure 2.15. The increase in grain size of the bed surface not only induces a degradational wave downstream of the nourishments, but also an aggradational wave on the upstream end of the nourishments. This aggradational wave causes an overall increase in the height of the sediment wave, and the magnitude of this increase in height is proportional to the change in surface grain size. This means that the accumulation of sediment on top of the sediment wave was largest for the model runs with less sand content in the nourishments.

The changes in maximum height presented in Figure 5.9 become more relevant when we consider that the flow velocities are larger for a taller sediment wave due to the Bernoulli effect. This provides an explanation as to why the initial celerity is higher for the sediment wave with the lowest sand content. This also highlights the impact of the grain size composition of the nourishments in morphodynamic

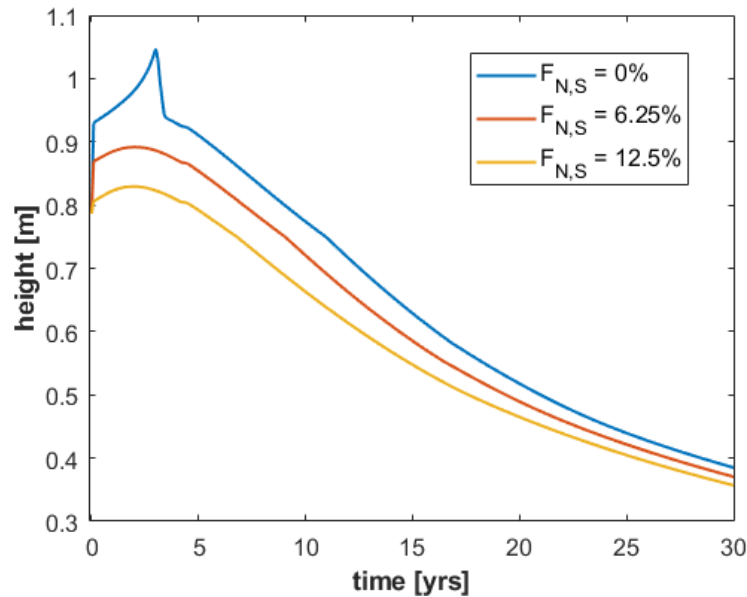


Figure 5.9: Maximum height of the sediment wave over time, set of model runs B (runs 1-3). $F_{N,S}$ indicates the fraction content of sand [% volume] in the nourished sediment in each model run.

response of the system. If we consider a river reach that needs to be protected against bed degradation, but also where excessive bed aggradation could be problematic, for navigation for example, then increasing the content of the finer fractions in the nourishments could lead to a more suitable solution.

5.2.2. Propagation of the degradational wave

The impact of the grain size composition of the nourishments on the morphodynamic response on the system also plays an important role on whether the nourishments are preceded by a degradational wave, and the severity of this effect, just as it did for the changes in height of the sediment wave presented in Figure 5.9. Over the nourished reach, sediment mobility is reduced due to the increase in grain size, which causes a deficit in sediment supply downstream and the formation of a degradational wave. We analyse how increasing the content of the finer fractions in the nourishments can counteract this effect by studying changes to the depth of the scour, and the celerity of the degradational wave front.

We first analyse the initial development of the degradational wave for each of the model runs by estimating the maximum depth of the incision over time (Figure 5.10). We observe that the depth of the incision changes significantly for each of the model runs. The higher the sand content in the nourishments, the less severe the incision becomes, not only initially but also on the longer term years after the nourishment supply. With these results we can conclude that including finer sediment in the nourishments improves sediment mobility, and that even if the surface texture is still coarsened by the nourishments, the improved mobility helps counteract the initial growth of the incision, as well as the overall depth of the degradational wave.

In Figure 5.11 we present the estimates for the celerity of the degradational wave front for each of the model runs. We observe that the largest change in celerity comes shortly after the nourishment supply (between 5 and 10 years). This particular decrease in celerity is related to the changes in surface grain size. In Figure 2.17 we explain how the coarsening of the surface induces the formation of a fining wave which starts propagating from the upstream end of the nourishments. This fining wave plays an important role in levelling the gradients in surface grain size and improving sediment mobility along the domain, and once it reaches the front of the degradational wave, the incision stops growing, and the propagation of the wave front significantly slows down.

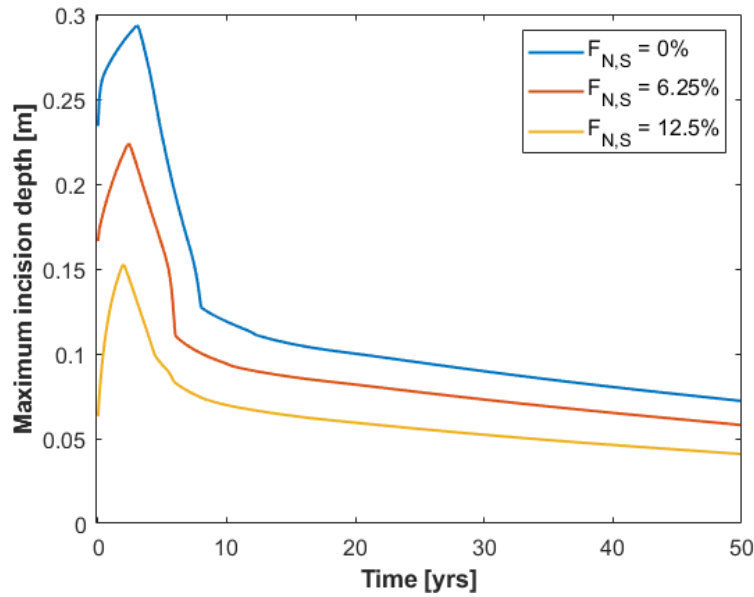


Figure 5.10: Maximum depth of incision [m] over time [yrs], set of model runs B (runs 1-3). $F_{N,S}$ indicates the fraction content of sand [% volume] in the nourished sediment in each model run.

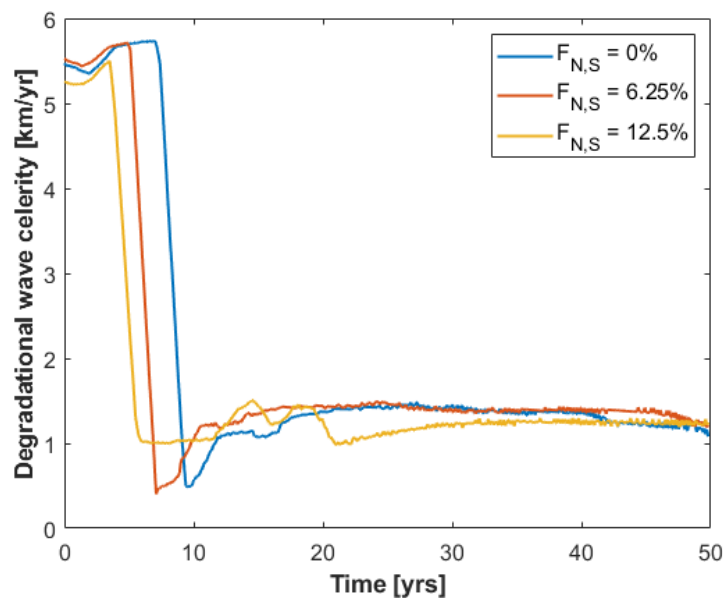


Figure 5.11: 1-year moving average value of the celerity [km/yr] of the front of the degradational wave, set of model runs B (runs 1-3). $F_{N,S}$ indicates the fraction content of sand [% volume] in the nourished sediment in each model run.

The main difference between the celerity of the waves in each model run is that they slow down at different times. This follows from the fact that by increasing the sand content in the nourishments, the coarsening effect of the bed surface becomes less severe, and the time it takes for the system to adjust the gradients in surface grain size becomes shorter. After the degradational wave has slowed down, the celerity of the front of the wave varies around a value of approximately 3.5 km/yr for all three model runs.

We study the propagation of the degradational wave by analysing how far downstream it travels for each of the model runs. We present these results in Figure 5.12 by analysing the distance the wave front travels over time. The results show that the main difference between the three model runs is due

to the time it takes for the growth of each of the waves to slow down, since this happens later for the wave with the coarser nourishment composition ($F_{N,S} = 0$) this wave propagates further downstream than the others.

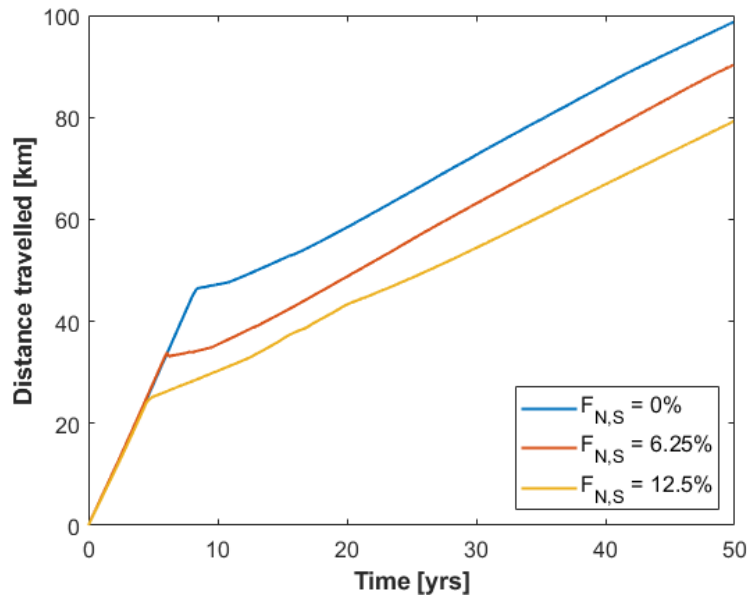


Figure 5.12: Distance travelled [km] over time by the front of the degradational wave, set of model runs B. $F_{N,S}$ indicates the fraction content of sand [% volume] in the nourished sediment in each model run.

5.2.3. Model run 4 - Decrease in grain size

In this last model run of the set of model runs B, we increase the content of sand in the nourishments such that their overall composition was finer than the bed surface. We first describe how the theoretical morphodynamic response changes in this situation, then we analyse the possible implications for the propagation of the sediment wave in this scenario, and the changes we expect with respect to the previous model runs.

By increasing the contents of fine sediment in the bed surface, the sediment mobility over the nourished reach is increased. This leads to a morphodynamic response opposite to the previous cases discussed in this section so far, as the increased sediment mobility leads to a sedimentation front on the downstream end of the nourishments (opposite to a degradational wave) and to enhanced degradation on the upstream end, as sketched in Figure 5.13.

If we now consider this morphodynamic response in combination with the ones depicted in Figures 2.8 and 2.11 for the Bernoulli and backwater effects respectively, we observe that all the effects promote the migration of the sediment wave, and that as a result the wave should be more mobile.

The results for bed elevation (Figure 5.14) in this model run show that the sediment wave is now preceded by an aggradational wave, and that the sediment wave rapidly decreases in height. Additionally, we observe that 5 years after the nourishments, the preceding aggradational wave has migrated much further downstream, and that the sediment wave is once again preceded by a (much smaller) degradational wave.

In these results we see that the bimodal composition of the nourishments causes two separate bed waves to propagate in the system, one for each grain size. The finer fraction is more mobile, and this is why we see it being eroded away much sooner than the coarser one, causing a rapid decrease in bed

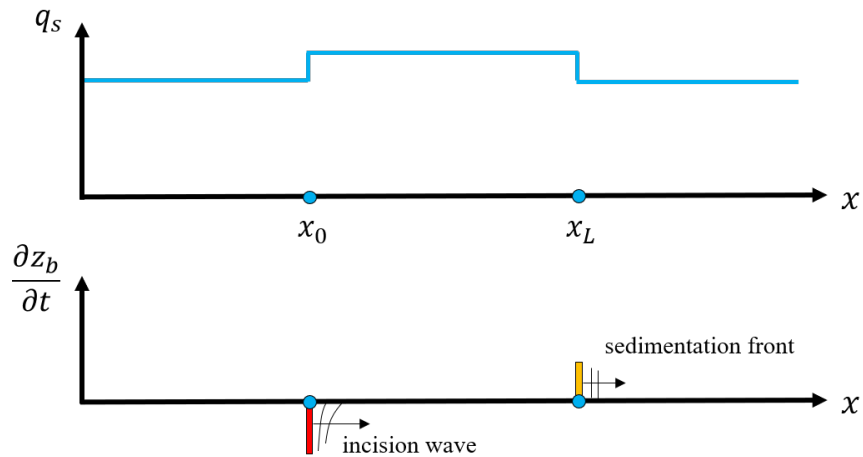


Figure 5.13: Sediment transport gradients (top) and the corresponding morphodynamic response (bottom) to a decrease in surface grain size over the nourished reach.

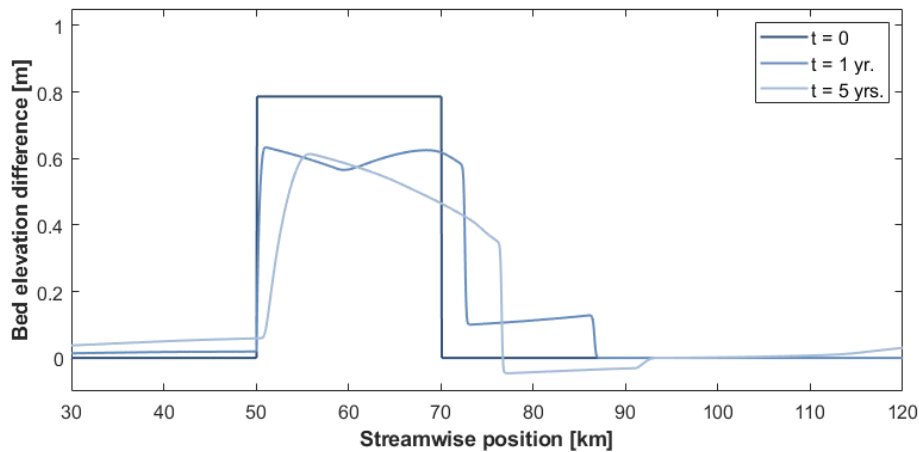


Figure 5.14: Bed elevation difference [m] with respect to initial bed level at times $t = 0, 1,$ and 5 years. Model run 4: fraction content of sand $F_{N,S} = 25\%$ of the total volume of nourished sediment. Flow direction from left to right.

elevation of the nourished reach, and an aggradational wave that migrates downstream significantly faster.

The adjustment in surface grain size does not happen simultaneously with the changes in bed level. In this case, the volume of the finer fraction propagates downstream so fast that it leaves the nourished reach before the gradients in grain size have adjusted, such that there is a time window in which the surface of the nourished reach is coarser than the surface downstream, and leads to the formation of a degradational wave. This is observed in Figure 5.14 5 years after the nourishment supply, where a degradational wave is seen to precede the sediment wave.

We compare the celerity of the sediment wave centroid to the previous model runs in Figure 5.15. The initial celerity of the wave ($F_{N,S} = 25\%$) is significantly higher than for the other 3 model runs. We hypothesise that this happens because unlike in the other model runs, this sediment wave is not preceded (initially) by a degradational wave to slow it down, and is able to propagate downstream more efficiently. This is also seen for the wave celerities 20 years after the nourishments, once the waves have decayed enough that increased flow velocities due to the Bernoulli effect have less impact on their propagation, then the waves with the smaller preceding degradational wave propagate faster.

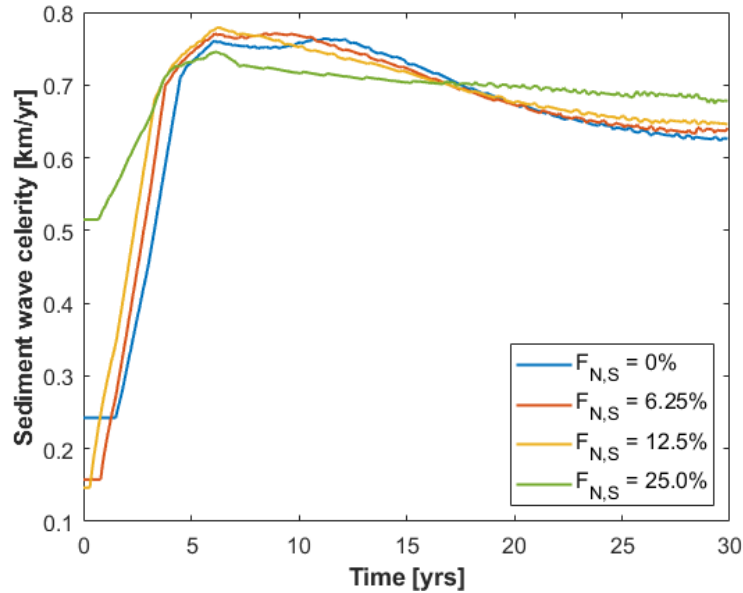


Figure 5.15: 1-year moving average value of the celerity [km/yr] of the centroid of the sediment wave, set of model runs B. $F_{N,S}$ indicates the fraction content of sand [% volume] in the nourished sediment in each model run.

Nourishment pilot project

In this chapter we study in detail the data gathered from a nourishment pilot project carried out in the Bovenrijn (see Figure 1.5) between 2016-2019. We first introduce the specifications of the nourishment pilot project, including the area of study, the data available, and the main objective of the project. We then present the changes in bed level in the affected reach for different time periods, where we analyse the evolution of the sediment wave and its propagation celerity for different discharge events. We then study the data available on measurements of grain size and tracer sediment, and analyse the related trends to bed level changes.

The objective of this analysis is to better understand the advantages and limitations of the one-dimensional analysis by comparing the results from the field experiment with the results from the numerical simulations. We can expect the results from the field experiment to be different due to the temporal variability of the flow rate, as well as due to 2D effects such as secondary flow.

In the model we assume a steady and representative value of the water discharge, the celerity of the nourishments is proportional to this value, and therefore, the celerity estimated with the model is only a representative value as well. In reality, discharge varies over time and affects the mobility of the nourishments, we can expect high discharge events to be more effective at dispersing the nourishments, and low discharge events to have little effect on them.

Due to the 1D character of the numerical model, bed level along the cross-section does not vary. In the study site for the field experiment, the channel is deeper along the outer bends, which causes secondary flow effects that influence the direction of propagation of the nourishments. Additionally, we assume in the model that the nourishment is supplied instantly, whereas in reality this can last multiple months. This means that dispersion of the nourishments can already start to occur before the entire intended volume of nourished sediment is supplied.

6.1. Project specifications

Bed degradation has been a problem in the Bovenrijn and Waal for some decades. Between 1985 and 1990 the river bed seems to have stabilised in the Bovenrijn, even showing aggradational tendencies afterwards. However, downstream in the Waal bed degradation trends are still observed (Ylla Arbós et al. 2019). In the Niederrhein, sediment nourishments have shown to stabilise bed level (Quick et al. 2019). In fact, it is hypothesised that these sediment nourishments have now migrated to the Bovenrijn, and are one of the reasons why bed level change has stabilised in this downstream reach.

With the objective to better understand how sediment nourishments propagate in the river system, and how effective they are as a sediment management measure to counteract bed degradation, Dutch authorities decided to carry out a nourishment pilot project in the Bovenrijn. Since the objective is mainly to study the propagation of these nourishments, the project is heavily monitored, and detailed measurements of bed level and tracer sediment are available.

The area where the sediment nourishments were supplied is schematised in Figure 6.1. The site is located in the Bovenrijn, near the German-Dutch border. The river bifurcates into the Waal and the

Pannerdensch Kanaal just 3 km downstream (Rhine-km 867). The nourishments were distributed between Rhine-km 862-864.3 in the outer bend of the river during a 3 month period. The main channel width at this location is approximately 350 m.

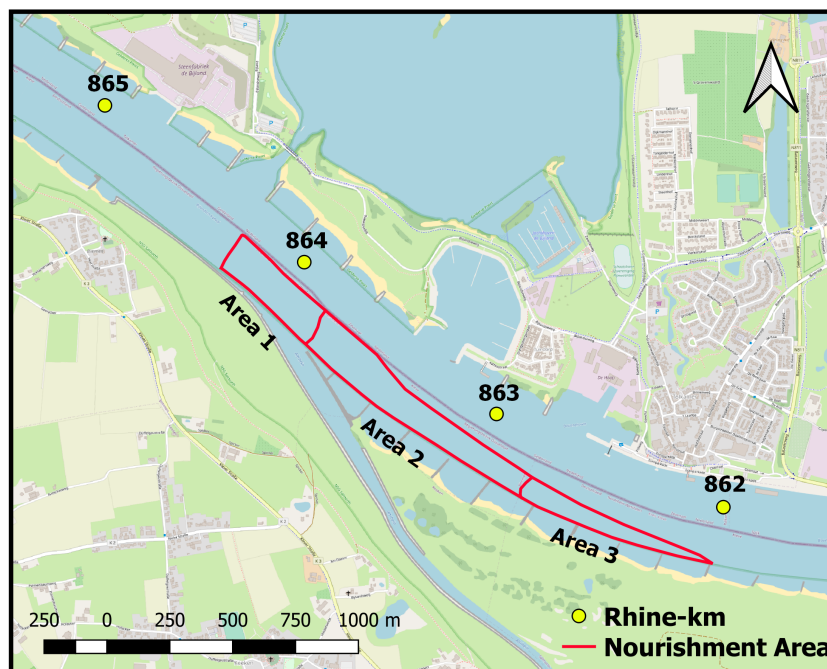


Figure 6.1: Site location for the nourishment pilot project in the Bovenrijn (2016). In red, the areas defined for the artificial sediment supply. Flow is from right to left.

The nourished reach was divided in three areas as seen in the Figure 6.1. The nourishment of the upstream area (Area 3) was interrupted for about a month due to a high discharge event. The dates and specifications of the nourishments for each of the areas are presented in Table 6.1. The total sediment volume of 70,000 m³ amounted to a layer thickness of 30 cm, such that the OLR-4m (Lowest agreed water level) navigability condition is satisfied.

Reach	River-km	Surface area	Volume	Material	Date
Area 1	863.848 – 864.3	58,337 m ²	17,500 m ³	Granite	11/Apr/16 – 26/Apr/16
Area 2	863.848 – 862.84	116,667 m ²	35,000 m ³	Gravel	26/Apr/16 – 25/May/16
Area 3	862 – 862.840	57,163 m ²	17,500 m ³	Granite	25/May/16 – 01/Jun/16, 05/Jul/16 – 12/Jul/16
Total	862 – 864.3	232,167 m ²	70,000 m ³	–	11/Apr/16 – 12/Jul/16

Table 6.1: Nourishments specifications for the Bovenrijn pilot project (source: RWS).

The sediment used for this project is composed of gravel and granite. The granite has a higher natural radioactivity than the natural gravel in the river due to its contents of Potassium (K), Uranium (U) and Thorium (Th), and is therefore traceable with radioactivity measurements (K/10 + U + Th). Specifically, before the nourishments, radiometries of the river showed an average radioactivity level of 49 Bq/kg with a standard deviation of 7 Bq/kg, and on the other hand measurements of the granite material then presented a much higher radioactivity level of 240 Bq/kg. The specifications for the grain size of the nourished sediment and bed material are presented in Table 6.2.

The available surveys of radioactivity and bed level are presented in Table 6.3 with the dates in which

Material	ρ [kg/m ³]	D_{10} [mm]	D_{50} [mm]	D_{90} [mm]
Bed surface	2650	0.4	7.4	19.5
Gravel supply	2620	4.3	9	18.8
Granite	2740	4.3	11.6	22.8

Table 6.2: Specifications of the present bed surface material, and the nourished sediment (source: RWS).

the measurements were carried out. We keep the same nomenclature used in the original analysis for clarity purposes. For our analysis, we divide the available data in three characteristic time periods based on discharge conditions. These are presented in Table 6.4.

Survey	Radiometry	Bed level survey
T1	17-Mar-16	6-Apr-16
T4	14-Jun-16	16-Jun-16
T5	12-Jul-16	6-Jul-16
T6	9-Aug-16	5-Aug-16
T10	20-Dec-16	30-Dec-16
T12	21-Feb-17	21-Feb-17
T14	18-Apr-17	28-Apr-17
T18	7-Nov-17	23-Oct-17
T19	13-Feb-18	26-Feb-18
T20	11-Jul-18	18-Jun-18

Table 6.3: Nomenclature and dates of the available measurements of bed level and radioactivity (source: RWS).

Period	Surveys	Days	Discharge [m³/s]			Description
			Mean	Max.	Min.	
Initial	T4 - T1	89	2692	4704	1778	High discharge event
	T5 - T4	28	3867	4757	2447	Right after supply to area 3
	T6 - T5	28	2187	2621	1883	After high discharge receded
Low water	T10 - T6	133	1358	2108	938	Low discharge period
	T14 - T12	56	2150	3778	1192	Short flood wave
	T18 - T14	203	1568	2189	1176	Low discharge period
High water	T19 - T18	98	3854	7553	1299	Extreme discharge event
	T20 - T19	148	2079	3056	1205	Receding discharge

Table 6.4: Characteristic time periods, with compared surveys, corresponding days in-between, and discharge statistics for the respective time period.

6.2. Changes in bed level

The nourishment supply induces an increase in bed level which propagates in the river as a sediment wave. We first analyse the evolution of this wave at each of the characteristic time periods (Table 6.4), and then compare the changes observed in its propagation celerity.

The initial time period is divided in three stages (Figure 6.2). First we compare (T1) the initial bed level before the nourishments to (T4) bed level after the sediment has been supplied to the downstream and middle reaches (Areas 1 and 2). The supply of the nourishments to Area 3 was interrupted by a high discharge event, so bed level for (T4) is measured shortly after this interruption. The next measurements (T5) were taken right after the high discharge event, once the supply of the nourishments to Area 3 was completed. Finally bed level was measured (T6) shortly after the high discharge event.

In Figure 6.2 we present the changes in sediment volume per surface area [m^3 / m^2] in the top layer (0.3 m) as estimated by Koolstra et al. (2019). The results compare the change in bed level with respect to the time elapsed between two surveys. The red areas indicate an increase in bed level, while the blue areas indicate bed erosion.

The following observations can be made from the measurements presented in Figures 6.2:

T4-T1:

- The wave started dispersing downstream of Area 1 before the sediment was supplied to Area 3. This is something we do not observe in the model results, where the nourishment is supplied all at once.
- The initial propagation of the wave seems to cross the main channel in the direction towards the next outer bend. This is probably related to 2D effects that we do not observe in the numerical model.

T5-T4:

- The sediment from Area 2 is transported to Area 3, where the material seems to be accumulating and creating a shoal. The difference in mobility between the sediment in the two areas seems mostly due to the differences in grain size of the supplied material, since the gravel in Area 2 is finer and less dense than the granite in Area 3 and hence more mobile.
- Bed degradation is observed in the inner bend downstream of Area 1. This could be related to bed erosion after a high discharge event, or as a reaction effect of reduced sediment mobility over the nourished reach.
- The increase in bed level observed in Area 3 indicates that the rest of the nourished sediment has been supplied to this area.

T6-T5:

- Deposition of sediment is observed in Area 3 just after the nourishment has been supplied to this area. In the model we observed that the coarsening of the bed surface was the dominant effect, reducing sediment mobility and enhancing aggradation over the nourished reach. This poses as a possible explanation to the changes in bed level observed in Area 3.

Regarding the propagation behaviour of the sediment wave, we can conclude from these results that the initial behaviour of the wave is predominantly dispersive, as the tail of the wave (Area 3) presents no degradation even for the time period after the nourishment has been fully supplied, and the front propagates downstream at a significantly faster rate.

The next time period (Figure 6.3) we analyse is characterised by low discharges during prolonged periods of time. We again present the estimations of changes in volume per surface area made by Koolstra et al. (2019). During the second stage of this period (T14-T12) a short peak in discharge was measured

at the nearest gauge station in Lobith.

During this low discharge period there are hardly any visible changes in the evolution of the sediment wave, which is indicative of a low mobility of the coarse material used for the nourishments. This is to be expected, since the use of finer material would significantly reduce the effectiveness of the nourishment, as it would be washed away with more ease.

We observe that even after a high discharge event (T14-T12) the sediment wave barely propagated. This means that the propagation of the wave not only requires a higher than average discharge, but also that the high discharge event last a significant amount of time.

During the next time period (Figure 6.4) we observe how the sediment wave is affected by an extreme discharge event. This occurs during the first stage of this period (T19-T18). The stage afterwards shows the changes for the period when this high discharge event is receding (T20-T19).

The high discharge event mobilises the shoal in the downstream end of Area 1 and the bed material propagates further downstream at a faster pace than at previous events. Even after the event (T20-T19) the wave keeps propagating, which implies that once the wave decays, less significantly large and long discharge events are required to mobilise it. The erosion of the material in the wave tail (Area 3) indicates that the discharge was high enough to also promote translation of the sediment wave.

From the figures, we estimate the location of the sediment wave front for each of the surveys, and calculate the propagation celerity of the wave during each period. The results are presented in Table 6.5, and then plotted in Figure 6.5.

Surveys	Max. Q [m ³ /s]	Distance travelled [m]	Days	c [km/yr]
T4 - T1	4704	150	89	0.62
T5 - T4	4757	75	28	0.98
T6 - T5	2621	25	28	0.33
T10 - T6	2108	0	133	0.00
T14 - T12	3778	0	56	0.00
T18 - T14	2189	0	203	0.00
T19 - T18	7553	200	98	0.74
T20 - T19	3056	100	148	0.25

Table 6.5: Propagation celerity of the sediment wave front estimated for the nourishment pilot project in the Bovenrijn.

In Figure 6.5 we observe that there is a clear correlation between the water discharge and the celerity of the wave. Furthermore, we observe that the celerity of the wave during the later time period is lower than during the initial time period, even though the maximum discharges observed were larger.

We find two similarities with respect to the results obtained from the numerical model: 1) the order of magnitude of the celerity is the same (0.5 - 1.0 km/yr). 2) As the sediment wave disperses and decays in height over time, the celerity of the wave also decreases.

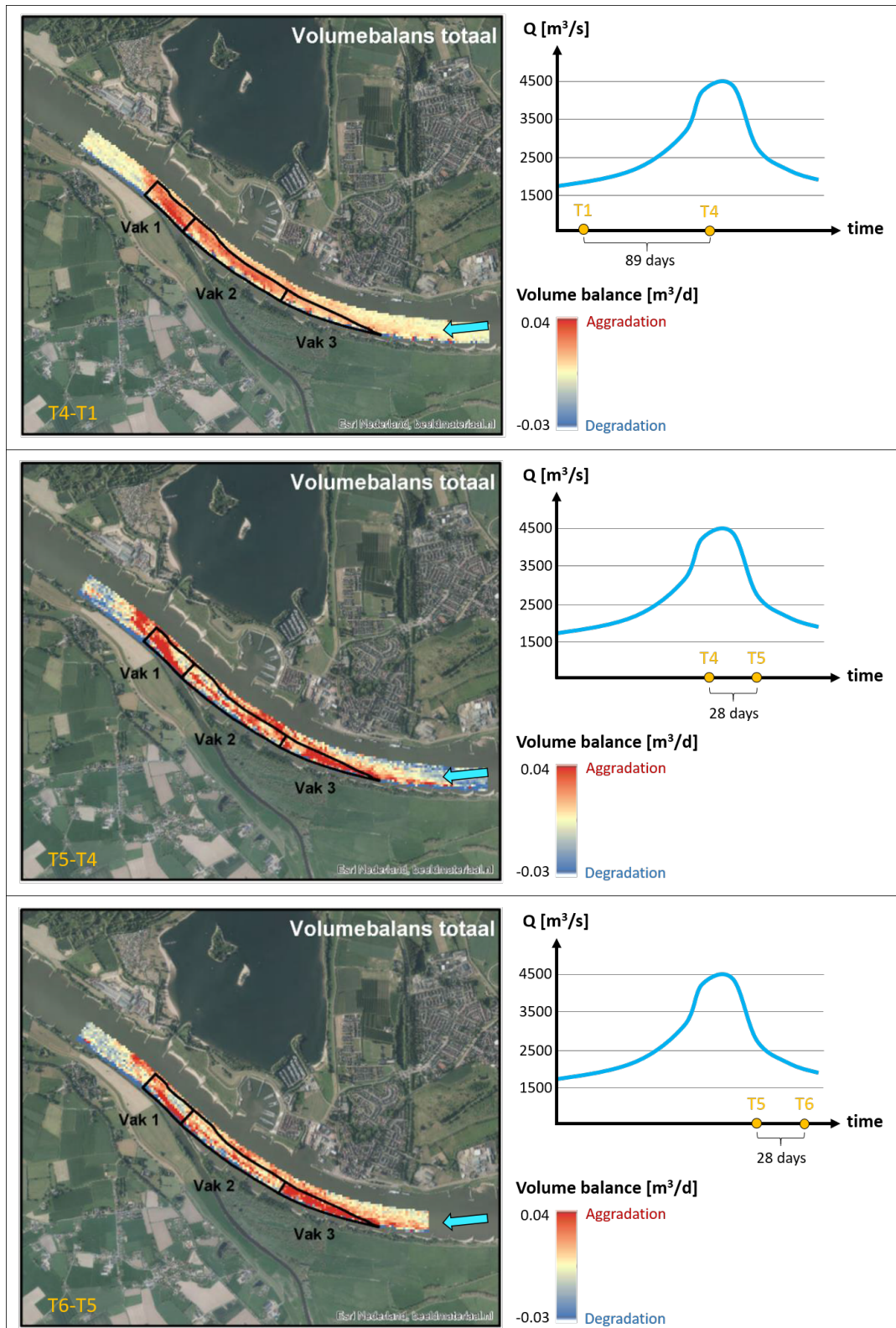


Figure 6.2: On the left figures, relative changes in sediment volume per bed surface area [m^3 / m^2] between surveys (images from Koolstra et al. (2019).), arrow indicates flow direction. On the right, sketch of the hydrograph, indicating the approximate values of the water discharge [m^3 / s] and the time [days] passed between each measurement.

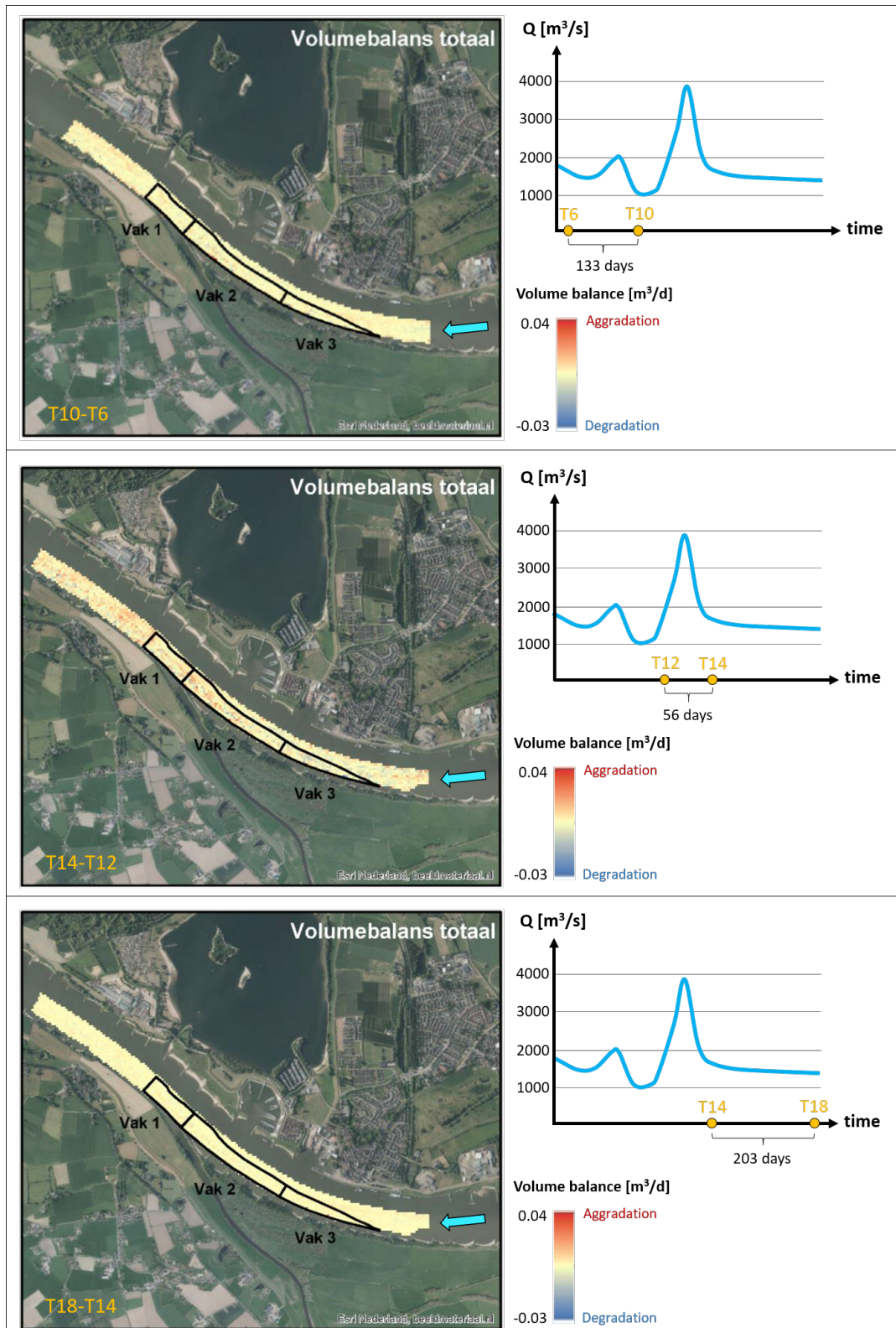


Figure 6.3: On the left figures, relative changes in sediment volume per bed surface area [m^3 / m^2] between surveys (images from Koolstra et al. (2019).), arrow indicates flow direction. On the right, sketch of the hydrograph, indicating the approximate values of the water discharge [m^3 / s] and the time [days] passed between each measurement.

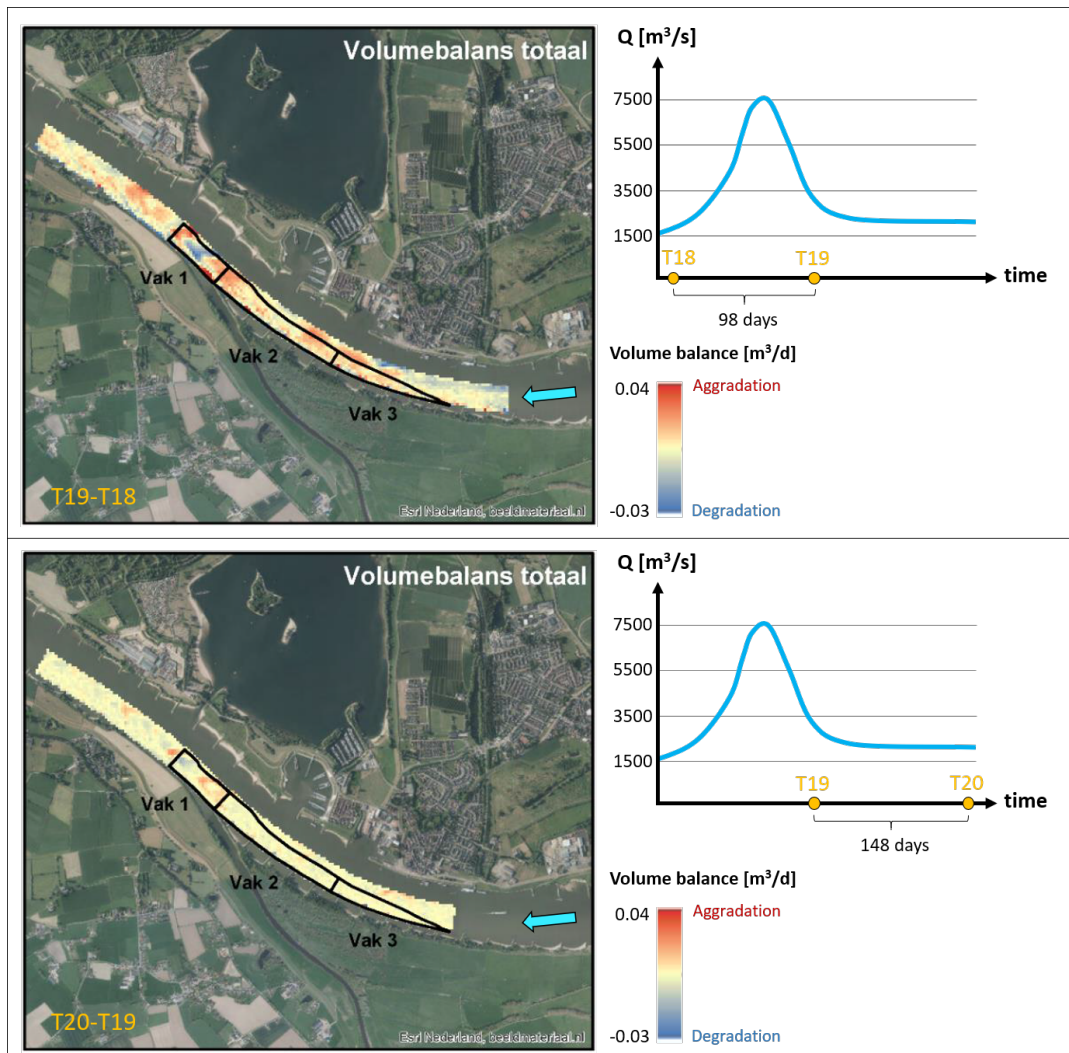


Figure 6.4: On the left figures, relative changes in sediment volume per bed surface area [m^3 / m^2] between surveys (images from Koolstra et al. (2019).), arrow indicates flow direction. On the right, sketch of the hydrograph, indicating the approximate values of the water discharge [m^3 / s] and the time [days] passed between each measurement.

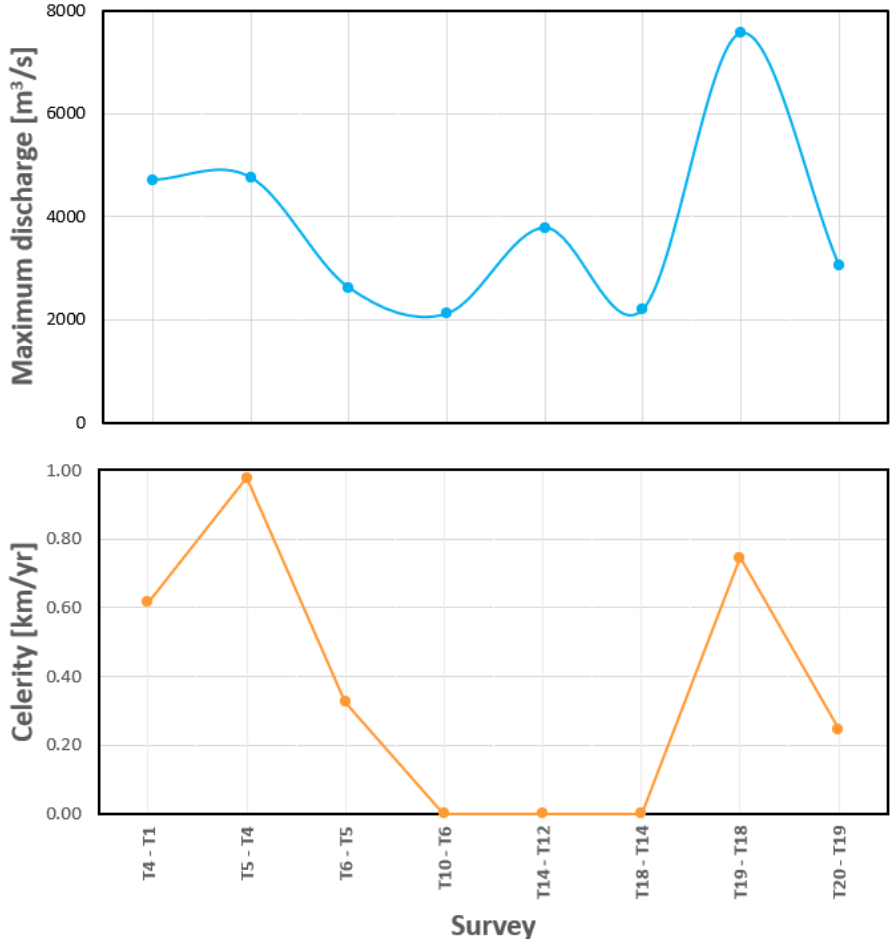


Figure 6.5: On the top, values for the maximum water discharge measured in Lobith for the same time periods as the bed level surveys. On the bottom, propagation celerity of the sediment wave front estimated for the nourishment pilot project in the Bovenrijn.

6.3. Changes in surface grain size

To analyse the changes in surface grain size, we first study the results from two Van Veen grab soil sampling campaigns, which are available from the months of March and August of 2016. In their analysis, Emmanouil (2017) compare the percentage of the grains larger than 2 mm between the two measurements. A ratio larger than 1 indicates surface coarsening, and a ratio smaller than 1 surface fining. Their results for the area of study are presented in Figure 6.6.

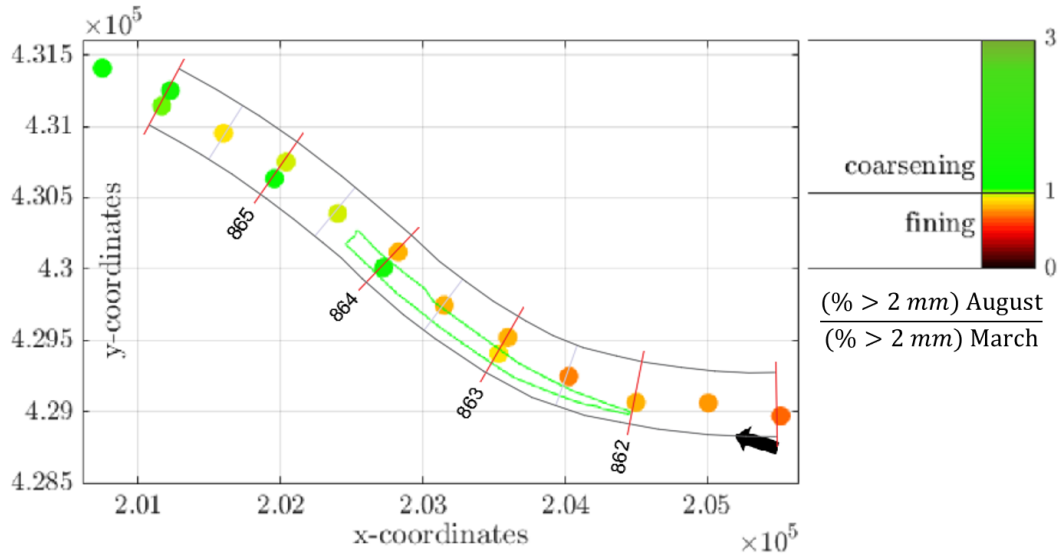


Figure 6.6: Ratio between percentage of the grains larger than 2 mm between grab soil samples of the bed surface for August and March 2016. The green area indicates the nourishments site. Arrow indicates flow direction. (Image modified from: Emmanouil 2017).

The spatial resolution of the measurements is too small to draw conclusions with certainty, but observations can be made regarding the results obtained. In the upstream end of the nourished reach bed surface has become finer with respect to the situation before the nourishments, even after the addition of the coarser sediment. This fining could be derived from a different process migrating from upstream, as the fining of the surface is observed even more predominantly both upstream of the nourishments and on the inner bend next to the nourished area. However, this fining also coincides with the theoretical response analysed in Figure 2.17, where the coarsening of the bed surface is met with a fining wave that originates on the upstream end of the nourished reach, and a coarsening wave that originates downstream. This fining wave has seemingly not yet reached the downstream end of the nourished reach, where surface grain size still shows a tendency to become coarser. We can expect that the fining wave will eventually overtake the coarsening wave, and over time, the reach coarsened by the nourishment will be preceded by surface fining, as was observed in the analysis by Berkhout (2015) presented in Figure 2.2.

To better understand how the tracer sediment propagates in the system, we analyse the radioactivity measurements carried out during the initial stages of the nourishment pilot project. These are presented in Figure 6.7. High measures of radioactivity are indicated in yellow and they represent high concentrations of granite (tracer material) in the top layer.

In Figure 6.7 we observe that the trajectory of the tracer material (granite) differs from that of the sediment wave observed in Figure 6.2. The granite tends to stay closer to the outer bend, while the sediment wave tends to cross the main channel in the direction towards the next outer bend. In the analysis made by Emmanouil (2017) they found that the wave tends to follow the deepest part of the main channel, this can be observed in better detail in the topography map presented in Figure 6.8.

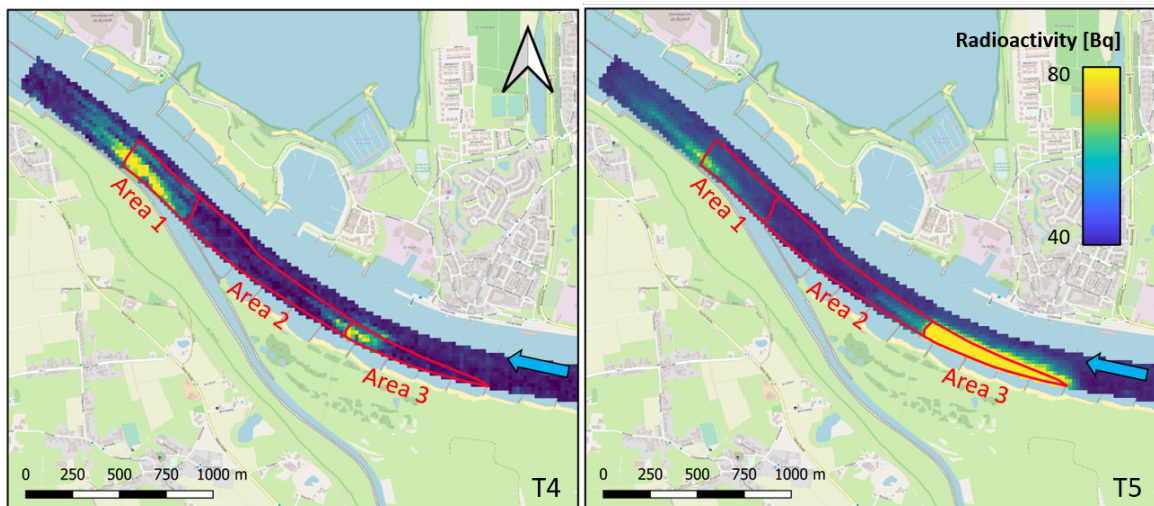


Figure 6.7: Measurements of radioactivity [Bq]. Nourishment areas marked in red. On the left, survey right after the nourishment supply to Area 1. On the right, survey right after nourishment supply to Area 3. Arrow indicates flow direction.

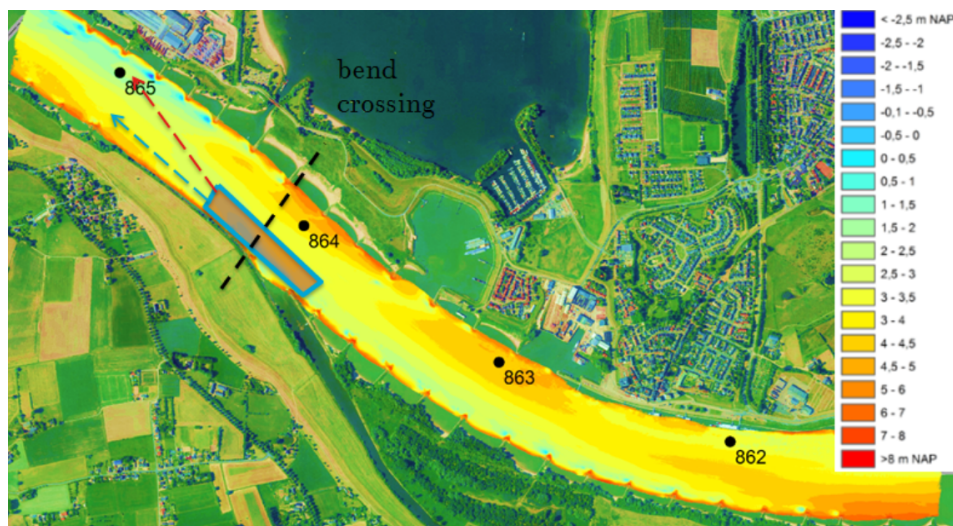


Figure 6.8: Topography of the river bend estimated with multi-beam measurements. Area 1 is marked with a blue box. The red arrow indicates the path of the deepest areas of the main channel. The blue arrow indicates the observed granite migration. Flow direction from right to left. (Image from: Emmanouil 2017).

Emmanouil (2017) hypothesised that this different path of the tracer sediment is due to spatial lag in the lateral sorting effect for the coarser particles. Lateral sorting effects are generally responsible for coarser outer bends in a meandering river. The centrifugal forces in the flow cause a differential in the pressure gradients between the inner and outer bends, and this pressure differential causes a circulation current that transports the sediment from the inner to the outer bends, which in turns leads to deeper outer bends and shallower inner bends (see Figure 6.9). This causes a lateral bed slope which enhances the lateral transport of the coarser fractions to the outer bend. This lateral sorting effect then does not correspond to the deepest locations in the main channel, but rather a bit further downstream. This secondary flow effect is schematised in Figure 6.8

In Figure 6.2 we observe bed degradation downstream of the nourished area, close to the outer bend. If we compare this with the radiometries shown in Figure 6.7, we see that bed degradation occurs in the direction of propagation of the tracer sediment. This probably means that the degradation observed is potentially related with the coarsening of the bed surface caused by the nourishment. However, the magnitude of this degradational wave is rather small, almost negligible, which means that the grain size

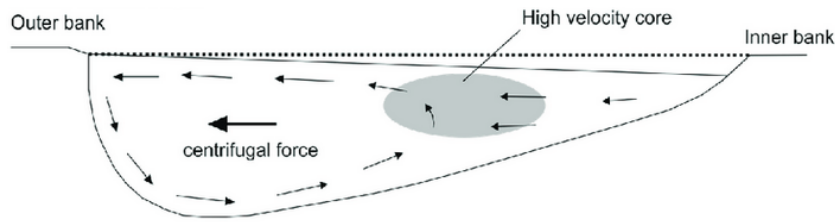


Figure 6.9: Secondary flow in river bends, image from Kasvi et al. (2017).

of the nourishments were neither too coarse to cause significant bed degradation downstream, not too fine that they were easily transported away from the reach of interest.

To better understand the accumulation of sediment observed in Figure 6.2 in the areas right after the nourishment, we analyse the contents of gravel (bed material) in the top layer (0.3 m) as estimated by Koolstra et al. (2019) in Figure 6.10 for the measurements available right after the nourishment was supplied.

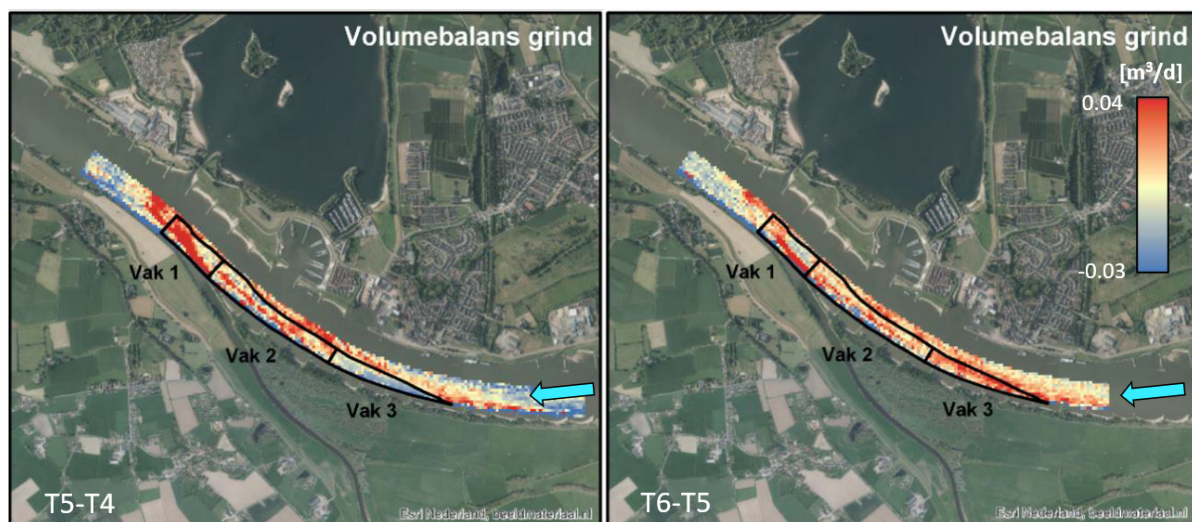


Figure 6.10: Relative changes in gravel volume per bed surface area [m^3 / m^2] between surveys. On the left, survey 28 days after the nourishment supply to Area 1. On the right, survey 28 days after nourishment supply to Area 3. Arrow indicates flow direction. (images from Koolstra et al. (2019).)

We observe that in both surveys (Area 1 in T5-T4 and Area 3 in T6-T5) the content of gravel has increased. These measurements are taken just 28 days (in both cases) after the nourishment supply, which means that in little time sediment coming from upstream has deposited in the areas where the coarser sediment (granite) was supplied. This possibly indicates adjustments in the surface grain size of these areas, and show that these adjustments occur at a much faster rate than the adjustments in bed level, as was observed in the model results.

6.4. Chapter conclusions

Regarding the propagation of the sediment wave associated with the sediment nourishments, we can conclude that the temporal variations of the flow play a large role in the propagation of the wave. This is highlighted by the low mobility of the sediment wave during low discharge periods. The results from the steady-flow model then only represent an average of the temporal variations in the wave propagation.

The initial propagation of the wave was predominantly dispersive, as the wave tail practically remained in place while the wave front propagated. During the extreme discharge event, the wave showed both

dispersive and translational behaviour, this confirms the findings from the model that the evolution of the wave becomes increasingly translational for a higher ratio between flow depth and sediment wave height.

The spatial variations in bed material proved important to the evolution of the wave. Since the gravel material in the middle reach (Area 2) was more mobile, it quickly migrated to the downstream reach (Area 1), leading to the formation of a shoal. Should an accumulation of sediment as observed in this case occur in a larger magnitude, it could potentially cause problems for navigation as the available draught is reduced.

We also find that the transverse variations in bed level in the cross-section significantly affect the trajectory of the sediment wave and should therefore be taken into account. However, in previous studies that worked with validated 1-dimensional models, it is found that the results from these models can provide decent estimates of the propagation of sediment waves (Lisle et al. 2001). This is somewhat corroborated with our model results as we find the propagation celerities to be of the same order of magnitude as those observed in the field.

The trends in bed level induced by the spatial variations in surface grain size are still observed even for a mild increase in grain size. The reach downstream of the nourishments (in the trajectory of the coarser granite fraction) did seem to show degradational tendencies. Likewise, the upstream area of the nourished reach initially favoured bed aggradation. And although the small resolution of the surface grain size data does not allow for conclusions, the observed trends match what was expected from the numerical simulations.

Discussion

In this chapter we discuss the broader application of the findings in this study and the limitations of our analysis. In rivers such as the Rhine, artificial sediment nourishments carried out during the past decades have certainly played a role in the morphodynamic changes of the river system. Sediment budget analysis show that gravel nourishments represent the largest source of the coarser sediment fractions (< 2mm) in the river (Frings et al. 2019). Furthermore, studies based on bed level data analysis of the German Rhine show that bed degradation rates have significantly slowed down in recent times (Quick et al. 2019). However, the same cannot be said for the Dutch Rhine where bed degradation rates of up to 1.5 cm/yr have persisted (Ylla Arbós et al. 2019).

In this project we aimed to better understand not only how nourishments propagate, but also the changes they cause to bed level and bed surface grain size in the river system. We take a closer look at the nourishments carried out between 1991 and 2010 in the Niederrhein. In this time period a total of about 3.6 Mt of coarse gravel (8 - 150 mm) were supplied to the 37 km reach between Rhine-km 820-857, just upstream of the German-Dutch border.

The parameters used in the numerical simulations in this study are roughly inspired on the Niederrhein. The results show that the nourishments in this schematised river system propagate with a celerity in the order of magnitude of 0.5 km/yr. This allows us to roughly estimate that at the present time (10 years after) the nourishments have dispersed 5 km downstream. Furthermore, the model results indicate that the nourishments are preceded by bed degradation, which propagates downstream with a celerity of approximately 5 km/yr, such that for the same 10-year time period, bed degradation has propagated 50 km further downstream than the nourishments. This means that in the context of the Rhine river, after 10 years, the nourishments could have propagated as far as the Dutch-Rhine border in the Bovenrijn (approx. Rhine-km 862), and bed degradation as far as the downstream areas of the Waal in Tiel (approx. Rhine-km 912).

These initial estimates stem from a very rough schematisation of the river, with several simplifications and large uncertainties, so they should not be considered to be accurate. However, they highlight just how relevant the difference in celerities of the adjustment waves are, as well as demonstrate the importance of considering not only what happens in the area where the nourishment is distributed, but also what happens downstream of it.

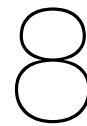
These findings also raise the question on whether sediment nourishments are an effective measure to mitigate bed degradation. Data suggests that they have a very positive effect in the areas where they are supplied, as the coarser sediment is harder to erode and may even enhance sediment deposition. Additionally, the increase in bed level caused by the nourishment may also lead to a backwater effect that enhances aggradation on the reach upstream from where it is supplied. The main problem is the negative degradational effect the nourishments have on the downstream areas, so while they are very effective at mitigating localised bed degradation problems, in a larger scale it then becomes unfeasible to try and use them to stop bed degradation along the entire river length. Furthermore, a lot is still unknown about the long-term effects of these nourishments on the morphodynamic changes of the river system.

Between the years 2000-2010 an additional sediment nourishment campaign was implemented in the Niederrhein, a total of around 2 Mt of sediment were distributed along this river reach. The main difference with the nourishment campaign mentioned earlier, was that the nourishments had a similar grain size composition to the river bed (4-32 mm). In this study we analysed how increasing the content of finer sediment in the nourishments helps mitigate the contribution of the nourishments to degradation in the downstream areas. It is then possible that this nourishment campaign has helped reduce degradation downstream by partly compensating for the deficit in sediment supply.

One of the limitations of the numerical model is that we assumed the river started from an equilibrium state, in order to be able to analyse the morphodynamic changes to the system related with the sediment nourishment. In reality, the river is not in an equilibrium state, and due to the combination of processes that affect the morphology of the system, it is not easy to determine the extent to which the nourishments in the German Rhine have impacted bed level and bed surface grain size in the Dutch Rhine downstream.

In the model schematisation of the nourishments, we assumed the nourishment supply was uniformly distributed and was executed instantly. When in reality, nourishment supply projects may last several months, and migration of the nourished sediment might already occur within this time span, just as it was observed for the nourishment pilot project in the Bovenrijn analysed in this study. This means that the shape of the sediment wave associated with the nourishments can become quite irregular, as opposed to uniform, and this can directly influence how it disperses. As an example, we observed in the nourishment pilot project in the Bovenrijn that the sediment accumulated in the most downstream area, and it was this area that eroded the most (relatively) during the high discharge event, as the accumulated sediment was dispersed further downstream.

Another important simplification of the model was that the longitudinal bed slope is assumed constant, which neglects the typical concavity of the river profile. The implications are that in reality, bed slope decreases in the downstream direction and this tends to slow down the migration of the nourished sediment. At some point the nourished sediment might become completely immobile which could potentially lead to an undesired accumulation of sediment that would have to be dredged out of the river.



Conclusions and Recommendations

8.1. Conclusions

1. What adjustment waves can be observed in a river system after a sediment nourishment?

We distinguish between two types of adjustment waves, bed and sorting waves. Bed waves originate due to changes in bed level in the river system, and sorting waves due to changes in bed surface grain size. A sediment nourishment causes an immediate increase in bed level over the reach where it is supplied, which leads to an increase in flow velocity and sediment transport, and induces a degradational wave on the upstream end of the nourished reach, as well as an aggradational wave downstream of it. We make the analogy that the accumulated sediment in the nourished reach after the nourishment travels downstream as a sediment wave, and that the adjustment waves describe the dispersion of this sediment wave through the system, as bed level decreases at the upstream end of the wave, and increases downstream of it.

In order to prevent the nourished sediment from being easily transported downstream, a sediment composition coarser than the bed surface texture is typically used in the nourishment. This causes an immediate coarsening of the bed surface over the reach where the sediment is supplied, which increases the fraction volume of the coarser sediment transported downstream and induces a fining wave on the upstream end of the nourished reach, and a coarsening wave on the downstream end. Furthermore, the immediate coarsening of the bed surface reduces sediment mobility and enhances sediment deposition over the nourished reach, and consequently also causes a deficit in the sediment supplied downstream inducing bed degradation.

The adjustments waves that are observed in a river system after a nourishment depend on which physical process is dominant in determining the morphodynamic response of the system. Previous research as well as the results in this study show that in the initial morphodynamic response, the immediate coarsening of the bed surface over the nourished reach is generally the dominant effect. This is not the case only when the immediate increase in bed level caused by the nourishment is large with respect to the flow depth, and the ensuing increase in flow velocity is so large enough that the reduced mobility of the coarser nourished sediment becomes negligible. This is generally not the case in an artificial sediment nourishment, since the thickness of the nourished sediment layer in the bed is limited to maintain a navigable water depth in the river channel.

2. What physical processes determine the propagation celerity of the adjustment waves?

The main physical processes that determine the propagation celerity of the adjustment waves are the thickness of the sediment wave resulting from the nourishment, and the grain size composition of the bed surface.

The propagation celerity of bed waves is directly proportional to flow velocity and sediment transport. The increase in bed level induced by the nourished sediment increases flow velocity and creates a backwater effect where flow velocities on the downstream end of the nourished reach are larger than on the upstream end. This means that the celerity of the aggradational wave at the downstream end

is larger than the celerity of the degradational wave at the upstream end. In other words, the front of the sediment wave associated with the nourishment disperses faster than the tail of the wave erodes, which leads to a predominantly dispersive behaviour of the sediment wave.

Over time, as the sediment wave disperses and becomes thinner, flow velocities decrease and the spatial gradient in flow velocity associated with the backwater effect becomes milder. This means that the sediment wave front gradually slows down over time, and the propagation of the wave becomes less dispersive the more the wave has dispersed.

The propagation celerity of the sorting waves depends on the sediment transport per grain size fraction and the thickness of the active layer. Sorting waves propagate several times faster than bed waves, and thus the time scale of the changes in the system related to sorting waves is significantly shorter than the time scale of changes related to bed waves. The upstream fining wave travels faster than the downstream coarsening wave, and when these waves meet the changes in surface grain size are offset. This fining wave has an accelerating effect on the sediment wave, and a decelerating effect on the preceding degradational wave.

3. What is the impact of variations in the height and length of the sediment wave induced by the nourishment on the adjustment waves?

We found that taller sediment waves lead to faster propagation of the bed waves. This is due to the Bernoulli effect, since there is a larger increase in flow velocity over the nourished reach as the ratio between the flow depth and the height of the sediment wave becomes smaller. Additionally, due to the backwater effect over then nourished reach, flow velocity at the downstream end is larger than at the upstream end, this gradient in flow velocity becomes steeper the taller the sediment waves. This means that the propagation of the taller sediment waves can be described as predominantly dispersive, and for the shorter waves the propagation is mainly translational.

The propagation of the sorting waves appears to remain mostly unaffected by variations of the height of the sediment wave. One might expect the incision downstream of the nourishment to become deeper for the taller sediment waves, since these cause larger increases in flow velocities over the nourished reach. However, we found that this is not always the case, as flow velocities can become large enough to be more effective at carrying the nourished sediment downstream.

The main impact of variations in the length of the nourished reach is in how far downstream the degradation preceding the nourishment propagates before it is slowed down. This is related to the distance both of the sorting waves (i.e. the fining and the coarsening wave) travel before they offset each other. The longer the nourished reach, the larger the distance the fining wave has to travel before it meets the coarsening and offsets the initial changes to surface grain size caused by the nourishment. This means that degradation is found further downstream a lot earlier the larger the nourished reach is.

4. What is the impact of variations in the grain size distribution of the nourishments on the adjustment waves?

We found that a finer composition of the nourishment helps mitigate the growth of the incision downstream of the nourished reach. This means that for finer nourishments, not only is the depth of incision smaller, but also it takes longer for the incision to propagate further downstream. The reason is that when the content of fines in the nourishment is larger, the deficit in sediment supply to the downstream reach is reduced. Additionally, the larger content of fines available for transport increases the celerity of the fining wave, which means that it takes a shorter time for the initial coarsening of the bed surface caused by the nourishment to be counteracted, and that the downstream propagation of the incision is slowed down significantly sooner.

However, we also found that simply increasing the contents of the finer sediment in the nourishment is not necessarily a solution to the growth of the incision, as adding too much may actually potentially

cause aggradational problems in the downstream areas. This is due to the surplus of finer sediment being mobilised too easily and causing an increase in the sediment load supply downstream. Enhanced aggradation downstream creates problem in navigation channels and ports, where the sediment has to be dredged out to keep the waterway navigable.

The deposition of sediment over the nourished reach was found to be more prominent the coarser the composition of the nourishment. This means that for the coarser nourishments, the sediment waves become taller, which lead to larger increases in flow velocity and therefore a larger initial propagation celerity of the waves. One may expect the incision preceding the sediment waves to have an influence on their propagation celerity, as a larger incision might present a larger obstacle for the wave. We found that this was not the case, as the celerity of the sediment waves was practically the same regardless of the composition of the nourished sediment, the only significant difference found was related to the height of the wave and its relation this has with the flow velocity.

5. How do these results compare to a nourishment field experiment?

The main difference is that the nourishments in the field experiment are not supplied across the entire river width as was schematised in the numerical model. The direction of propagation of the nourished sediment differed from the direction of propagation of the sediment wave, probably due to spatial lag in lateral sorting effects. This highlights the main limitation of using a one-dimensional model as it is unable to predict these 3-dimensional flow effects.

A strong similarity was found in the initial morphodynamic response in the field experiment to that of the numerical model. In this initial response the increase in surface grain size is the dominant effect, sediment deposition is favoured over the nourished reach, and bed degradation occurs just downstream of it. Additionally, surface grain size measurements also indicate a fining of the bed surface on the upstream end, and a coarsening on the downstream end, just as is observed in the initial response in the numerical model.

Furthermore, the differences in mobility of the nourished sediment between the middle and downstream area of the nourished reach (the middle area being more mobile) potentially led to an accumulation of sediment in the downstream area. This again highlights how the grain size composition of the nourished sediment is determining factor in the initial evolution of the sediment wave.

As was observed in the numerical model, the propagation of the sediment wave in the later stages is entirely determined by the flow conditions, and the size and shape of the wave. In the model, we observed that the dispersion of the nourished sediment occurred more prominently at the sediment wave front where the flow velocities were higher due to backwater effects. In the field experiment, the sediment wave practically remains unchanged during low flow rate conditions, and during extreme discharge conditions it is also the sediment at the wave front, where the height of the wave was larger due to the initial sediment accumulation in this area, that disperses further downstream.

8.2. Recommendations

To continue the ongoing research on the effects of sediment nourishments in a river system presented in this study, we recommend the following:

- To analyse the effects of changes in bed slope in the propagation of the adjustment waves after a nourishment. This will provide insight on how the downstream changes in the slope might affect the mobility of the nourished sediment, which could have implications for the river system not considered in this study. This can be done with a numerical model like the one used in this study, by setting up a series of model runs with the bed slope as the control parameter, and analysing the changes in the propagation of the adjustment waves in the system.
- To study the effect of changes in the composition of the substrate in the propagation of the adjustment waves after a nourishment. This will allow for a better understanding of the influence of the composition of the substrate on the propagation celerity of the sorting waves in the system, as well as in the degradation observed downstream of the nourishment. This can be done by studying a set of numerical model runs with different compositions of the substrate.
- To include a river bifurcation in the schematisation of the river system. This will provide insight on how the changes in the system caused by the nourishment can impact the water and sediment discharge partition, as well as the stability of the river bifurcation. This can be done with numerical simulations, or even with a physical model, where the propagation of the nourished sediment can be more thoroughly studied.

Bibliography

- Arkesteijn, Liselot et al. (2019). "The Quasi-Equilibrium Longitudinal Profile in Backwater Reaches of the Engineered Alluvial River: A Space-Marching Method". In: *Journal of Geophysical Research: Earth Surface* 124.11, pp. 2542–2560. DOI: [10.1029/2019jf005195](https://doi.org/10.1029/2019jf005195).
- Berkhout, Bart (2015). *Waves arising from Hirano's conservation model for mixed-size sediment morphodynamics*.
- Blom, Astrid (2016). *Flows platform*. URL: <https://flowsplatform.nl/#/bed-degradation-in-the-rhine-river-1479821439344>.
- Blom, Astrid, Liselot Arkesteijn, et al. (2017b). "The equilibrium alluvial river under variable flow and its channel-forming discharge". In: *Journal of Geophysical Research: Earth Surface* 122.10, pp. 1924–1948. DOI: [10.1002/2017jf004213](https://doi.org/10.1002/2017jf004213).
- Blom, Astrid, Víctor Chavarrías, et al. (2017a). "Advance, Retreat, and Halt of Abrupt Gravel-Sand Transitions in Alluvial Rivers". In: *Geophysical Research Letters* 44.19, pp. 9751–9760. DOI: [10.1002/2017gl074231](https://doi.org/10.1002/2017gl074231).
- Blom, Astrid, Jan S. Ribberink, and Huib J. de Vriend (2003). "Vertical sorting in bed forms: Flume experiments with a natural and a trimodal sediment mixture". In: *Water Resources Research* 39.2. DOI: [10.1029/2001wr001088](https://doi.org/10.1029/2001wr001088).
- Blom, Astrid, Enrica Viparelli, and Víctor Chavarrías (2016). "The graded alluvial river: Profile concavity and downstream fining". In: *Geophysical Research Letters* 43.12, pp. 6285–6293. DOI: [10.1002/2016gl068898](https://doi.org/10.1002/2016gl068898).
- Chavarrías, Víctor, Liselot Arkesteijn, and Astrid Blom (2019). "A Well-Posed Alternative to the Hirano Active Layer Model for Rivers With Mixed-Size Sediment". In: *Journal of Geophysical Research: Earth Surface* 124.11, pp. 2491–2520. DOI: [10.1029/2019jf005081](https://doi.org/10.1029/2019jf005081).
- Chavarrías, Víctor, Guglielmo Stecca, and Astrid Blom (2018). "Ill-posedness in modeling mixed sediment river morphodynamics". In: *Advances in Water Resources* 114, pp. 219–235. DOI: [10.1016/j.advwatres.2018.02.011](https://doi.org/10.1016/j.advwatres.2018.02.011).
- De Way, M. (2014). *Sediment augmentation and the migration of shoals*.
- Emmanouil, Antonios (2017). *Morphodynamic trends in the freely flowing Rhine*.
- Frings, R. M., Ricarda Döring, et al. (2014b). "Fluvial sediment budget of a modern, restrained river: The lower reach of the Rhine in Germany". In: *Catena* 122, pp. 91–102. DOI: [10.1016/j.catena.2014.06.007](https://doi.org/10.1016/j.catena.2014.06.007).
- Frings, R. M., Nicole Gehres, et al. (2014a). "Today's sediment budget of the Rhine River channel, focusing on the Upper Rhine Graben and Rhenish Massif". In: *Geomorphology* 204, pp. 573–587. DOI: [10.1016/j.geomorph.2013.08.035](https://doi.org/10.1016/j.geomorph.2013.08.035).
- Frings, R. M., G. Hillebrand, et al. (2019). "From source to mouth: Basin-scale morphodynamics of the Rhine River". In: *Earth-Science Reviews* 196, p. 102830. DOI: [10.1016/j.earscirev.2019.04.002](https://doi.org/10.1016/j.earscirev.2019.04.002).
- Hillebrand, G. and Roy M. Frings (2017). *Von der Quelle zur Mündung: Die Sedimentbilanz des Rheins im Zeitraum 1991 – 2010. Lelystad: Internationale Kommission für die Hydrologie des Rheingebietes. KHR-Bericht I-22. KHR/CHR II-22*. DOI: [10.5675/KHR_22.2017](https://doi.org/10.5675/KHR_22.2017).
- Hirano, Muneo (1971). "River-bed degradation with armoring". In: *Proceedings of the Japan Society of Civil Engineers* 1971.195, pp. 55–65. DOI: [10.2208/jscej1969.1971.195_55](https://doi.org/10.2208/jscej1969.1971.195_55).
- Kasvi, Elina et al. (Feb. 2017). "Flow Patterns and Morphological Changes in a Sandy Meander Bend during a Flood—Spatially and Temporally Intensive ADCP Measurement Approach". In: *Water* 9, p. 106. DOI: [10.3390/w9020106](https://doi.org/10.3390/w9020106).
- Koolstra, FJ, RL Koomans, and K. de Vries (2019). *2019-P-677 Suppletion Upper Rhine, part II: analysis and interpretation 2019-P-677*.
- Lisle, Thomas E., Yantao Cui, et al. (2001). "The dominance of dispersion in the evolution of bed material waves in gravel-bed rivers". In: *Earth Surface Processes and Landforms* 26.13, pp. 1409–1420. DOI: [10.1002/esp.300](https://doi.org/10.1002/esp.300).

- Lisle, Thomas E., James E. Pizzuto, et al. (1997). "Evolution of a sediment wave in an experimental channel". In: *Water Resources Research* 33.8, pp. 1971–1981. DOI: [10.1029/97wr01180](https://doi.org/10.1029/97wr01180).
- Mark, C. F. van der, A. Blom, and S. J. M. H. Hulscher (2008). "Quantification of variability in bedform geometry". In: *Journal of Geophysical Research* 113.F3. DOI: [10.1029/2007jf000940](https://doi.org/10.1029/2007jf000940).
- Paarlberg, A. et al. (Jan. 2007). "Modelling dynamic roughness during floods". In:
- Quick, Ina et al. (2019). "Evaluation of depth erosion as a major issue along regulated rivers using the classification tool Valmorph for the case study of the Lower Rhine". In: *International Journal of River Basin Management* 18.2. DOI: [10.1080/15715124.2019.1672699](https://doi.org/10.1080/15715124.2019.1672699).
- Ribberink, J.S. (1987). "Mathematical modelling of one-dimensional morphological changes in rivers with non-uniform sediment". PhD thesis. Delft University of Technology.
- Sklar, Leonard S. et al. (2009). "Translation and dispersion of sediment pulses in flume experiments simulating gravel augmentation below dams". In: *Water Resources Research* 45.8. DOI: [10.1029/2008wr007346](https://doi.org/10.1029/2008wr007346).
- Stecca, G., A. Siviglia, and A. Blom (2014). "Mathematical analysis of the Saint-Venant-Hirano model for mixed-sediment morphodynamics". In: *Water Resources Research* 50.10, pp. 7563–7589. DOI: [10.1002/2014wr015251](https://doi.org/10.1002/2014wr015251).
- Venditti, J. G. et al. (2010). "Effect of sediment pulse grain size on sediment transport rates and bed mobility in gravel bed rivers". In: *Journal of Geophysical Research* 115.F3. DOI: [10.1029/2009jf001418](https://doi.org/10.1029/2009jf001418).
- Vries, M. de (1965). *Considerations about non-steady bed-load-transport in open channels*. Hydraulics Laboratory.
- Ylla Arbós, Claudia et al. (2019). *Bed level change in the upper Rhine Delta since 1926 and rough extrapolation to 2050*.



Model convergence

In this sub-section we present the results of the model simulation using different time and spatial steps, with the aim to show that the numerical results converge to a solution independent of the numerical settings. We do so by showing the resulting bed elevation difference for different time steps, spatial steps and storage time steps. The latter are the temporal intervals in which the results are stored.

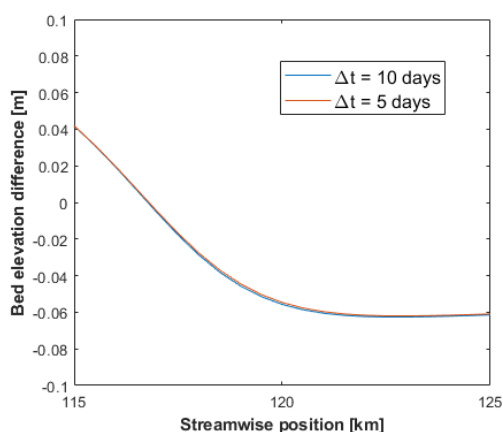


Figure A.1: Time step convergence.

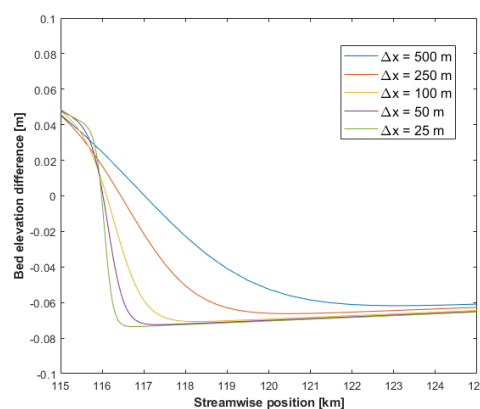


Figure A.2: Spatial step convergence.

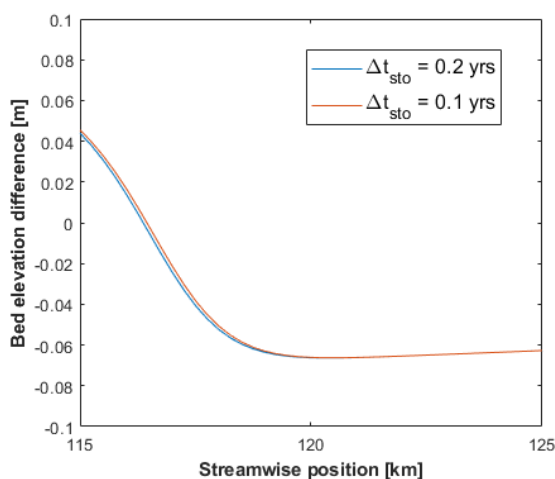


Figure A.3: Convergence of the storage time step.

In Figure A.1 we show that the results converge for a time step Δt of 10 days, this is later reduced to a value of $\Delta t = 0.5$ days to comply with the CFL condition with respect to the spatial step. Figure A.2

shows that the results converge for a spatial step $\Delta x = 50$ meters. Finally the selection of the storage time step $\Delta t_{sto} = 0.1$ yrs is made with the convergence of the results shown in [Figure A.3](#).

B

Wiggles

The propagation celerities of the waves are calculated based on the location of the wave at every time step, and because this location is found for discrete grid sizes, the computed celerity oscillates or wiggles around its true values. In this appendix we provide further explanation on why these wiggles occur, and how using a moving average of the celerity provides a good approximation of the true celerity values.

To elaborate on the occurrence of the wiggles in the celerity value, in Figure B.1 we first present in more detail the location of the wave centroid for the mixed-size base case analysed in Section 4.2. We observe in this figure that the slope (and therefore the celerity of the wave centroid) varies at every time step.

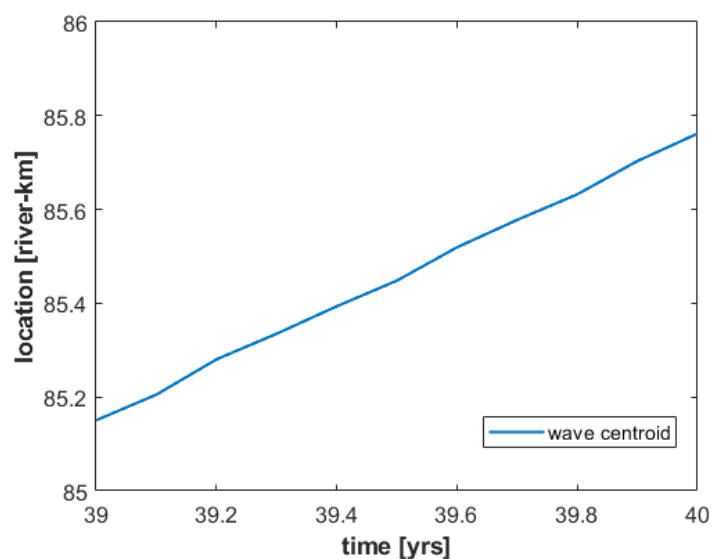


Figure B.1: Location of the nourishment wave centroid for the mixed-size base case.

From Figure B.1 we can observe that in total the centroid propagates approximately 0.6 km in one year. However, when we estimate the celerity value at each time step, the resulting celerity is affected by the small variations in slope, as is presented in Figure B.2.

We observe in Figure B.2 that even though the celerity values do wiggle around the approximate value of 0.6 km/yr, this value of the celerity is not easily deduced from this figure. An attempt was made at reducing the time and spatial steps used in the model, and while this effectively reduced the magnitude of the wiggles, it did not prevent them. Instead, if we analyse what the celerity estimate is by taking a 1-year moving average of these values (Figure B.3), we observe that even though the wiggles still persist (although significantly milder), the value of the celerity of 0.6 km/yr is well approximated.

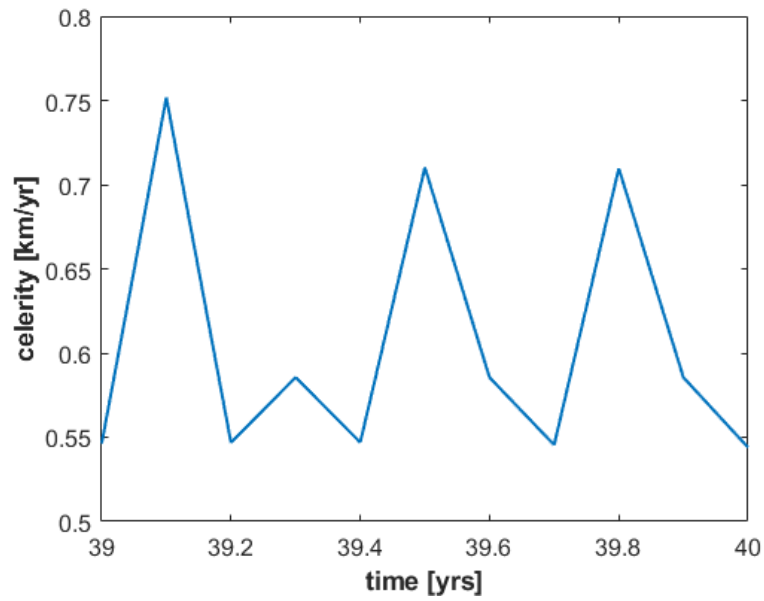


Figure B.2: Celerity of the nourishment wave centroid for the mixed-size base case.

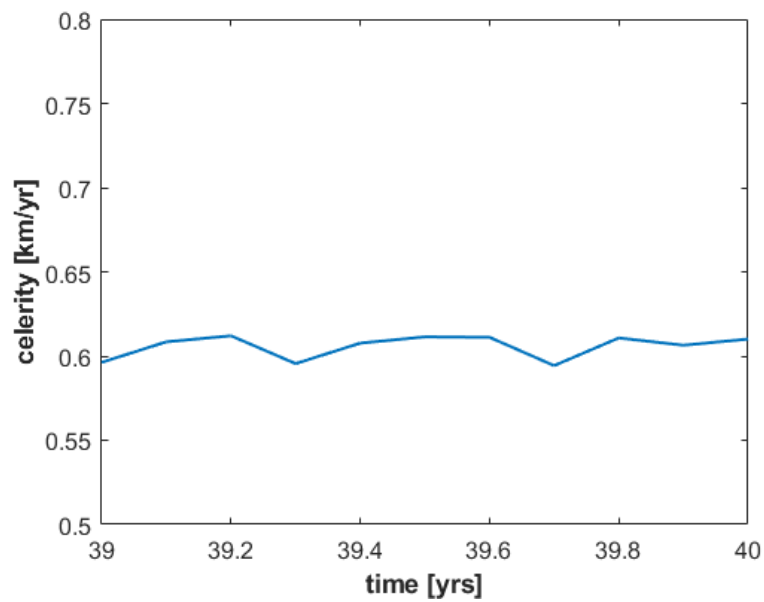


Figure B.3: 1-year moving average of the celerity of the nourishment wave centroid for the mixed-size base case.

List of Figures

1.1	Rhine reach between Weisweil and Marlen. On top the meandering river reach before the normalisation works. On the bottom the same straightened river reach afterwards. (Hillebrand et al. 2017)	1
1.2	Total dredged and re-allocated sediment volumes in the Niederrhein between 1991-2010. As presented by Frings et al. (2014a).	2
1.3	Total volume of nourished sediment with grain size of 8-150 mm in the Niederrhein between 1991-2010.	3
1.4	Total volume of nourished sediment consisting of additional bed-load supply (gravel of 4-32 mm) in the Niederrhein between 2000-2010.	3
1.5	Upper Rhine delta and downstream reach of the German Rhine (Niederrhein), city boundaries with respective (Rhine-km). PK: Pannerdensch Kanaal.	4
2.1	Schematic of the effect of a perturbation in bed elevation in a mixed sediment case as depicted by (Chavarrías, Guglielmo Stecca, et al. 2018). A perturbation in bed elevation introduces perturbations in flow, bed level and surface grain size distribution, hereby referred to as “water”, “bed”, and “sorting” waves respectively.	8
2.2	Results from experimental studies by Berkhout (2015) for the propagation of a shoal composed of coarse sediment. On the left, bed level measurements depicting the formation of a scour downstream of the shoal. On the right, measurements of the gravel volume content in the active layer, showing the fining of the surface downstream of the shoal.	9
2.3	Accumulation of the coarser sediment fractions in the trough of migrating bed forms due to vertical sorting, as depicted by Blom et al., (2003)	10
2.4	On top (a) the evolution of a purely translational sediment wave. On bottom (b) the evolution of a purely dispersive sediment wave.	11
2.5	On the left (A) the evolution of a gravel sand sediment wave. On the right (B) the evolution of a sand sediment wave. As depicted by Lisle et al. (2001).	12
2.6	Normalised tracer concentration per grain size fraction, almost 5 years after nourishments, as depicted by Emmanouil (2017)	12
2.7	Energy balance and Bernoulli effect over a bed level step, neglecting energy losses due to friction ($\frac{d(H)}{ds} = 0$).	13
2.8	Morphodynamic response corresponding to the increase in velocity caused by the Bernoulli effect.	14
2.9	Initial flow response and backwater effect.	14
2.10	Flow velocity gradients corresponding to the backwater effect.	15
2.11	Morphodynamic response to the backwater effect.	15
2.12	Resulting backwater curves for an increase in surface friction over the nourished reach.	15
2.13	Morphodynamic response to an increase in friction.	16
2.14	Sediment transport gradients resulting from a coarsening of a river reach.	16
2.15	Morphodynamic response to coarse sediment nourishments.	16
2.16	At the top, surface content of the coarser fraction (F_g) with respect to the equilibrium surface texture ($F_{e,g}$). At the bottom sediment transport gradients for the finer fraction ($q_{s,s}$) and the coarser fraction ($q_{s,g}$).	17
2.17	Sorting waves resulting from an increase in grain size.	18
2.18	Sediment transport gradients corresponding to the backwater effect for each grain size fraction.	18
2.19	Changes in grain size and sorting waves resulting from the gradients in flow velocity due to the backwater effect.	19

4.1	Bed elevation difference [m] with respect to initial bed level at times $t = 0, 10,$ and 50 years. Flow direction from left to right.	25
4.2	Flow velocity [m/s] at times $t = 0, 10,$ and 50 years. Flow direction from left to right.	25
4.3	Estimation of the sediment wave tail (x_{05}), centroid (x_c), and front (x_{95}).	26
4.4	On the left, the evolution of a purely translational sediment wave (top) and a purely dispersive sediment wave (bottom). On the right, the comparison between the location of the wave centroid (x_c) and the wavelength (l), for a purely translational wave (blue) and a purely dispersive wave (green).	26
4.5	Displacement of the centroid of the sediment wave with respect to its initial position in the streamwise direction, the dashed lines indicate the location of the centroid at times $t = 10$ and 50 years.	27
4.6	Celerity of the sediment wave centroid estimated with the results for the numerical simulation (blue) and with the analytical solution (orange).	27
4.7	Base case results for times $t = 0, 2,$ and 10 years. At the top (a) bed elevation difference [m] with respect to initial bed level. At the bottom (b) Bed surface gravel content [-]. Flow direction from left to right.	28
4.8	Base case results for times $t = 0, 2,$ and 10 years. At the top (a) Flow velocities [m/s] along the domain. At the bottom (b) Total sediment transport rates per unit width [m^2/s] along the domain. Flow direction from left to right.	29
4.9	Dispersion of the nourishment wave with respect to its centroid.	31
4.10	1-year moving average value of the celerity [km/yr] of the sediment wave tail (blue), centroid (red), and front (yellow).	31
4.11	Celerity of the sediment wave centroid estimated with the results for the numerical simulation (blue) and with the analytical solution (orange)	32
4.12	Streamwise location of the degradational wave tail (blue), centroid (red) and front (yellow) over time [yrs].	33
4.13	Streamwise location of the front of the degradational wave (blue), sediment wave (red), and fining wave (yellow) over time.	34
4.14	1-year moving average value of the celerity [km/yr] of the degradational wave tail (blue), centroid (red), and front (yellow).	34
4.15	Celerity of the degradational wave front estimated with the results for the numerical simulation (red) and with the analytical solution (blue).	35
4.16	1-year moving average value of the celerity [km/yr] of the centroid of the sediment wave (blue), and the front of the degradational wave (red).	35
5.1	Changes in wave length with respect to the displacement of the wave centroid for the sediment waves in the set of model runs A. ΔL indicates the length in [km] of the nourished reach in each model run.	37
5.2	1-year moving average value of the celerity [km/yr] of the centroid of the sediment wave, set of model runs A. ΔL indicates the length in [km] of the nourished reach in each run.	38
5.3	Maximum depth of the incision [m] over time [yrs], set of model runs A. ΔL indicates the length in [km] of the nourished reach in each run.	39
5.4	1-year moving average value of the celerity of the front of the degradational wave, set of model runs A. ΔL indicates the length in [km] of the nourished reach in each run.	40
5.5	Distance travelled by the front of the degradational wave, set of model runs A. ΔL indicates the length in [km] of the nourished reach in each run.	40
5.6	Changes in wave length with respect to the displacement of the wave centroid of the sediment waves in the set of model runs B. $F_{N,S}$ indicates the fraction content of sand [% volume] in the nourished sediment in each model run.	42
5.7	Distance travelled [km] over time by the front of the sediment wave, set of model runs B. $F_{N,S}$ indicates the fraction content of sand [% volume] in the nourished sediment in each model run.	42
5.8	1-year moving average value of the celerity [km/yr] of the centroid of the sediment wave, set of model runs B (runs 1-3). $F_{N,S}$ indicates the fraction content of sand [% volume] in the nourished sediment in each model run.	43

5.9	Maximum height of the sediment wave over time, set of model runs B (runs 1-3). $F_{N,S}$ indicates the fraction content of sand [% volume] in the nourished sediment in each model run.	44
5.10	Maximum depth of incision [m] over time [yrs], set of model runs B (runs 1-3). $F_{N,S}$ indicates the fraction content of sand [% volume] in the nourished sediment in each model run.	45
5.11	1-year moving average value of the celerity [km/yr] of the front of the degradational wave, set of model runs B (runs 1-3). $F_{N,S}$ indicates the fraction content of sand [% volume] in the nourished sediment in each model run.	45
5.12	Distance travelled [km] over time by the front of the degradational wave, set of model runs B. $F_{N,S}$ indicates the fraction content of sand [% volume] in the nourished sediment in each model run.	46
5.13	Sediment transport gradients (top) and the corresponding morphodynamic response (bottom) to a decrease in surface grain size over the nourished reach.	47
5.14	Bed elevation difference [m] with respect to initial bed level at times $t = 0, 1,$ and 5 years. Model run 4: fraction content of sand $F_{N,S} = 25\%$ of the total volume of nourished sediment. Flow direction from left to right.	47
5.15	1-year moving average value of the celerity [km/yr] of the centroid of the sediment wave, set of model runs B. $F_{N,S}$ indicates the fraction content of sand [% volume] in the nourished sediment in each model run.	48
6.1	Site location for the nourishment pilot project in the Bovenrijn (2016). In red, the areas defined for the artificial sediment supply. Flow is from right to left.	50
6.2	On the left figures, relative changes in sediment volume per bed surface area [m^3 / m^2] between surveys (images from Koolstra et al. (2019).), arrow indicates flow direction. On the right, sketch of the hydrograph, indicating the approximate values of the water discharge [m^3 / s] and the time [days] passed between each measurement.	54
6.3	On the left figures, relative changes in sediment volume per bed surface area [m^3 / m^2] between surveys (images from Koolstra et al. (2019).), arrow indicates flow direction. On the right, sketch of the hydrograph, indicating the approximate values of the water discharge [m^3 / s] and the time [days] passed between each measurement.	55
6.4	On the left figures, relative changes in sediment volume per bed surface area [m^3 / m^2] between surveys (images from Koolstra et al. (2019).), arrow indicates flow direction. On the right, sketch of the hydrograph, indicating the approximate values of the water discharge [m^3 / s] and the time [days] passed between each measurement.	56
6.5	On the top, values for the maximum water discharge measured in Lobith for the same time periods as the bed level surveys. On the bottom, propagation celerity of the sediment wave front estimated for the nourishment pilot project in the Bovenrijn.	57
6.6	Ratio between percentage of the grains larger than 2 mm between grab soil samples of the bed surface for August and March 2016. The green area indicates the nourishments site. Arrow indicates flow direction. (Image modified from: Emmanouil 2017).	58
6.7	Measurements of radioactivity [Bq]. Nourishment areas marked in red. On the left, survey right after the nourishment supply to Area 1. On the right, survey right after nourishment supply to Area 3. Arrow indicates flow direction.	59
6.8	Topography of the river bend estimated with multi-beam measurements. Area 1 is marked with a blue box. The red arrow indicates the path of the deepest areas of the main channel. The blue arrow indicates the observed granite migration. Flow direction from right to left. (Image from: Emmanouil 2017).	59
6.9	Secondary flow in river bends, image from Kasvi et al. (2017).	60
6.10	Relative changes in gravel volume per bed surface area [m^3 / m^2] between surveys. On the left, survey 28 days after the nourishment supply to Area 1. On the right, survey 28 days after nourishment supply to Area 3. Arrow indicates flow direction. (images from Koolstra et al. (2019).)	60
A.1	Time step convergence.	70
A.2	Spatial step convergence.	70

A.3	Convergence of the storage time step.	70
B.1	Location of the nourishment wave centroid for the mixed-size base case.	72
B.2	Celerity of the nourishment wave centroid for the mixed-size base case.	73
B.3	1-year moving average of the celerity of the nourishment wave centroid for the mixed-size base case.	73